8-30-2002

Modeling Corrosion in Oxygen Controlled LBE Systems with Coupling of Chemical Kinetics and Hydrodynamics-Task V: Final Report -Phase I 09/01/2001-08/30/2002

Samir Moujaes
University of Nevada, Las Vegas, samir@me.unlv.edu

Yitung Chen
University of Nevada, Las Vegas, yitung.chen@unlv.edu

Modeling Corrosion in Oxygen Controlled LBE Systems with Coupling of Chemical Kinetics and Hydrodynamics-Task V

Final Report -Phase I
09/01/2001-08/30/2002
UNLV-AAA University Participation Program

Principle Investigator: Samir Moujaes
Co-Principle Investigator: Yitung Chen

PURPOSE AND PROBLEM STATEMENT

The Lead-Bismuth eutectic (LBE) has been determined from previous experimental studies by the Russians and the European scientific community to be a potential material that can be used as a spallation target and coolant for the AAA proposed application. Properly controlling the oxygen content in LBE can drastically reduce the LBE corrosion to structural steels. However, existing knowledge of material corrosion performance was obtained from point-wise testing with only very sparse experimental data. Scientists have noticed that the concentration of oxygen dissolved in the liquid alloy could control the corrosion rate of steels exposed to Pb or Pb-Bi. At high oxygen concentration, an oxide layer could be formed on the steel surface (lead oxides are less stable than iron oxide), which protects it from corrosion. At low oxygen concentration, there is no oxidation and corrosion occurs by dissolution of the steel components in the liquid metal. The surface of the oxide layer in contact with the bulk flow of liquid metal may also be eroded under a high fluid velocity. Then the surface of the metal will no longer be protected because a porous oxide layer will be formed.

The first subtask of this project involves using a CFD code (3-D simulation) such as STAR-CD to obtain averaged values of stream wise velocity, temperature, oxygen and corrosion product concentrations at a location deemed close to the walls of the LBE loop at more than one axial location along it. The oxygen and corrosion product inside the test loop will be simulated to participate in chemical reactions with the eutectic fluid as it diffuses through towards the walls. Details of the geometry of these loops will be obtained from scientists at LANL. These values will act as a set of starting boundary conditions to the second task.

The second subtask and the more important objective of this project is to use the information supplied by the first task as boundary conditions for the kinetic modeling of the corrosion process at the internal walls of the test loop. The outcome of the modeling will be fed back to the first subtask, and the steady state corrosion/precipitation in an oxygen controlled LBE system will be investigated through iterations. The information is hoped to shed some light on the likely locations for corrosion and precipitation along the axial length of parts of the test loop.

PERSONNEL

Principle Investigator:

- Dr. Samir Moujaes (Mechanical Engineering)

Co-Principle Investigator:

- Dr. Yitung Chen (Mechanical Engineering)

Students:

- Mr. Kanthi Dasika, M.S. Graduate Student, (Mechanical Engineering)
- Mr. Chao Wu, M.S. Graduate Student, (Mechanical Engineering)

National Laboratory Collaborator:

- Dr. Ning Li, Project Leader, Lead-Bismuth Material Test Loop, LANL

MANAGEMENT PROGRESS

TECHNICAL PROGRESS

HYDRODYNAMICS:

Initial Code Testing:

The STAR-CD computer simulation code was chosen for the purpose of performing the Computational Fluid Dynamics (CFD) calculations for this project. STAR-CD is a commercially available code that is offered by ADAPCO Co. out of New York State. The code is a transient multidimensional simulator for Thermal hydraulics and chemical reactions occurring in the fluid flow itself. The project though required an additional capability in regards to the simulation of surface chemistry reactions such as those expected to take place on the inside of all the surfaces of the LBE loop. To handle these requirement conversations with ADAPCO indicated that the company was in the process of incorporating another code as a subroutine to STAR-CD named CHEMKIN. More will be discussed about this later.

STAR-CD is a general purpose code that solves numerically a set of differential equations that describe the following conservation laws: mass conservation, momentum, energy and chemical species. The following equations are solved by this code:

Continuity Equation:

$$u_{i,i} = 0 \qquad (1)$$

Momentum Equation:

$$\rho_0 [\frac{\partial u_i}{\partial t} + u_i u_{i,j}] = - P_{,i} + [\mu (u_{i,j} + u_{j,i})]_{,j} \qquad (2)$$

Energy Equation:

$$\rho_o C_p (\frac{\partial T}{\partial t} + u_i T_{,i}) = (K * T_{,i})_{,i} + \mu \Phi \qquad (3)$$

Species Transport:

$$\rho (\frac{\partial C_n}{\partial t} + u_i C_{n,i}) = (\rho \alpha_n C_{n,i}) + q_{c_n} + R_n \qquad (4)$$

Due to the Re number estimate for flow in a LBE loop a turbulent flow model should be used as a constitutive model for the momentum transport. It was decided that a κ-ε model is to be used to account for that behavior. The model consists of adding two more non-linear (transport equations) partial differential equations to each unknown nodal location. The κ denoted the turbulent kinetic energy $\overline{u_i u_i}$ and the ε is the viscous dissipation rate of the turbulent kinetic energy $\upsilon \overline{u_{i,j} u_{i,j}}$. The resulting equations are:

k – transport equation:

$$\rho_o\left(\frac{\partial k}{\partial t}+u_i u_{i,j}\right)=\left(\mu_o+\frac{\mu_t}{\sigma_k}k_{,j}\right)_{,j}+\mu_t\Phi+\mu_t g_i\left(\frac{\beta_T}{\sigma_t}T_{,j}\right)-\rho_o\varepsilon \qquad (5)$$

ε – transport equation:

$$\rho_o\left(\frac{\partial \varepsilon}{\partial t}+u_j\varepsilon_j\right)=\left(\mu_o+\frac{\mu_t}{\sigma_k}\right)_{,j}+c_1\frac{\varepsilon}{k}\mu_t\Phi+c_1(1-c_3)\frac{\varepsilon}{k}g_i-\rho_o c_2\frac{\varepsilon^2}{k} \qquad (6)$$

As this is a new code for the researchers some simple numerical benchmarking were performed to give more confidence in the results of the code. Basic velocity tests were initially performed for whose analytical results are known such as determining the fully developed flow in a pipe under laminar conditions as shown in Figure 1.

The inlet conditions in figure 1 are a uniform velocity profile at inlet and constant properties with flow in a circular pipe. The familiar laminar (parabolic) profile is generated after the liquid is allowed to develop a distance long enough inside the tube. Another benchmarking test was to see how the temperature profiles develop using the code.

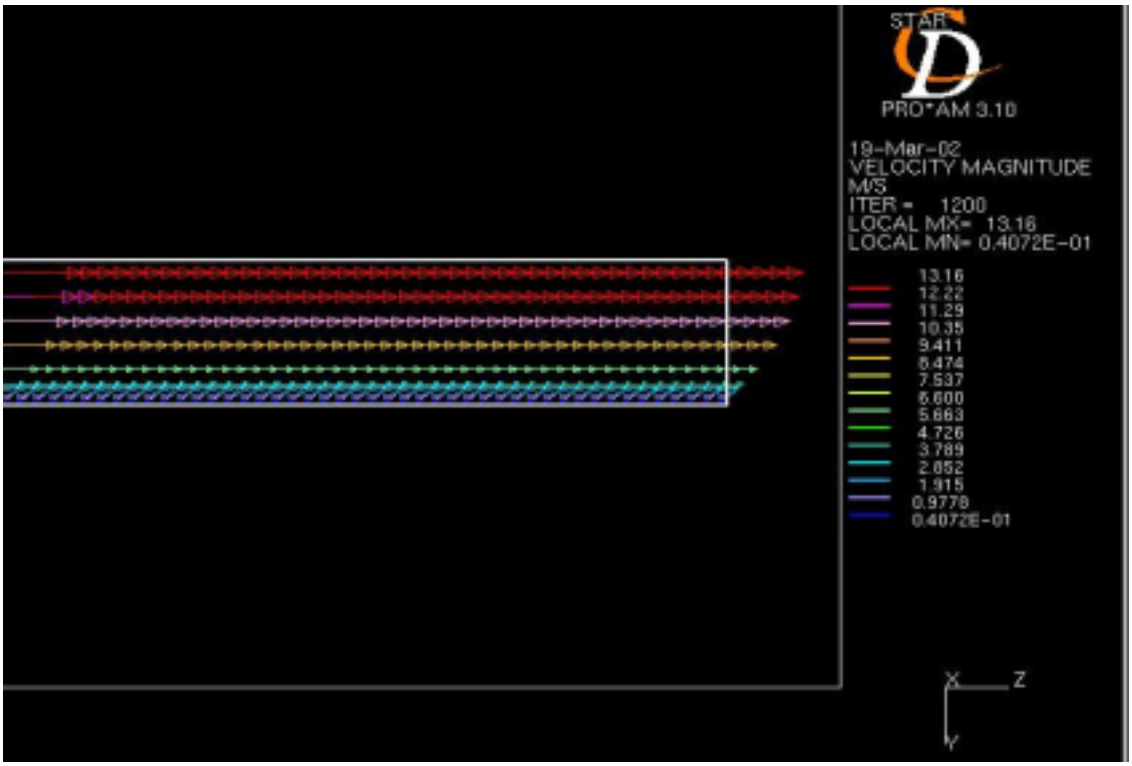

Figure 1: Fully Developed Laminar flow for a Pipe

Figure 2 shows the temperature profile along a diametrical plane along the pipe length. Here the inlet temperature to the pipe is 400K and there is a constant negative heat flow out of the pipe. The reduction in temperature is relatively small because the value of the wall heat flux is not large. Here the purpose is not to try to validate in great detail what those answers are, but rather to see that the physical trends are in the right order. Figure 3 shows the cross-sectional temperature contours across a section normal to the pipe axis.

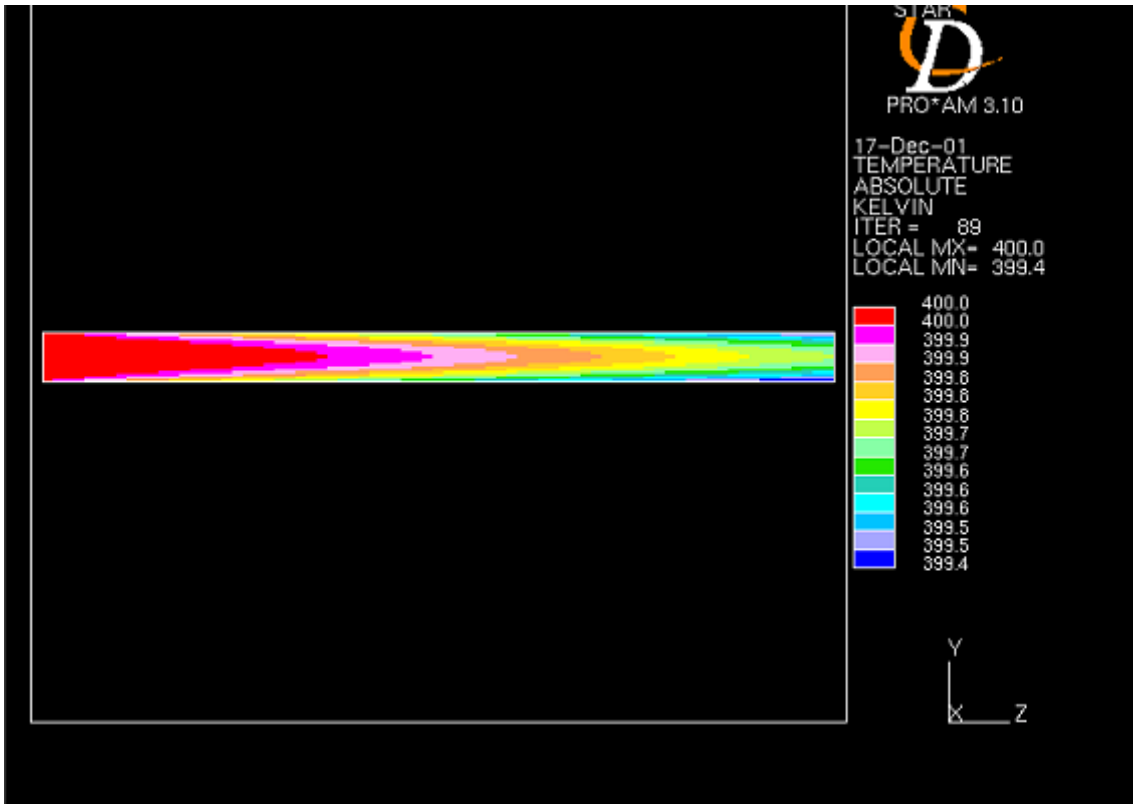

Figure 2: Temperature Profile Axially along a Pipe Flow

Figure 3 shows the expected symmetry in the solution as well as the monotonic increase of temperature from the outer wall strata to the central axis of the pipe.

Figure 4 shows a run of a uniform velocity imposed at the inlet to a pipe and chosen in such a way such as its value will generate a turbulent flow in the pipe. A κ-ε model is invoked in the code to allow the right shear stress and transport properties for a turbulent flow to exist. The relatively flat profile between 0.99 and 0.76 m/s is shown to exist.

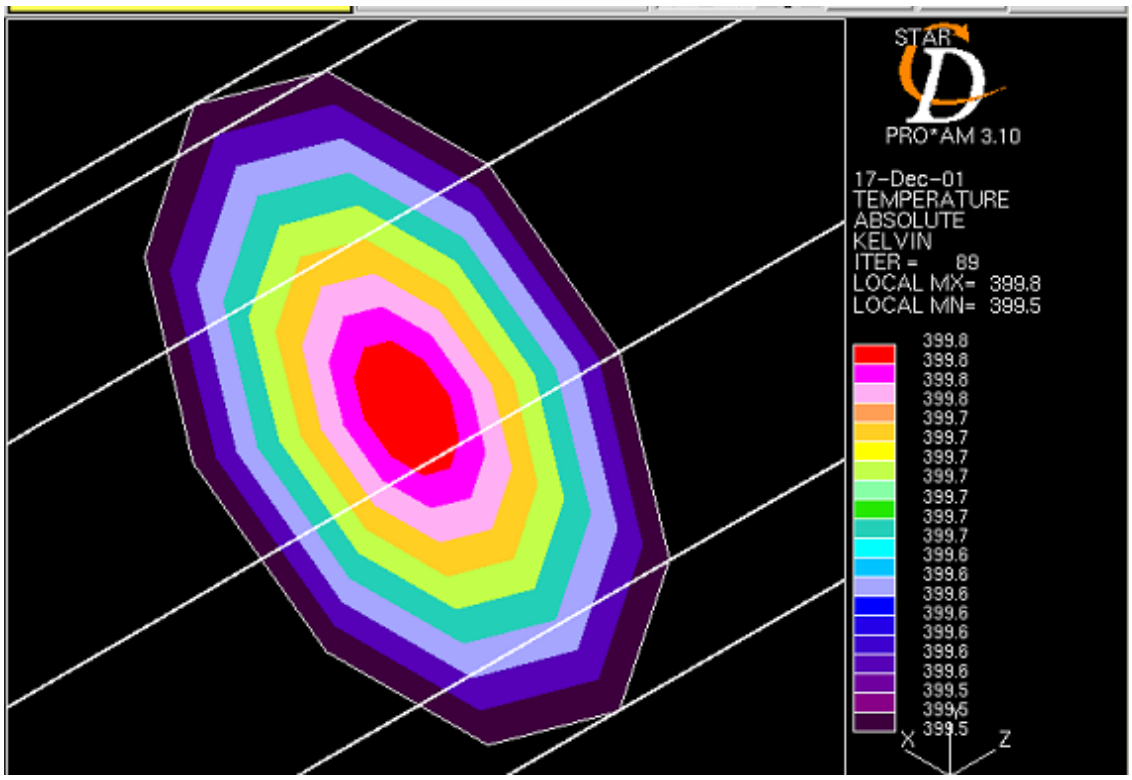

Figure 3: Transverse Temperature Contour Plot for the Previous Case

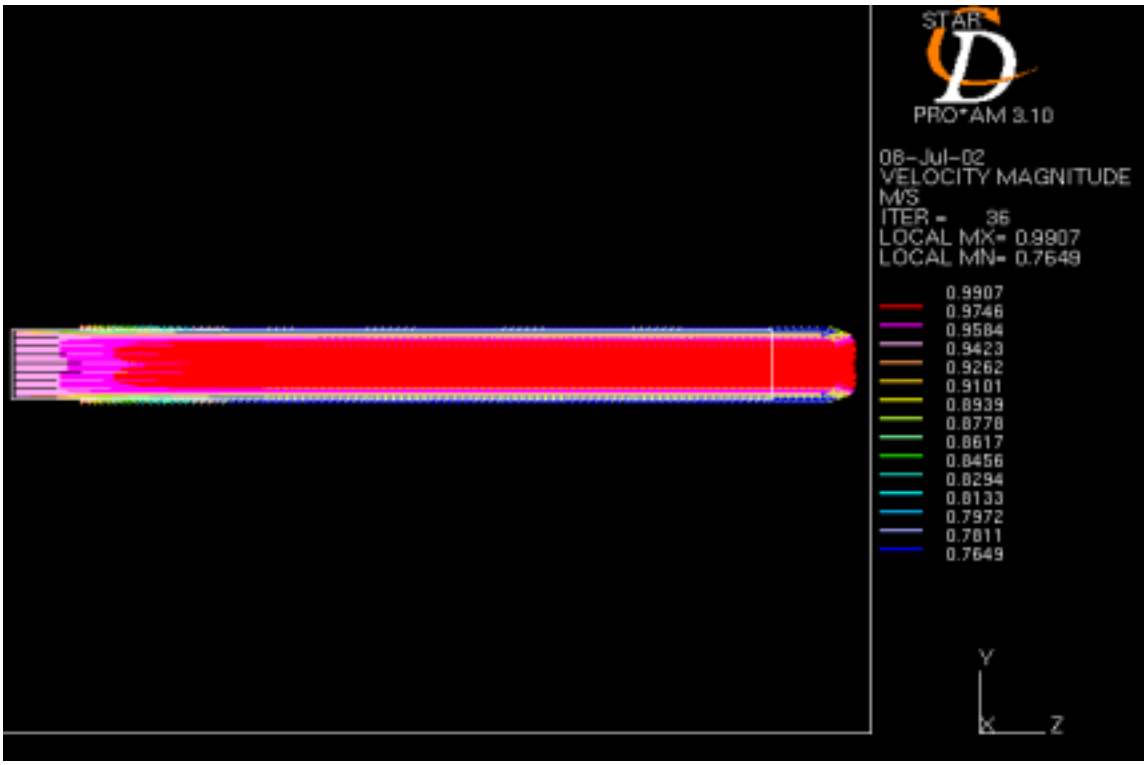

Figure 4: Transverse Velocity Profile in a Turbulent Pipe Flow

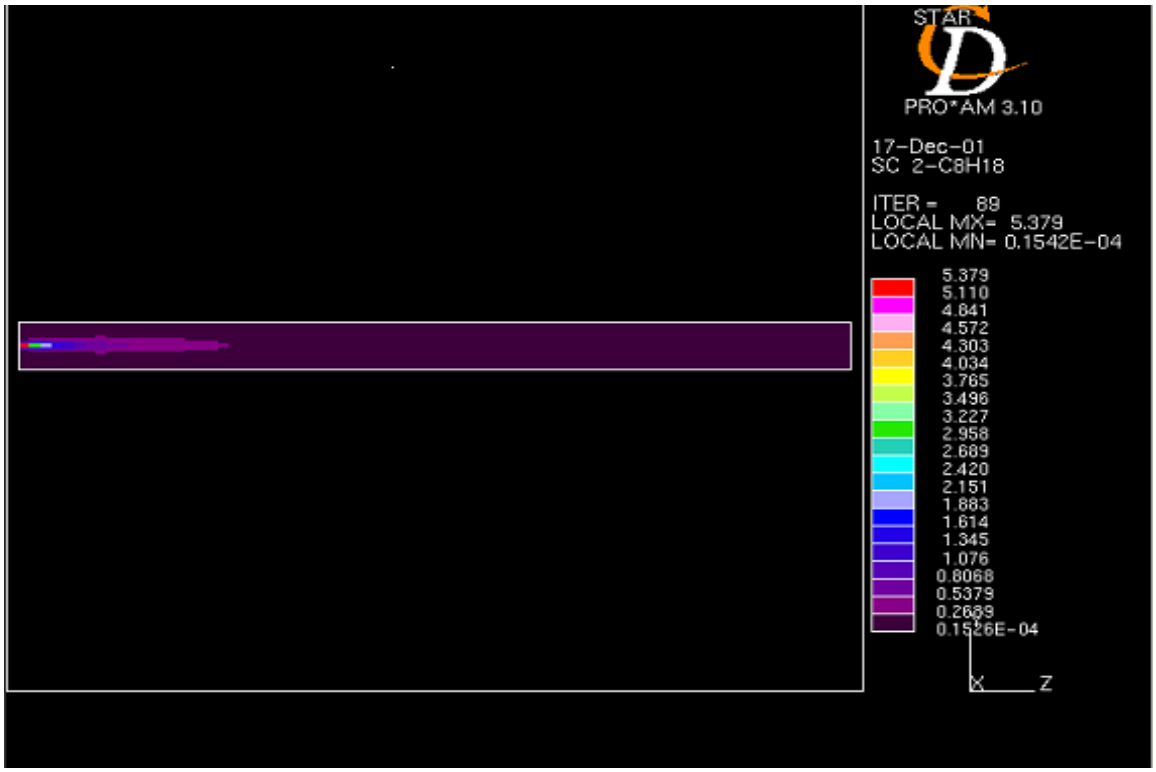

Figure 5: Plot of Axial and Diametrical Distribution of a Species in the Flow

Figure 5 shows the result of a test run to see how the species portion of the STAR-CD program work. We know that the code has the capability of predicting species transport phenomena when two or more fluid components are allowed to react. Provided the user chooses the right thermodynamic information for these reactions is chosen. As a simple test the flow of a chemical C_8H_{18} introduced into the flow from the central cell located at the axis of the pipe. A

turbulent flow condition was invoked as far as flow conditions and the concentration of this specie was tracked down the pipe. The figure shows clearly a small area of high concentration (red region) very close to the inlet and then followed by various decreasing values of the concentration until a few diameters away from the inlet one notices complete mixing between the specie and the base fluid flowing in the pipe. This is typical of what is expected in a turbulent flow i.e. rapid downstream mixing.

For testing the chemical analysis of STAR-CD, a simple model involving catalytic surface chemistry has been chosen and the results analyzed. A flow over a flat plate has been considered as the test model. A section of the plate has been chosen with dimensions of 2mm x 100mm for the analysis. Air along with propane is allowed to flow over a Vanadium plate. The fluids at a temperature of 600K are allowed to flow over the plate with temperature at 1290K. The mesh has been refined at the wall surface for clear depiction of the surface reactions. The propane gas disassociates by reacting with air at high temperatures. The fluids are allowed to flow at a velocity of 5m/s in the turbulent regime. The initial concentrations of the species of the gases are given below.

C_3H_8 ---------- 0.01746
O_2 ---------- 0.23922
N_2 ---------- 0.74332

The above values are specified in terms of weight percent.

Figure 6 describes the final concentration of the oxygen and shows that it decreases to 0.2240 weight percent at the outlet from an initial concentration of 0.2392 due to its partial consumption with the oxygen reaction. Figure 6 shows a closer view of the variation of oxygen concentration the oxygen velocity variation of the fluids along the surface of the flat plate. Figure 7 shows the variation of velocity magnitudes where these values vary from 5m/s at the inlet to 13m/s at the outlet. This is a realistic expectation of the flow and reaction conditions where the propane is reacting with the oxygen and generating more molar species which will increase the volumetric flow at each cross-section to preserve mass conservation at each cross-section since this is a steady flow steady state situation. The variations of the temperature along the flow direction of the plate are shown in Figure 8.

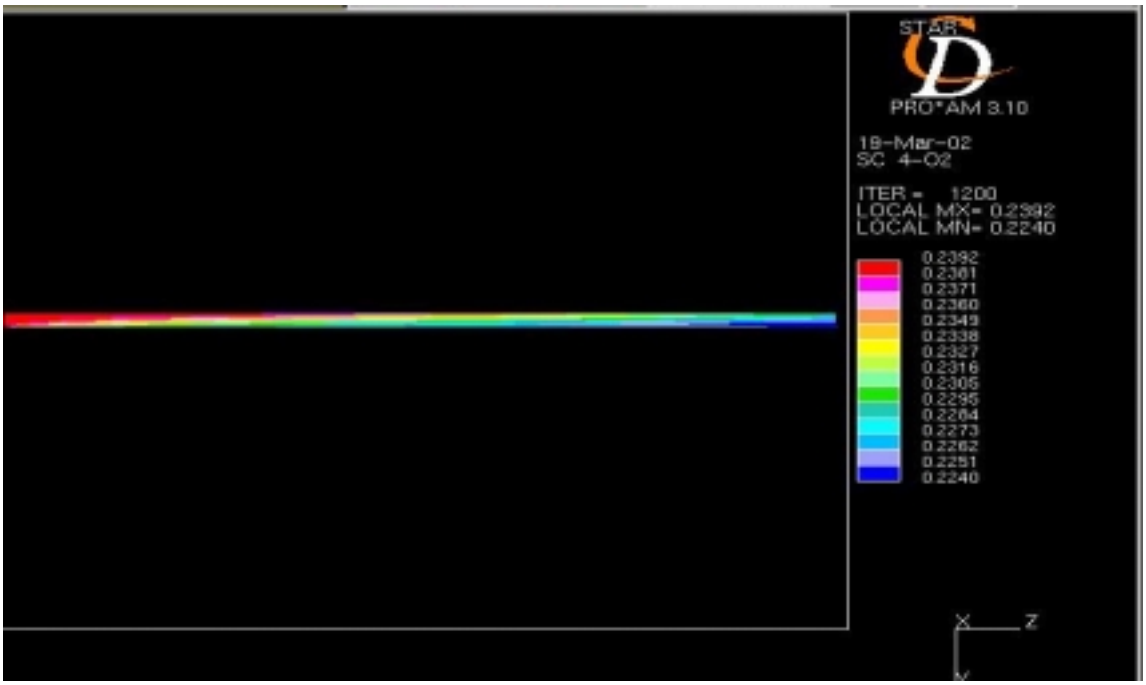

Figure 6: Oxygen Concentration along Plate Length

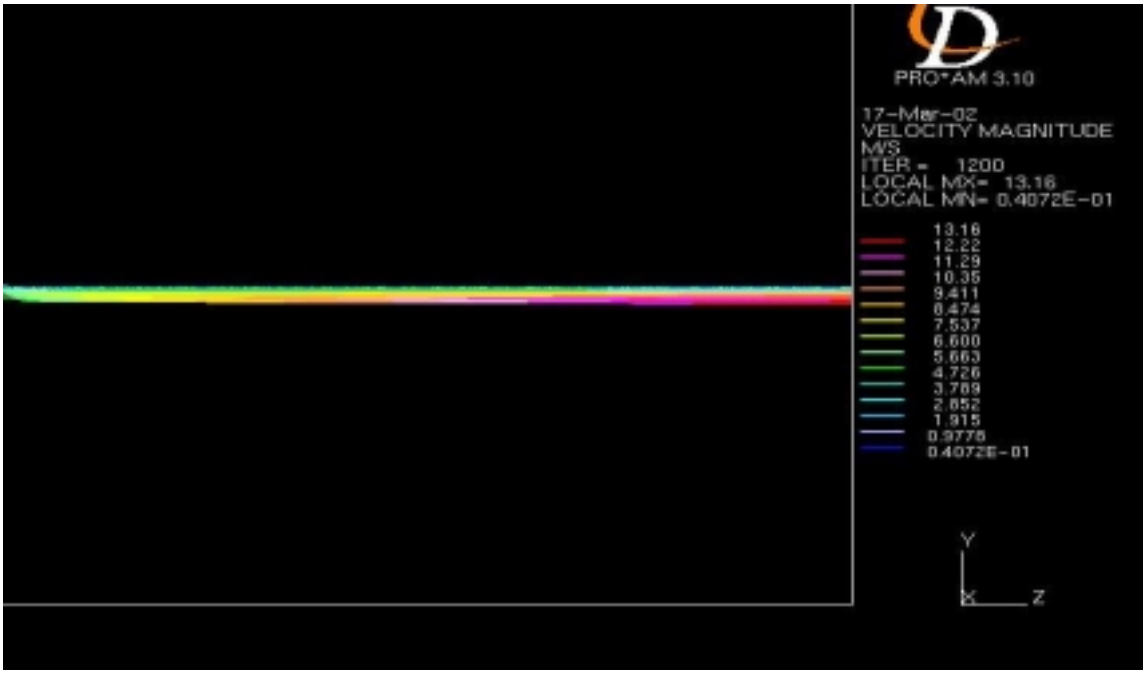

Figure 7: Velocity Profiles along the Plate Length in the Direction of Flow

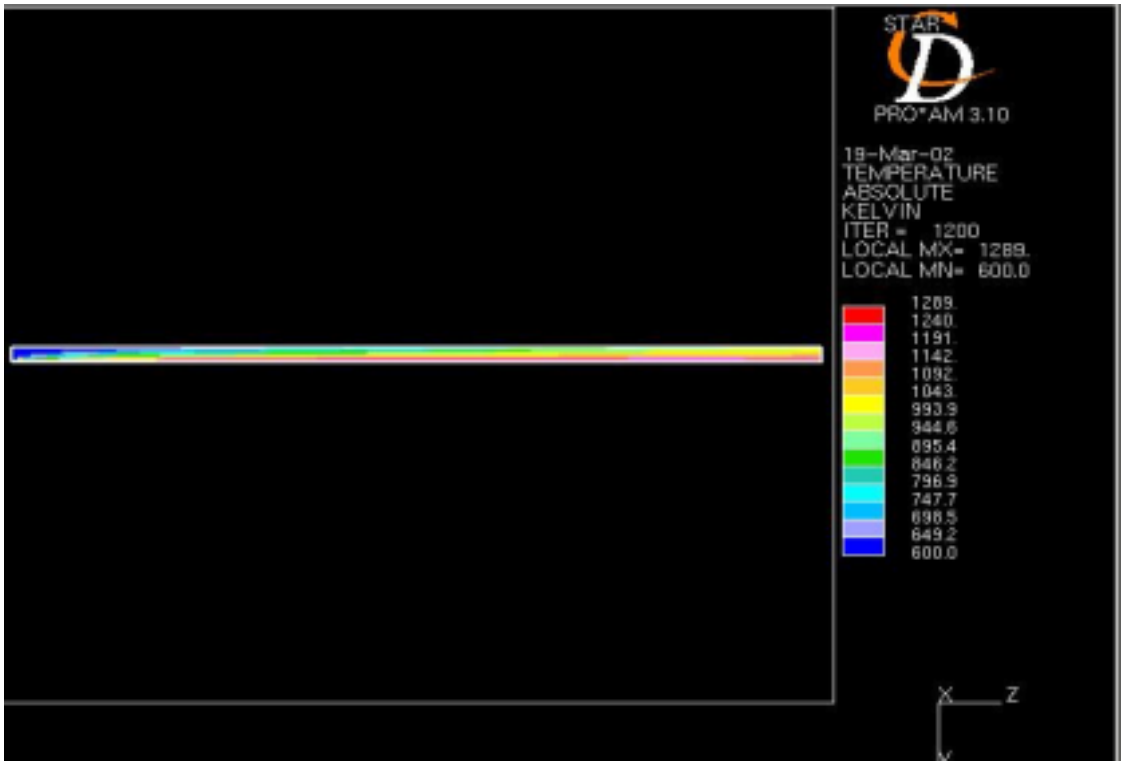

Figure 8: Temperature Profile along Plate for Particular Flow

In Figure 8 the flow temperature is shown to start at the lowest temperature possible and as the reaction continues to proceed to the right the temperature increases monotonically. Here it is seen that the temperature is not uniform across the flow direction because the density of the different reactants is probably coming into play and maybe contributing to the uneven distributions due to non homogeneous mixing in the flow. But the trend is certainly there as far as an expected exothermic reaction is concerned.

Since Lead is going to be one of the constituents of the flow inside the loop, another test of the reaction of Pb (lead) with oxygen in the core flow was simulated. It considered Pb in the

fluid state just to see how PbO (lead oxide) is represented as a concentration along the pipe flow. Figure 9 shows again the familiar decrease of oxygen concentration along the pipe axis.

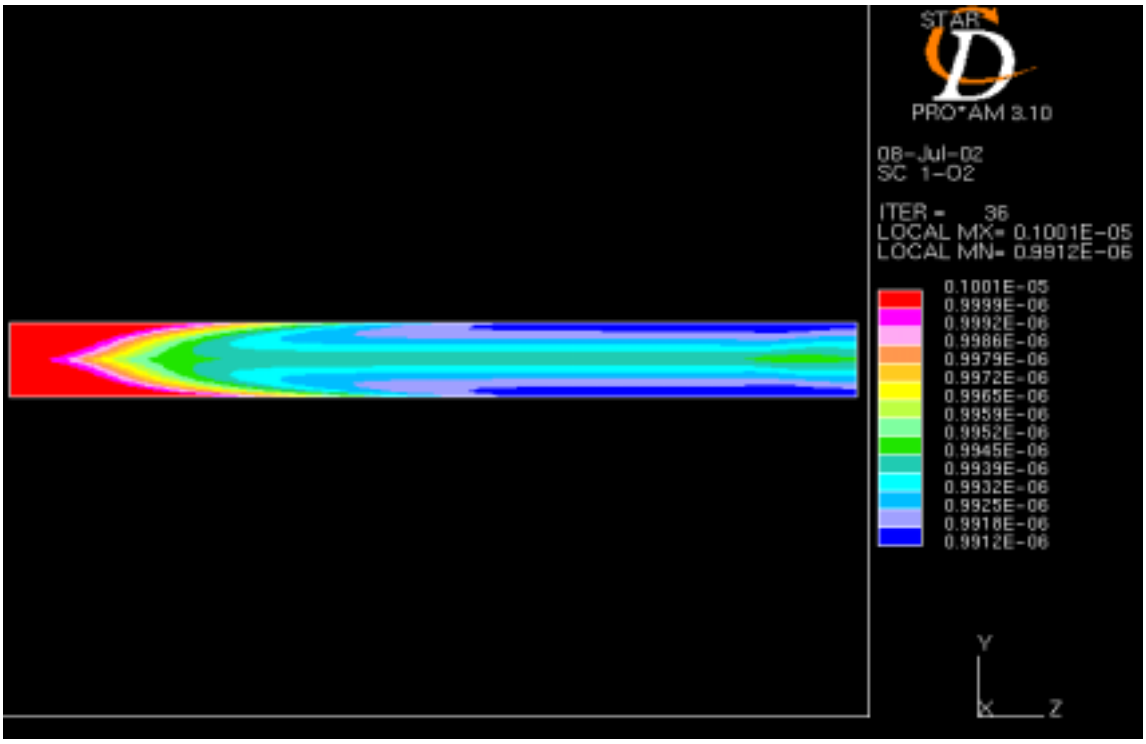

Figure 9: Profile of Oxygen Concentration along the Pipe Axis

Figure 10 shows the plot of lead oxide (PbO) profile axially due to the reaction of its components. It shows that as expected here again the PbO starts off with an extremely small concentration and then it is shown several orders of magnitude as it moves down the pipe. However some interesting transverse distributions are shown across the pipe which may indicates higher concentrations of the products near to the walls. One can theorize that due to the fact that the reactants move more slowly near to the wall regions that the expectation of higher product concentrations can be expected. At this point no experimental data is available to compare with.

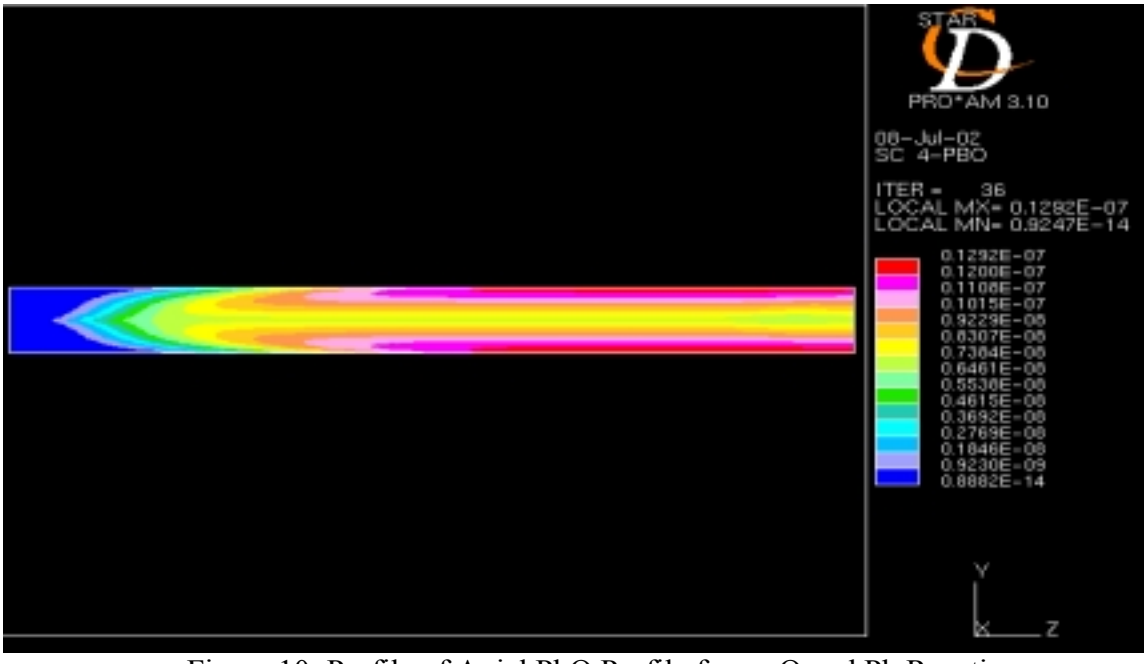

Figure 10: Profile of Axial PbO Profile for an O and Pb Reaction

CHEMICAL KINETICS OF CORROSIONS:

Corrosion is one of the major concerns with using of LBE loops. Liquid metal corrosion can proceed via various processes: dissolution, formation of inter-metallic compounds at the interface, penetration of liquid metal along grain boundaries, which depend on experimental factors such as: temperature, thermal gradients, solid and liquid compositions, velocity of the liquid metal. Research indicates that the corrosion rate of martens tic steels, at 475^0C (hot leg temperature) and for a temperature gradient of 60^0C (cold leg temperature is 415^0C), increases from 21 to 93 μm per year when the alloy of lead-lithium velocity increases from 0.019 to 0.18 meter per second. In the MTL, velocity of liquid lead-bismuth could reach values up from 3 to 5 meters per second in the spallation module.

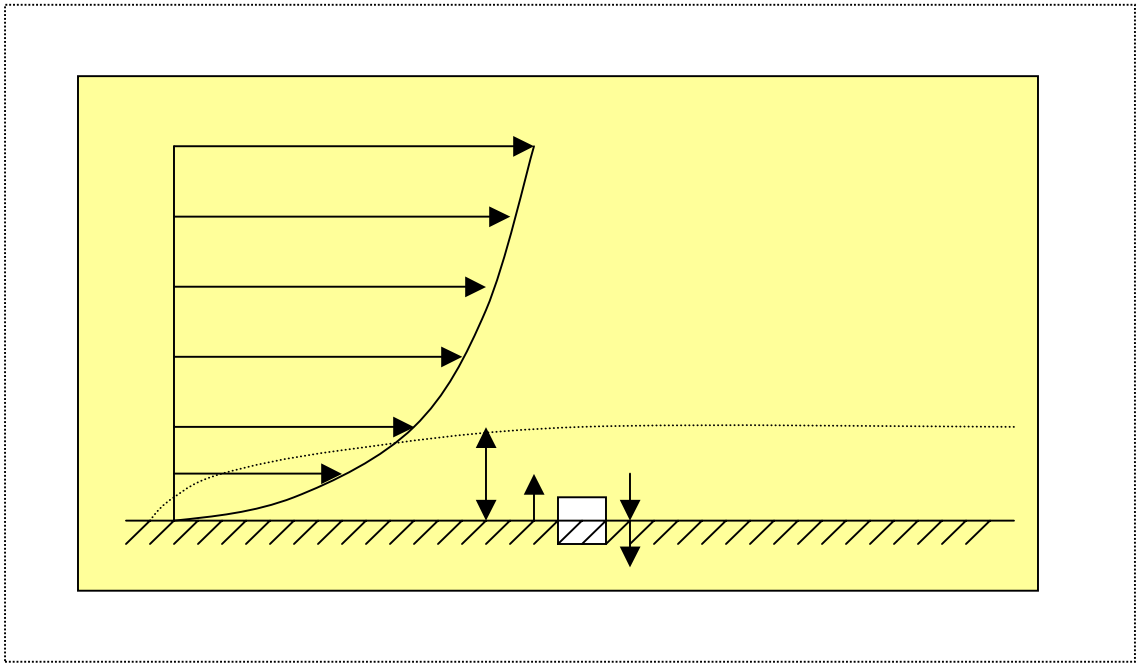

Figure 11: Diffusion Process through the Hydrodynamic Boundary Layer

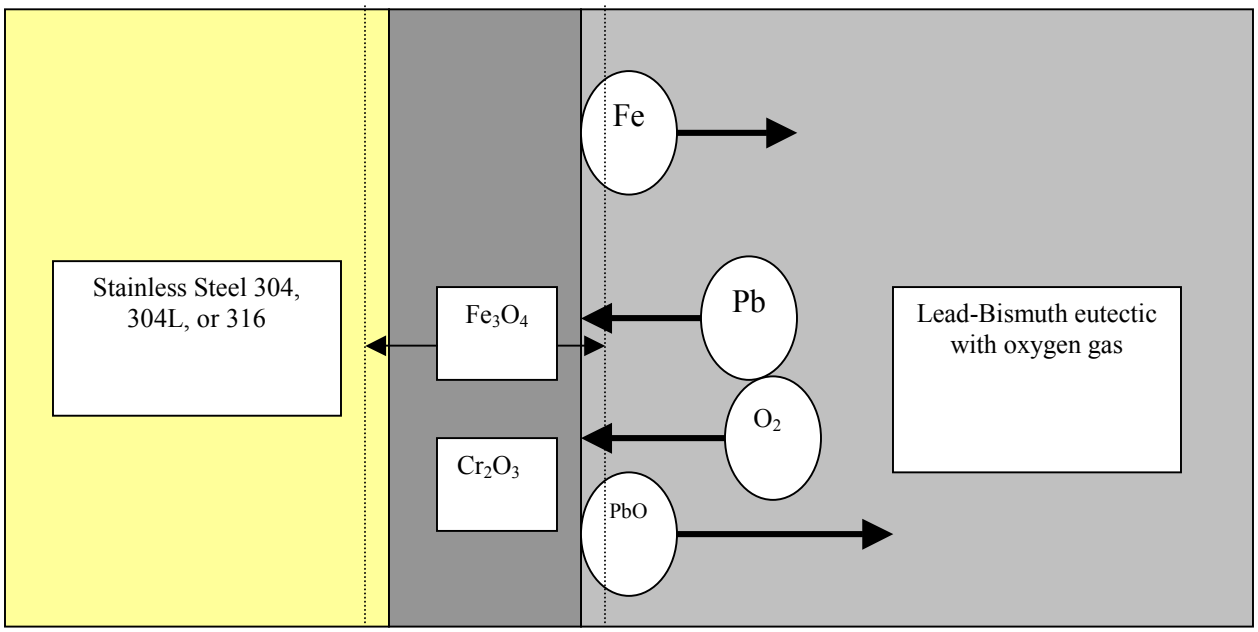

Figure 12: Schematics of Corrosion Processes between the Metal Surface and the Liquid Metal

The transport of oxygen and corrosion products, their interaction and variation of corrosion/precipitation along the flow are not well understood. An experimental study monitored corrosion history of specimens in one test loop over several thousand hours and showed that corrosion would occur at higher temperatures i.e. 550 ^{0}C but precipitation occurs around 460 ^{0}C, which is at the intermediate temperature. This confirms that the temperature distribution in an LBE system is important for understanding the system corrosion performance.

DEVELOPMENT OF MULTIDIMENSIONAL MODEL USING STAR-CD

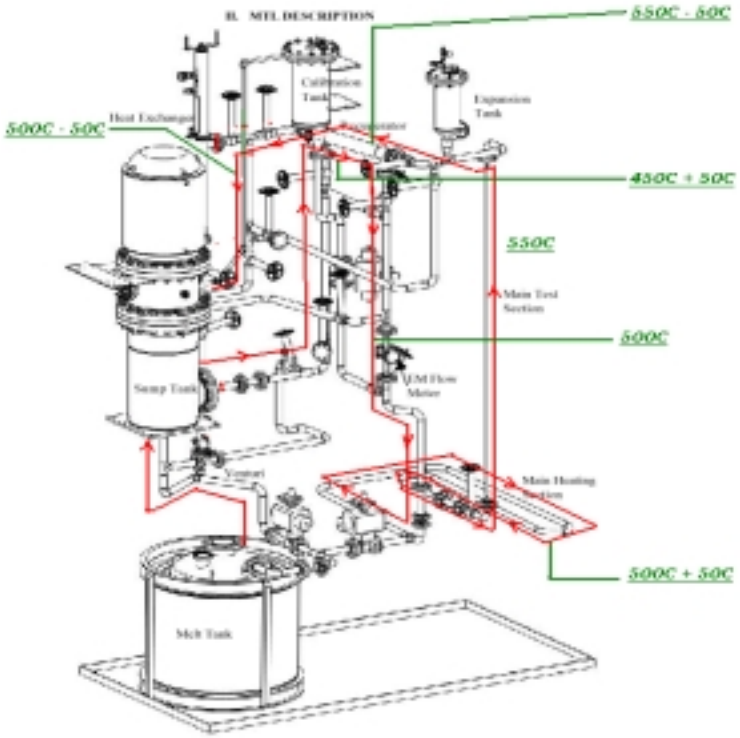

Fig-13: Materials Test Loop

Figure 13 shows the Materials Test loop with all the temperatures plotted along the flow paths. The task is to simulate and analyze the flow in a loop which has similar temperature variations in the MTL. The temperature distribution in the MTL is better shown in the picture below for a unit loop length. [1]

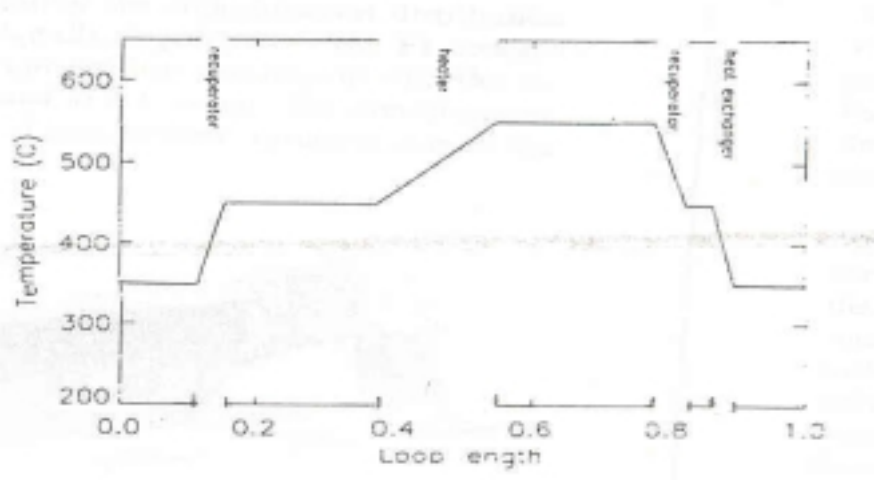

Fig- 14: Temperature Distribution in the LANL Materials Testing Loop. The Distance is scaled with the Total Loop Length.

The wall concentration is a function of the temperature given by the empirical formula:

$$C_{Fe} = C_0^{-4/3} * 10^{(11.35-(12844/T))} \text{ ------- (7)}$$

C_{Fe} – is the concentration of iron on the wall surface
C_0 – is the known concentration of oxygen in the flow.
T – is the wall temperature.
The approach followed here to achieve this task is described below.

MESH GENERATION AND DESCRIPTION:

The total loop length is estimated to be 30m (communications with LANL). Since, there is no option of creating a closed loop using STAR-CD (pumps are not allowed as part of the input), the loop length is divided into two U-sections of 15m each. The two sections are created as two different models and the output of one model is fed as an input for the second model. The output from the second model is again fed as an input for the first model and the procedure continues till a convergence is obtained. Figure 15 explains the simulated loop structure.

Fig-15: Schematic Diagram Showing the Loop Structure Adapted.

Two U-section numerical models of 15m and 5cm radius each have been created. The inlet velocity is given as 2m/s. A k-ε model has been considered. Lead-Bismuth Eutectic (LBE) of constant properties is allowed to flow through the geometry. The temperatures are interpolated from the fig.14 and applied to the inside surface of the walls accordingly. The temperatures on the walls vary from 350C to 550C. The concentration of oxygen is taken as 0.01ppm for the analysis purpose. The concentrations imposed on the walls vary from 0.5588E-07ppm to 0.2239E-01ppm (eq. 7) the lowest concentration corresponding to the lowest temperature region.

Figures 16&17 show the geometries created for the purpose of the flow analysis. The two shorter legs are 5m each in length and the middle section is 10m long in both the geometries. The mesh is created with 85500 cells each. In the radial direction, 5cm is divided in 15 equal grids. Theta direction is divided into 10 equal grid spacing. In the transverse direction, each meter is divided into 90 equally spaced grids.

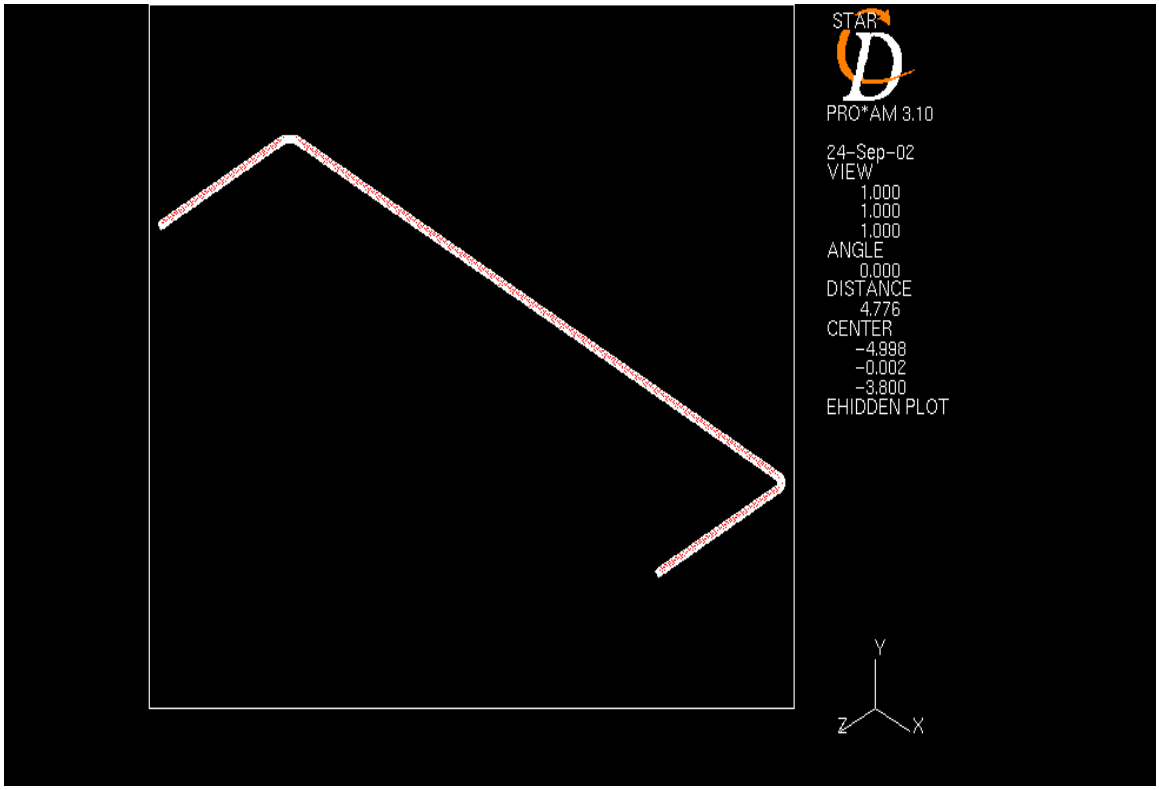

Fig-16: First Half of the Loop (referred to as loop 1).

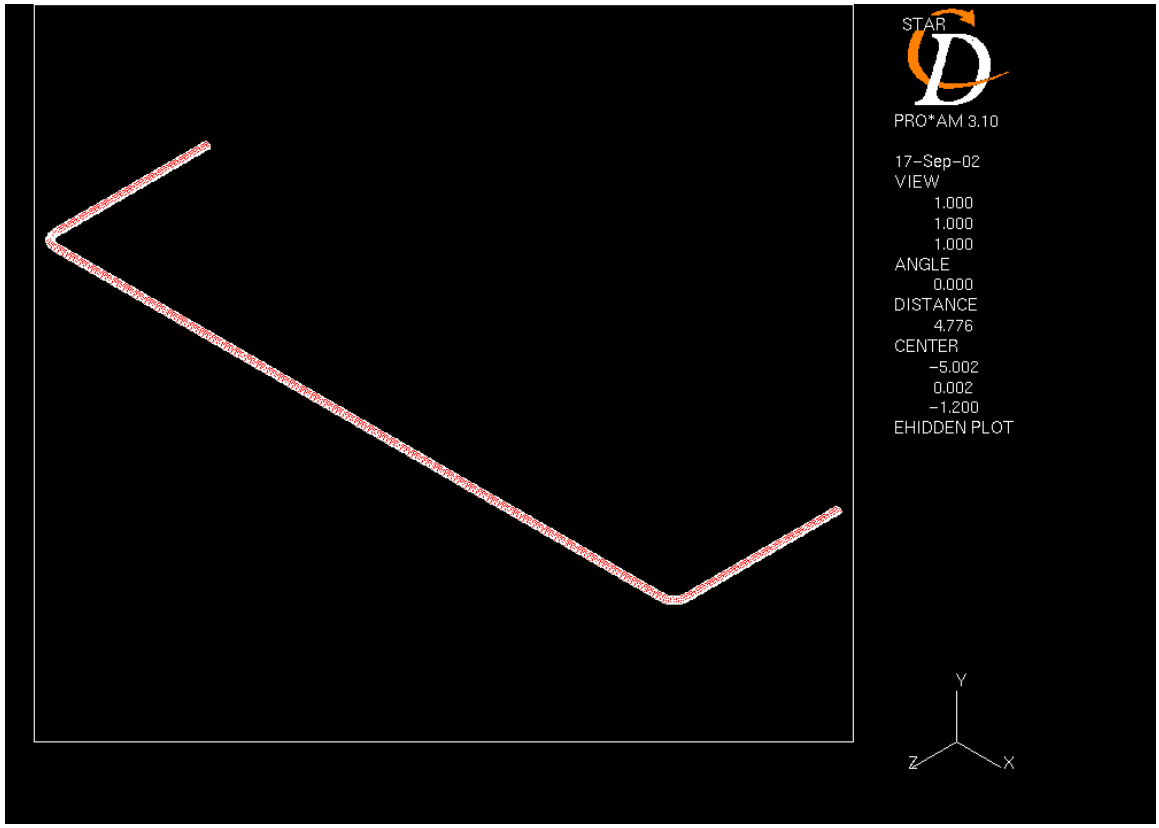

Fig-17: Second Half of the Loop (referred to as loop 2).

For ease of reference, the first half of the loop is referred to as loop1 and the second half of the loop as loop 2 in the entire discussion.

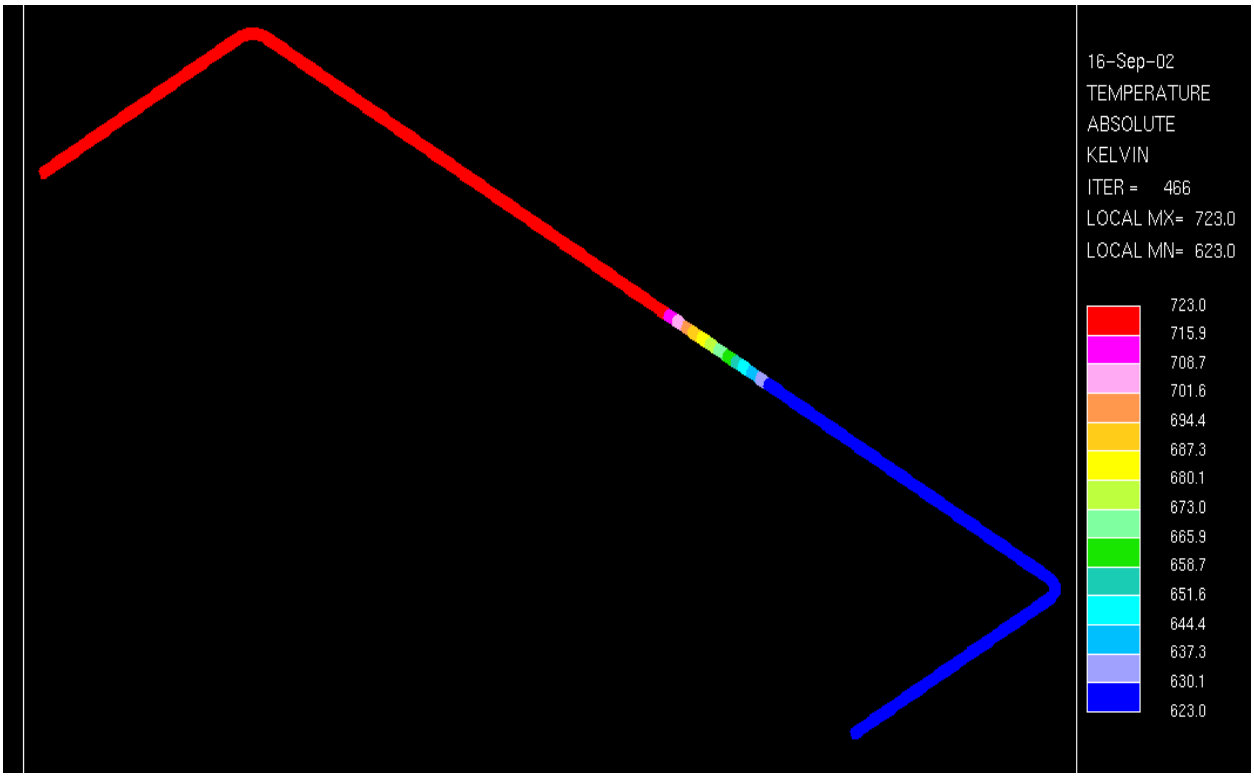

Fig-18: Imposed Wall Temperatures for Loop1

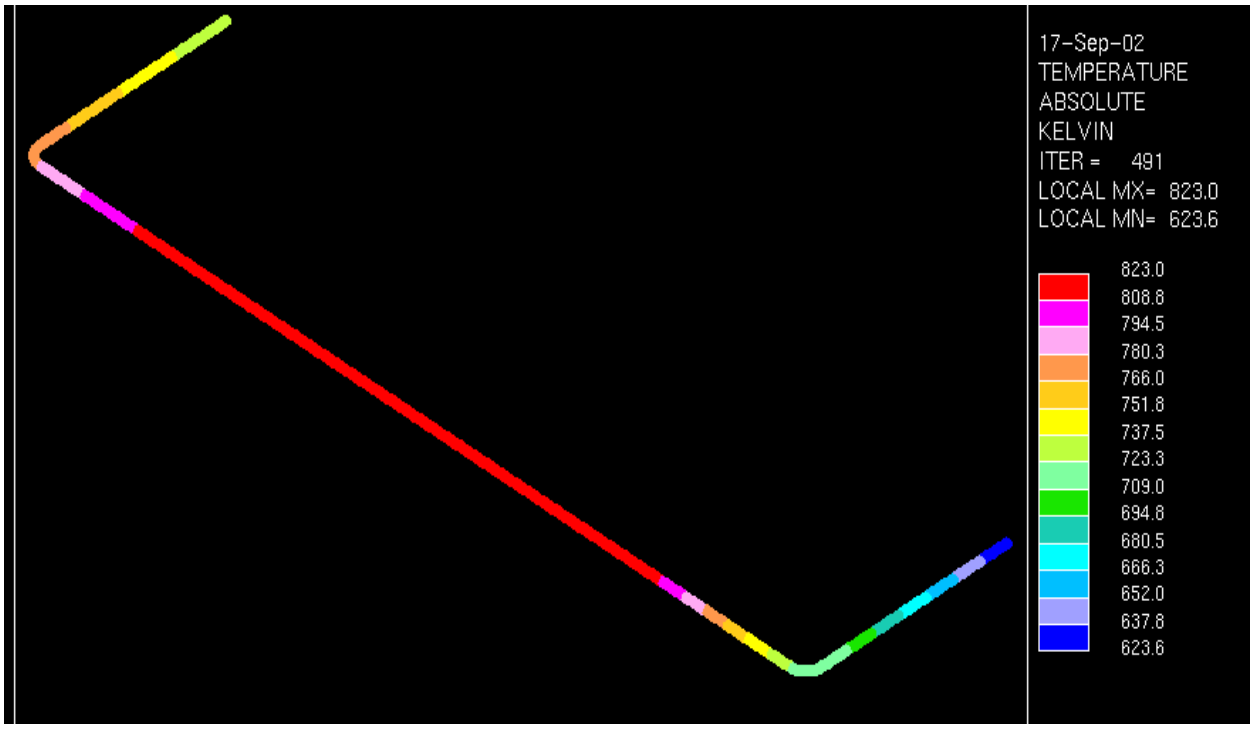

Fig-19: Imposed Wall Temperatures for Loop 2

The temperatures imposed on the walls as boundary conditions are shown in figures 18 & 19. Care is taken that the end temperature for loop 1 is same as the starting temperature for loop 2 and vice versa to satisfy the closure conditions of the total loop. Different temperature zones are shown in different colors.

Figures 20 & 21 show the fixed wall concentrations imposed on the walls of the loops. The concentrations are calculated by the program using equation (7). Again, it can be observed

here that the end boundary conditions of all variables for loop one are the same as the inlet boundary conditions for loop two.

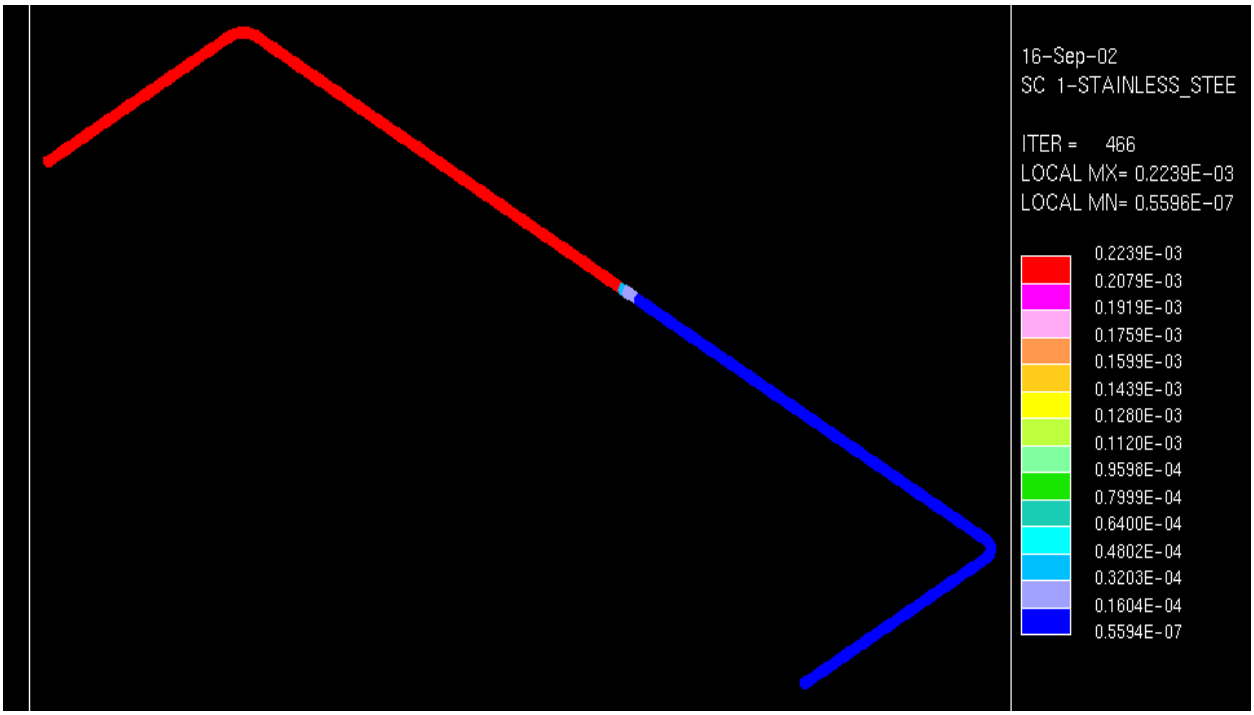

Fig-20: Imposed Wall Concentrations for Loop1

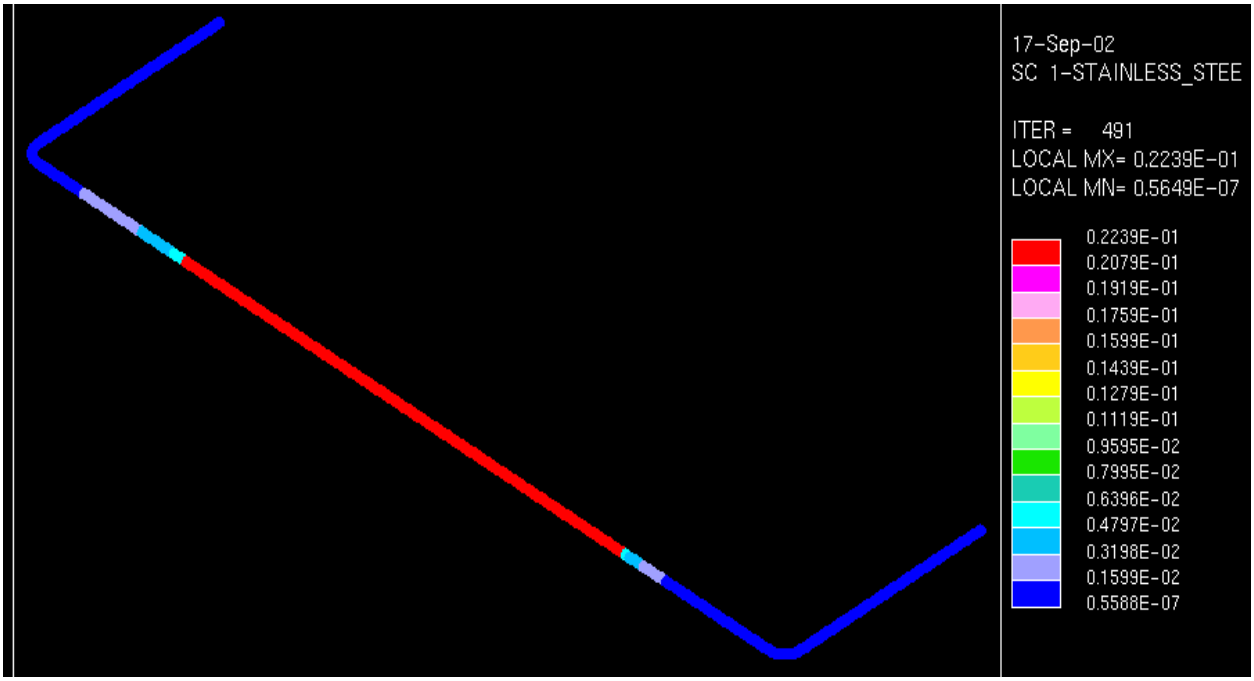

Fig-21: Imposed Wall Concentrations for Loop 2

RESULTS AND ANALYSIS OF THIS MODEL:

I) DISCUSSION ON THE RESULTS FROM LOOP1:

1. **Velocity and Pressure Distribution:**

The next few figures show the velocity profiles in the loop 1. These results shown are obtained after running the case for a few times by feeding the data from one loop to another.

Figures 22 & 23 show the velocity at the first and second elbow sections of the loop1. The profiles look very reasonable and are close to what are expected i.e. higher velocities on the inner radius than the outer one due to secondary flows developing in the elbow. The velocities shown are along a plane of loop1 passing through the central loop axis

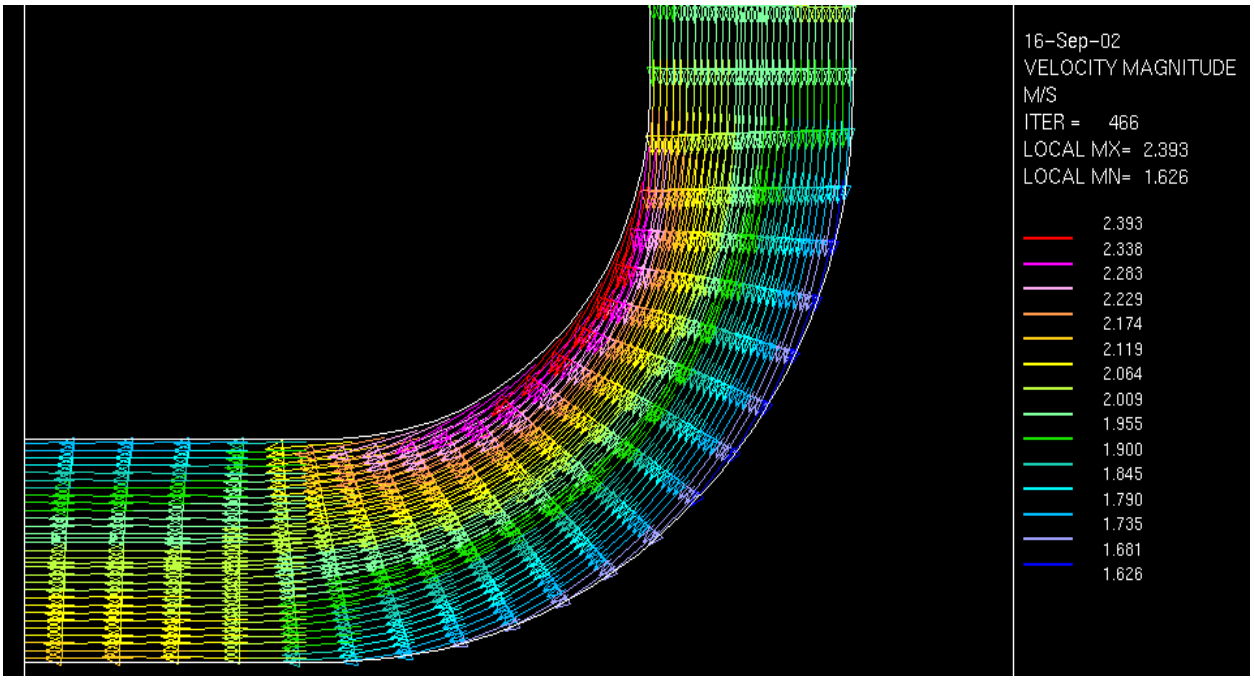

Fig-22: Velocity Profile at the First Elbow Section

Figure 24 depicts the velocity at the outlet of the loop1. Since a k-ε turbulent model has been applied, the velocity at the outlet is fairly flat. It can also be seen from the figure that the velocity at the inner edge is slightly lower than the velocity at the outer edge at the outlet. This trend is due to the developing nature of the fluid flow through the elbow section before coming out of the loop1. The velocities in the flow vary from 1.6m/s to 2.4m/s.

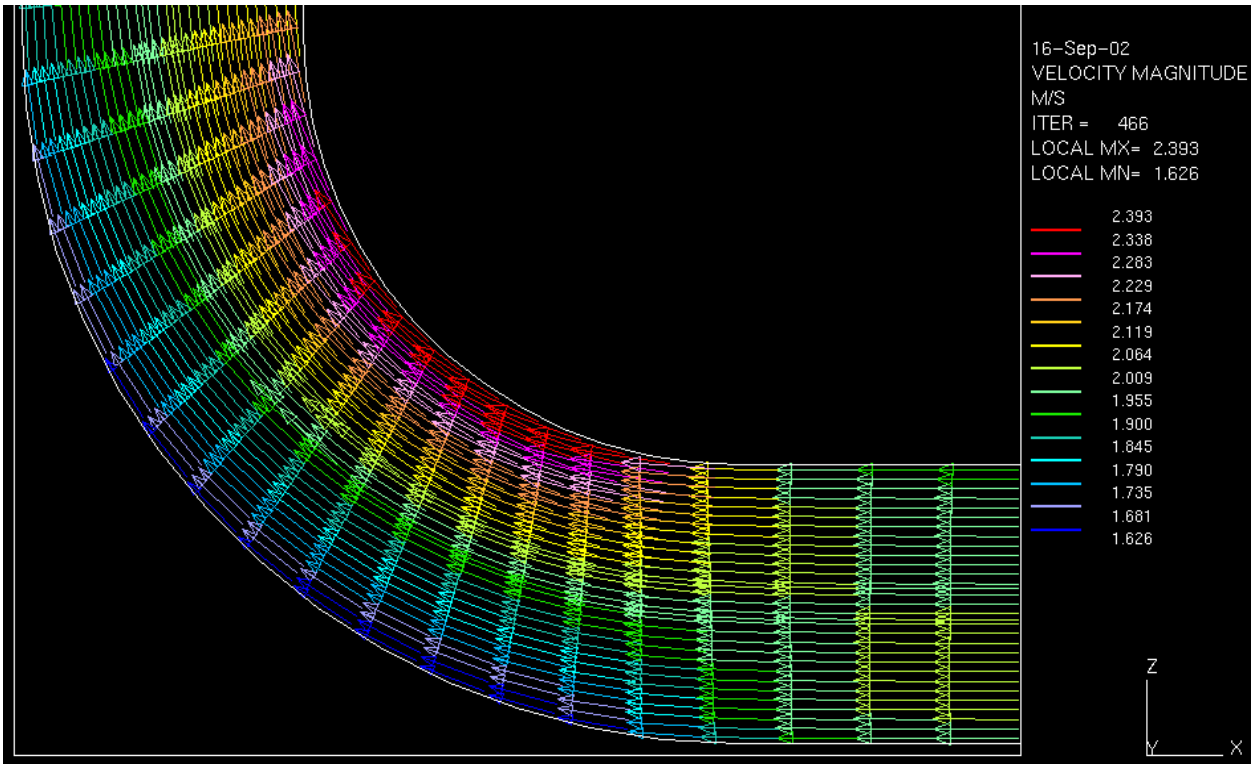

Fig-23: Velocity Profile at the Second Elbow Section

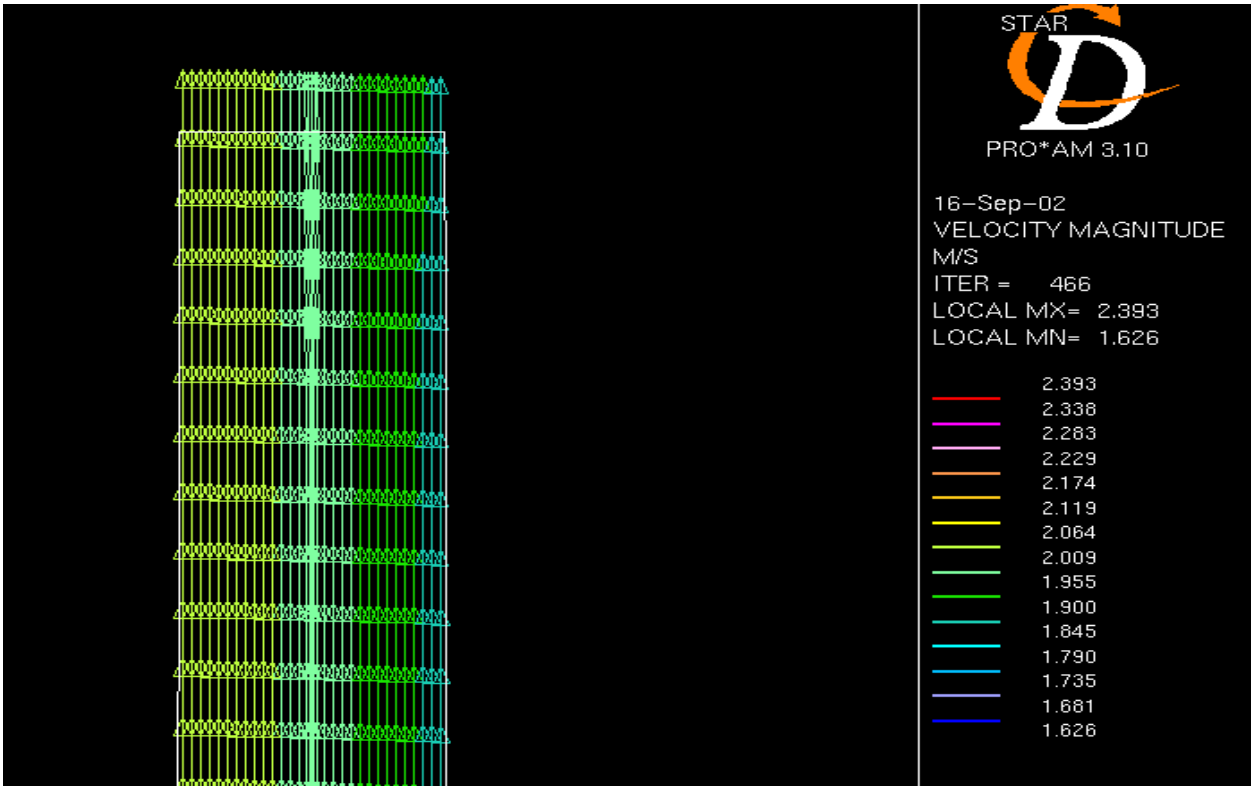

Fig-24: Velocity Profile at the Outlet

Figures 25, 26&27 show the velocity profiles in the three coordinate directions X, Y and Z respectively. This demonstrates the capability of STAR-CD to do three dimensional flow calculations and depicting the resulting secondary flows. These figures portray the velocity magnitudes in the u, v and w components respectively.

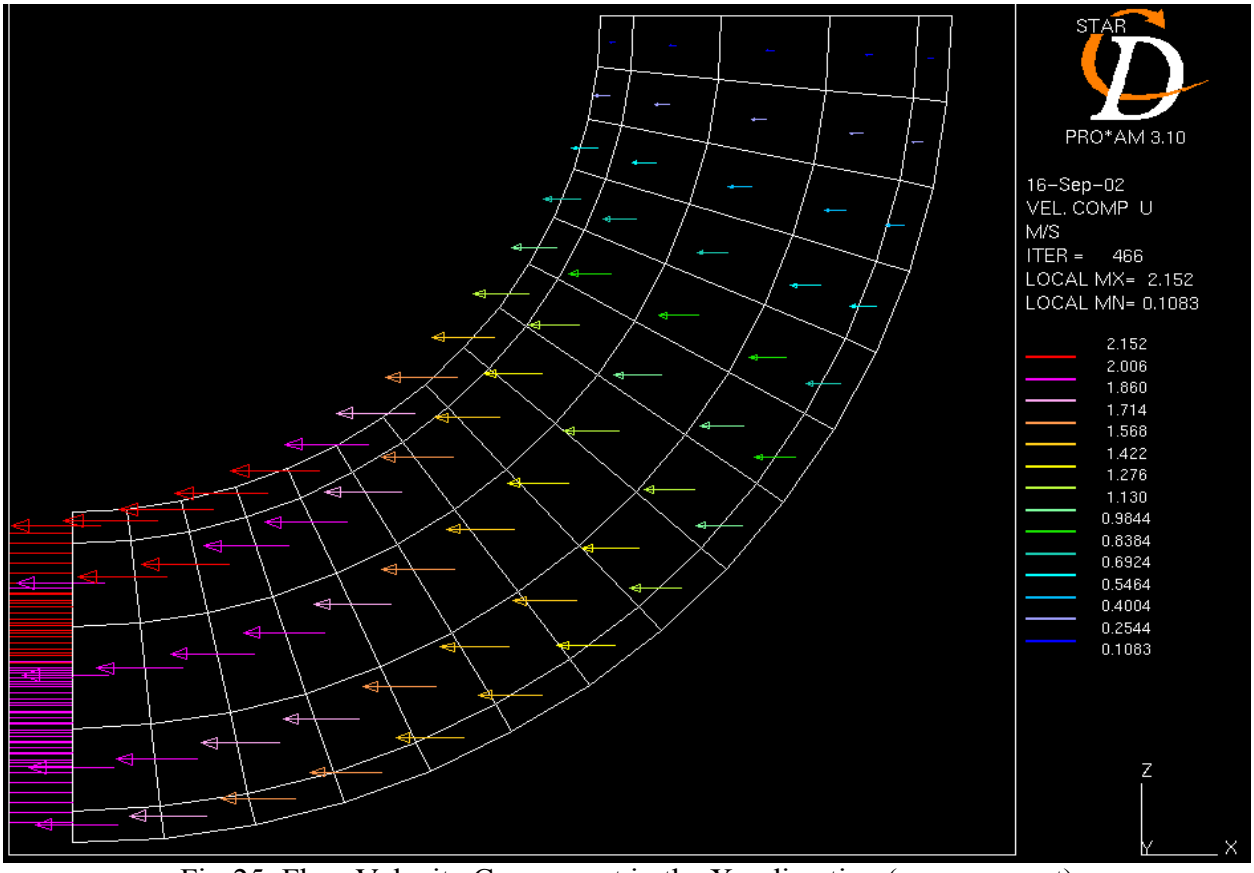

Fig-25: Flow Velocity Component in the X – direction (u component)

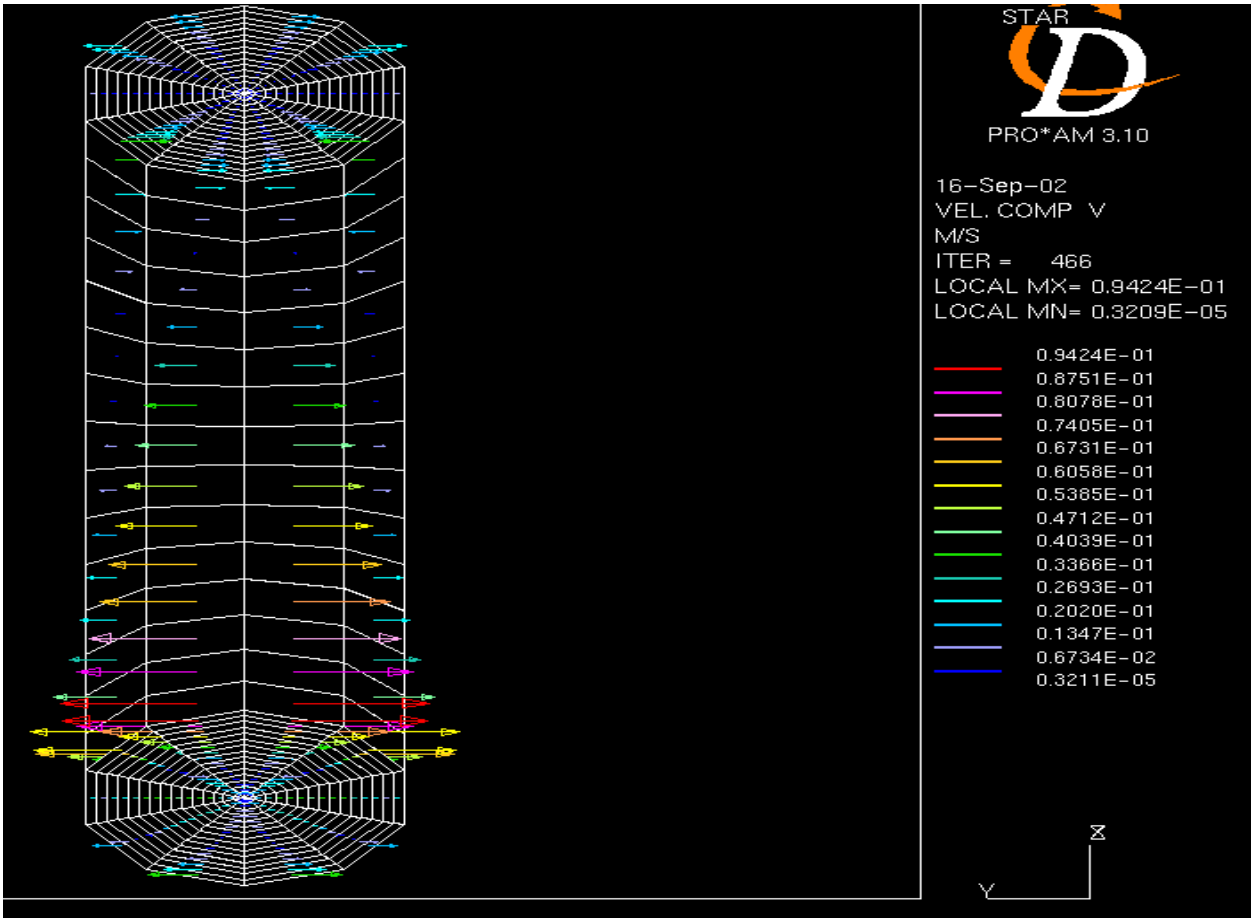

Fig-26: Flow Velocity component in the Y – direction (v component)

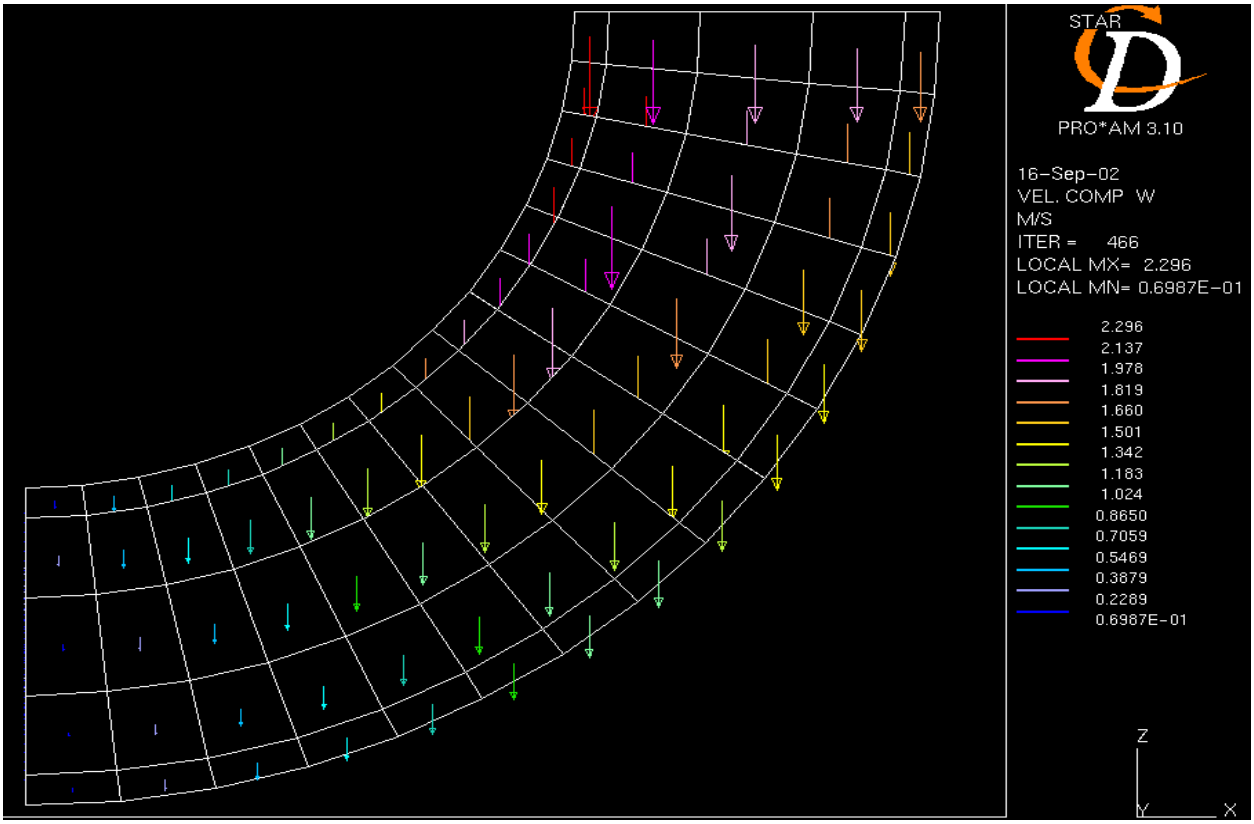

Fig-27: Flow Velocity Component in the Z – direction (w component)

Figure 28 shows the pressure distribution at the first elbow section of the loop1. It can be observed that the pressure at the outer edge of the elbow is more than at the inner edge resulting

in high velocity flows at the inner edge due to more favorable pressure gradients. Absolute pressure is in Pascal.

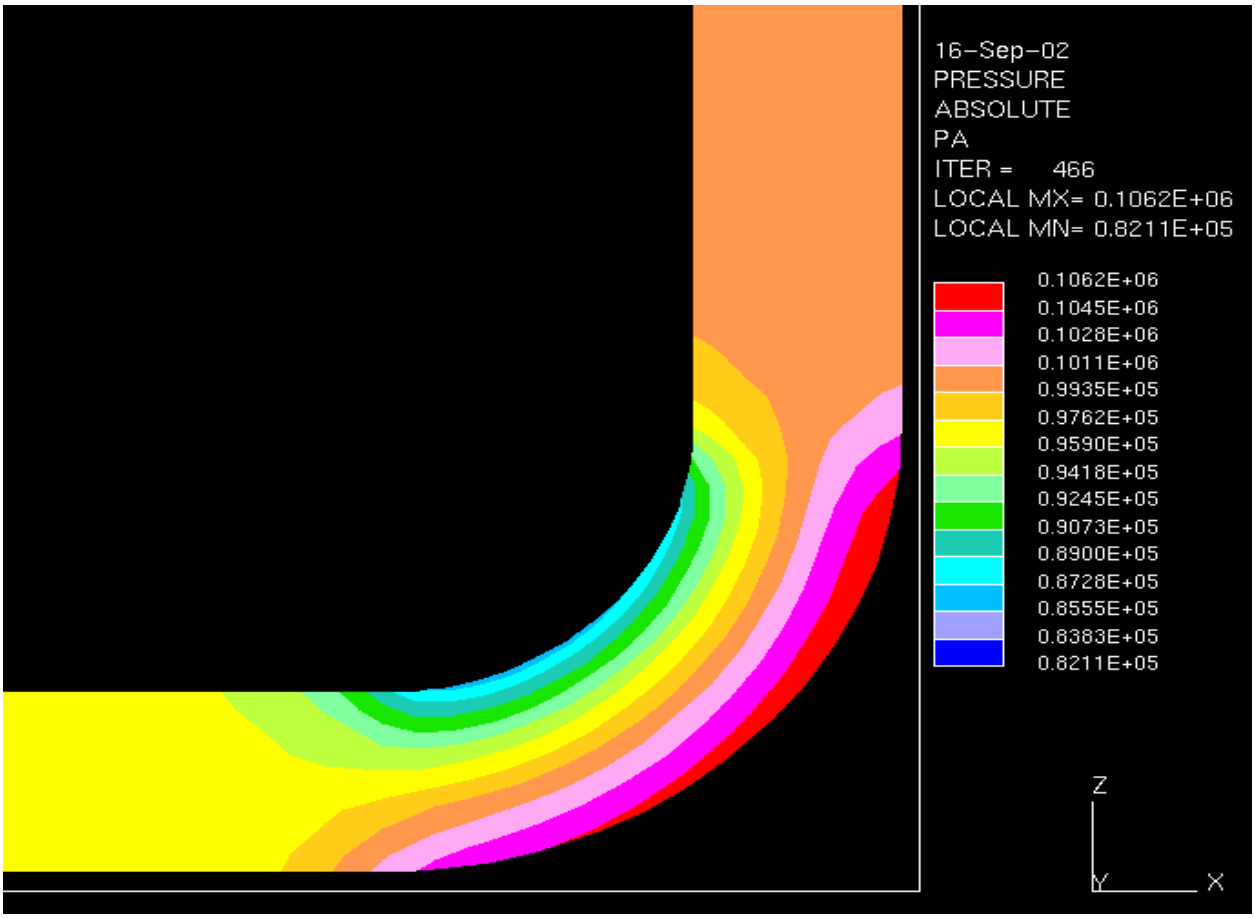

Fig -28: Pressure Distribution at the First Elbow Section.

Pressures at the second elbow section look similar to the above figure and hence have not been included in the discussion. Away from these two regions, the pressure remains almost uniform in the remaining regions of the flow and hence not shown here. This is due to the degree of resolution of pressure contour colors in the graph.

2. Temperature Distribution:

Different wall temperatures are imposed according to the graph shown in figure 14. For loop1, the wall temperatures imposed are as shown below:

0 – 5m: 623K
5 – 6.5m: linearly increases from 623K to 723K
6.5 – 15m: 723K

A user supplied subroutine is developed to impose the wall boundary temperatures and concentrations.

Figure 29 shows the temperature of the fluid at the wall. The temperature values in some regions in the figure have higher values than the maximum temperature imposed on the wall for that section. This is because the fluid is coming out from the other half of the loop i.e. loop2, where the temperature zones are higher than the temperature zones in loop1. The temperatures in the loop2 vary from 623K to 823K. So, when the fluid enters the loop1, it has slightly higher

temperature than the wall temperature at the inlet region. After the fluid enters the loop1, it starts cooling down after coming in contact with comparatively cooler wall temperatures.

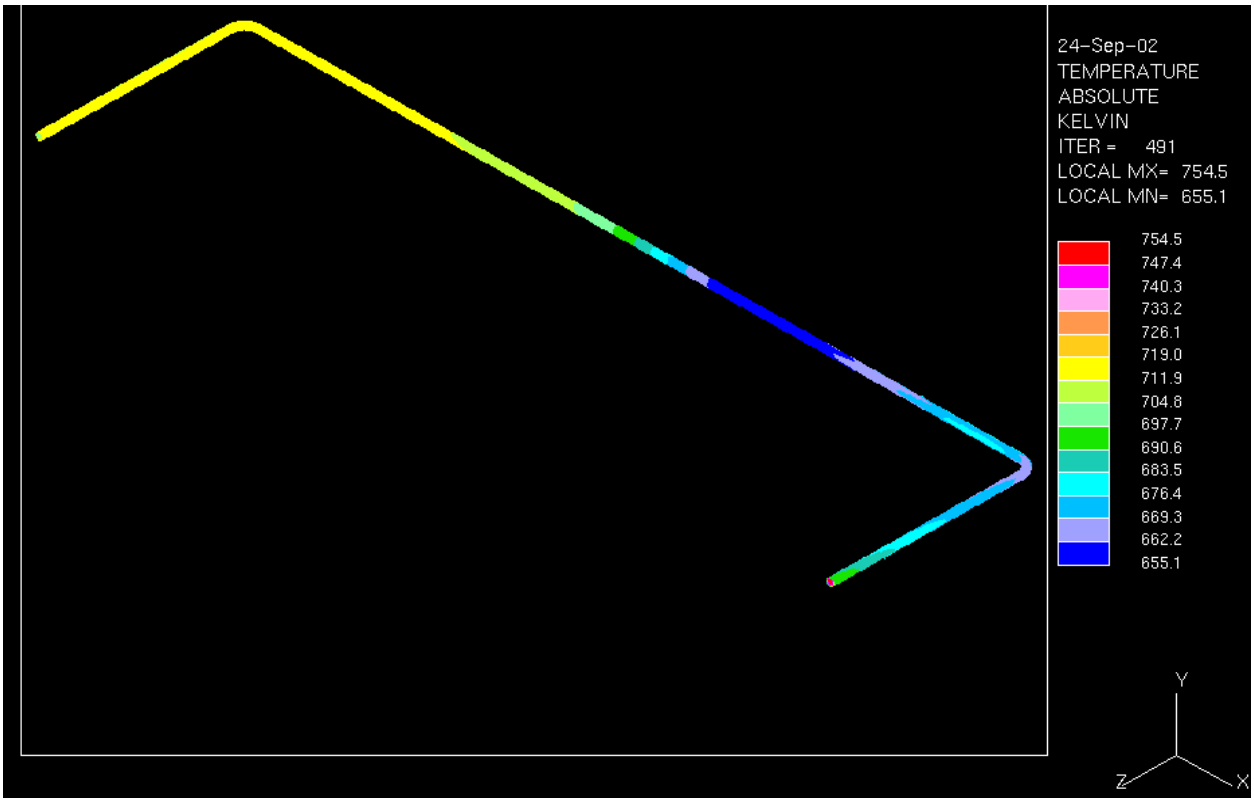

Fig -29: Fluid Surface Temperature for Loop1

The above phenomenon can be better explained by figure 30, which is a planar view of the temperature distribution in the fluid along a section cut through the axis of the pipe. Figure 31 shows the temperature distribution at the inlet of the loop1. It can be seen that the fluid enters the loop1 at 755K.

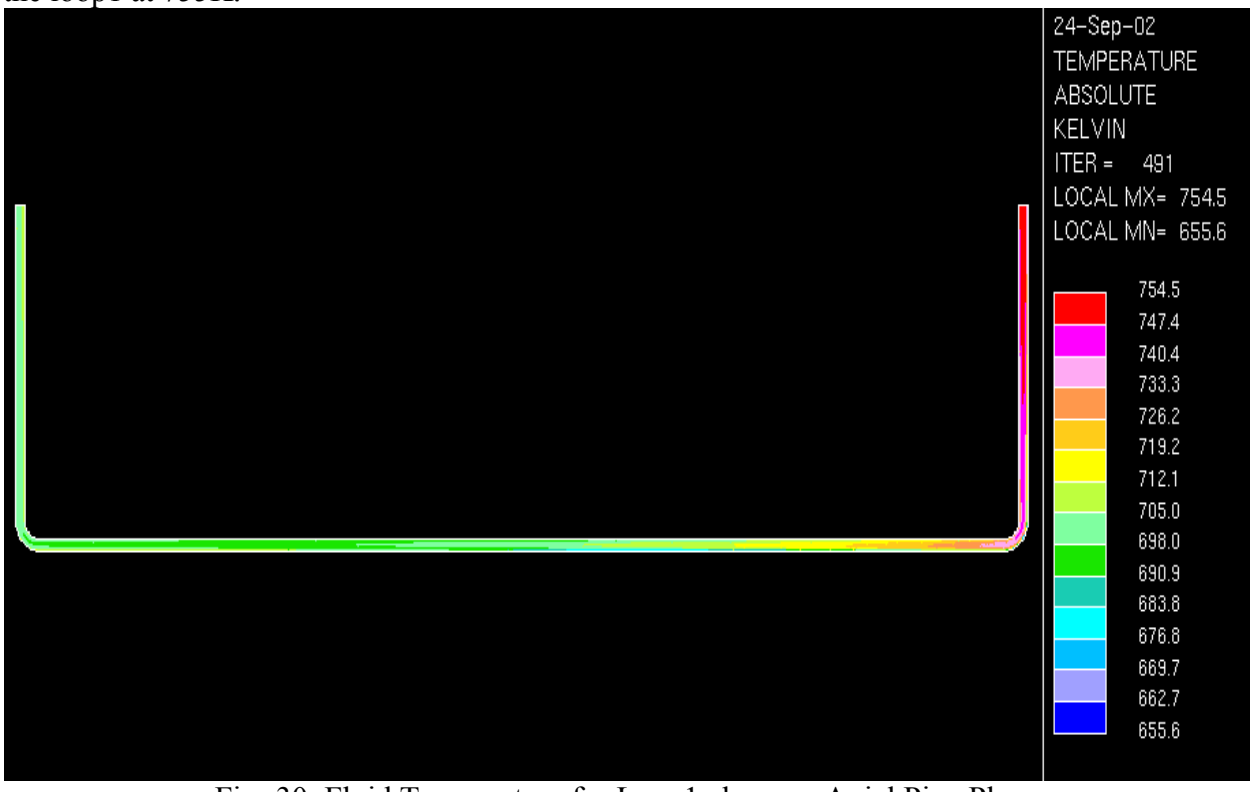

Fig -30: Fluid Temperature for Loop1 along an Axial Pipe Plane

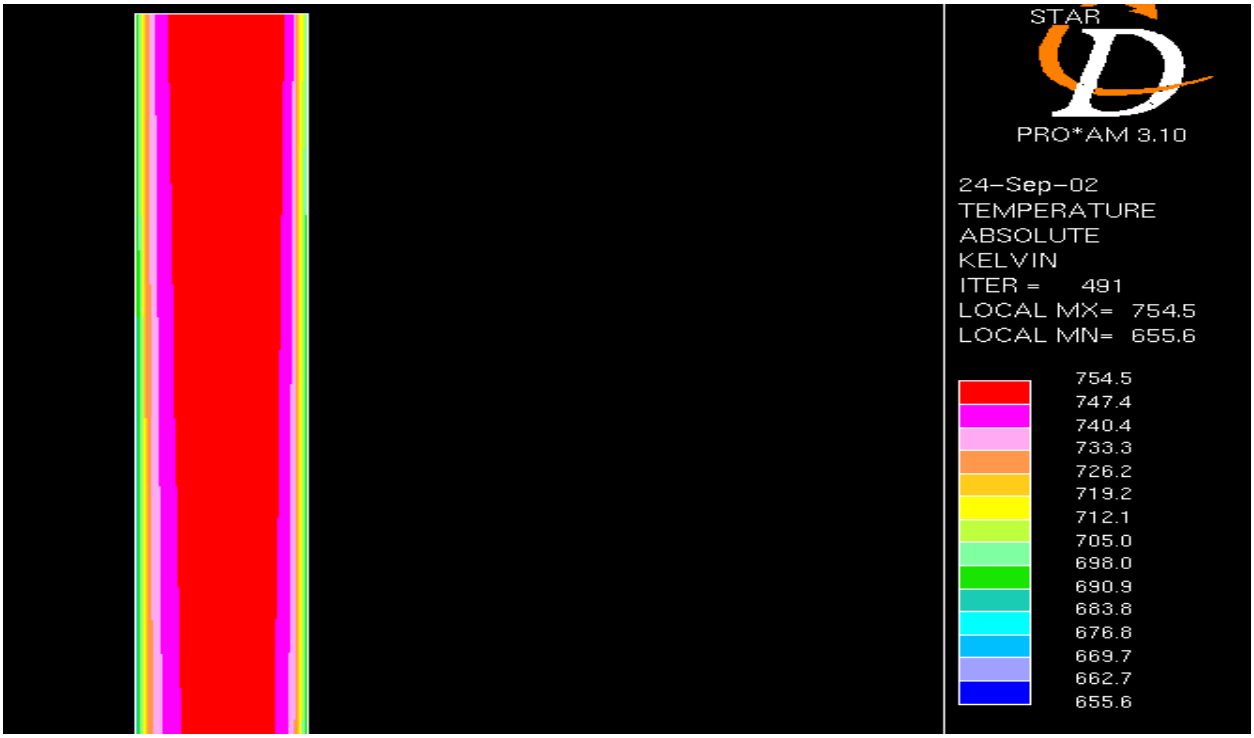

Fig -31: Fluid Temperature at the Inlet for Loop1

The temperature slowly diffuses into the fluid and the fluid temperatures show a decreasing trend. Figure 32 shows the temperature distribution at the first elbow section in the loop1. The loop wall temperature for this whole region is 623K.

Careful observation of figure 33 shows an interesting behavior in temperature variation. It can be seen that the temperature at the center of the pipe is more compared to fluid adjacent to

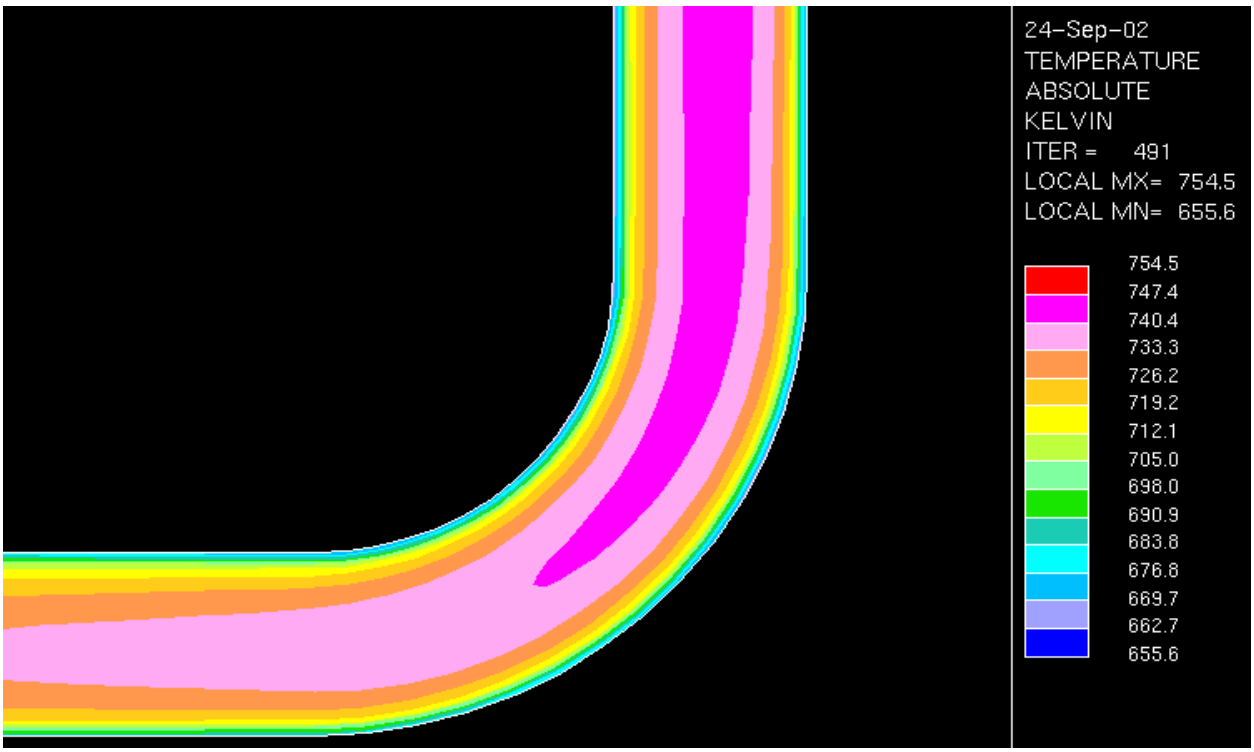

Fig -32: Fluid Temperature at the First Elbow Section for Loop1

it, and again, the temperature of the fluid near to the wall is almost equal to the fluid temperature at the center of the pipe. The reason for this is, since the diffusion occurs from the wall surface

region to the center of the pipe, and the wall temperature before this fluid passes through this region is at 623K, the temperature at the center of the fluid is higher than the temperature of the fluid adjacent to it.

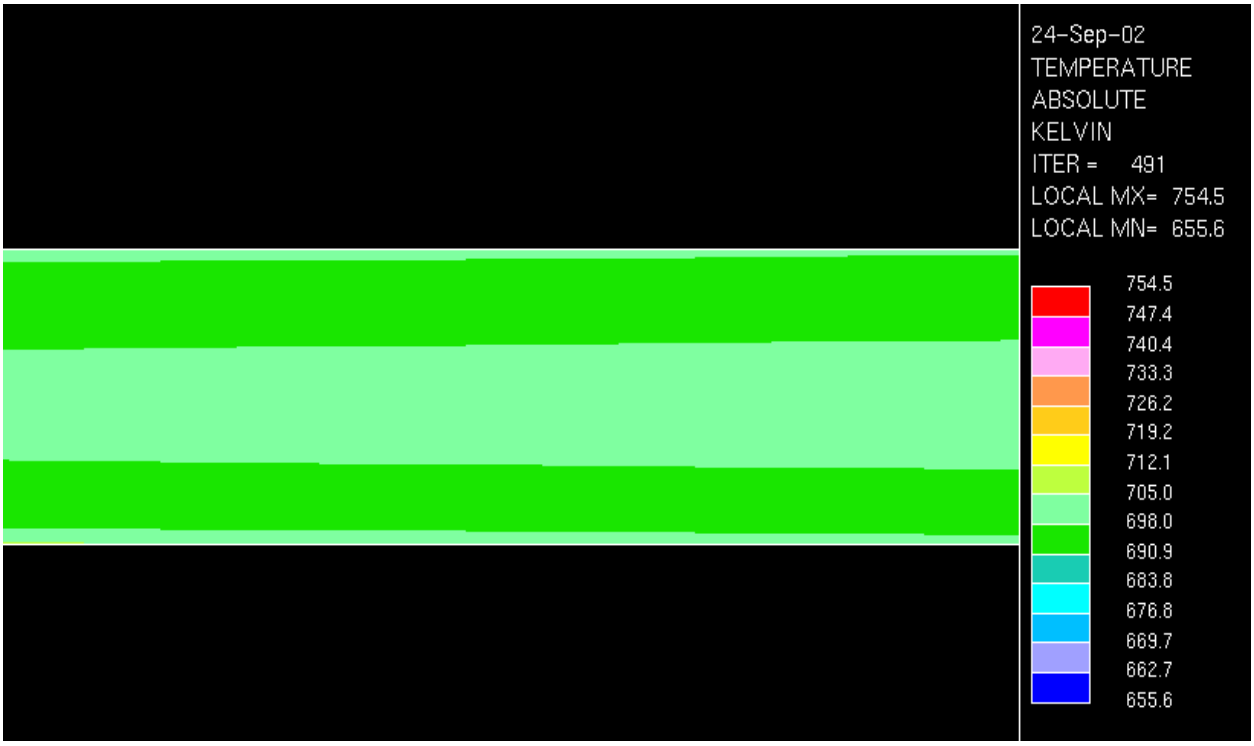

Fig -33: Fluid Temperature at the Heating Zone in the Loop1

In this figure, the fluid temperature at the wall shows a higher temperature than the fluid adjacent to it, because, this section shown in the figure is actually a heating zone, where the temperature of the wall surface increases from 623K to 723K.

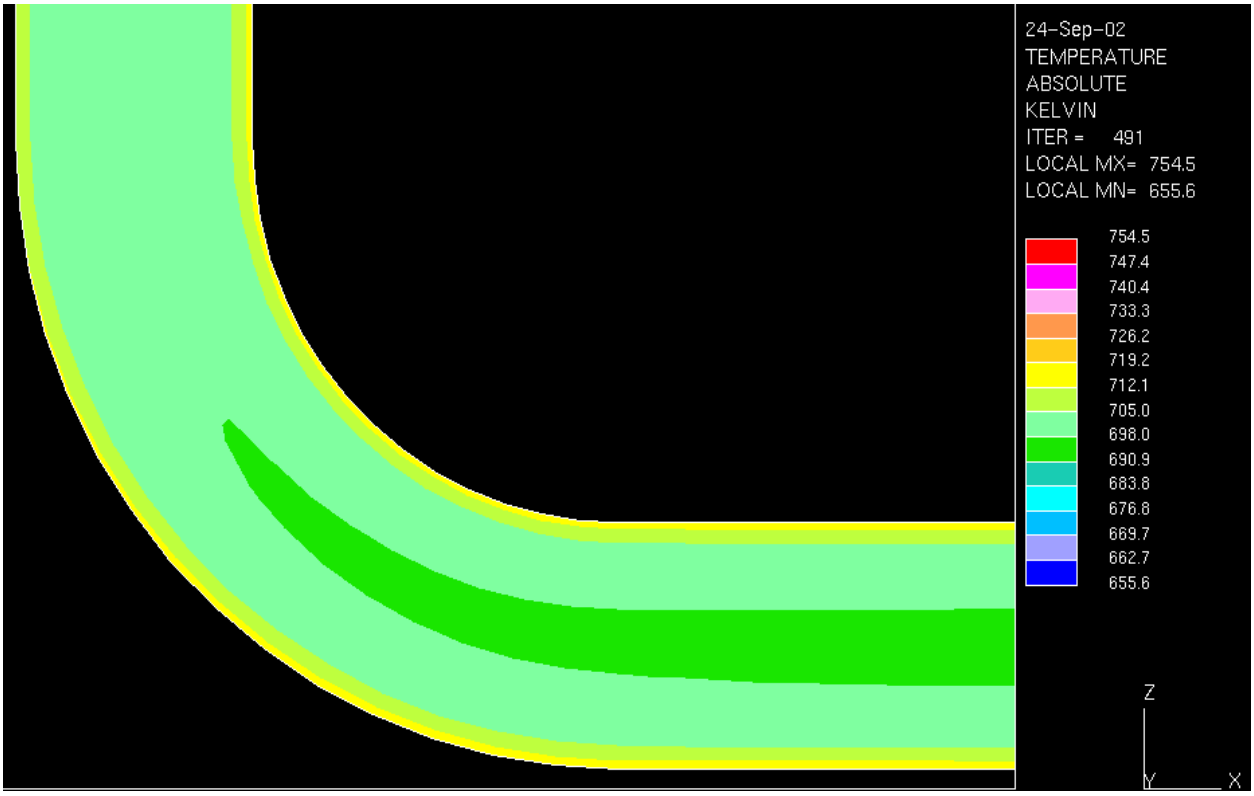

Fig -34: Fluid Temperature at the Second Elbow Section for Loop1

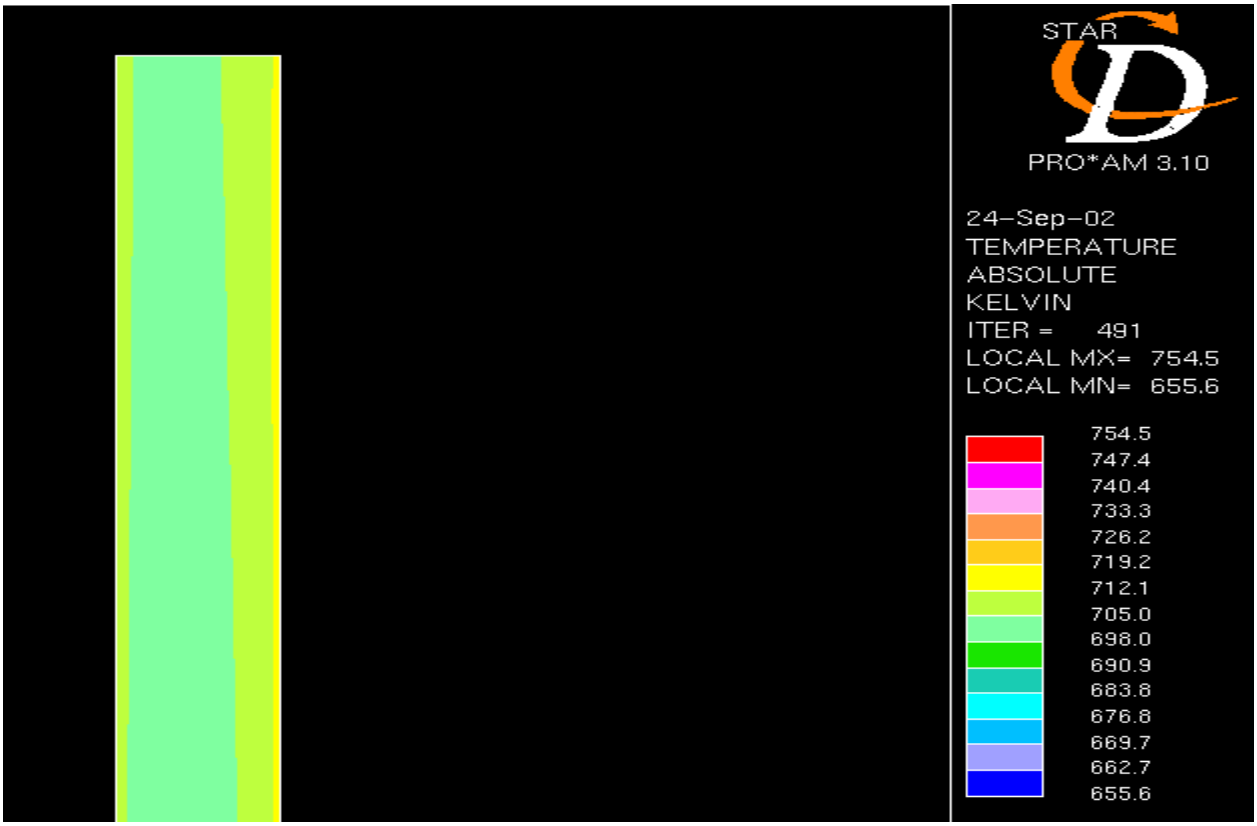

Fig -35: Fluid Temperature at the Outlet from Loop1

Figures 34 & 35 depict the temperature distribution in the fluid at the second elbow section and the outlet respectively. It can be seen that the temperature of the fluid increases steadily as the fluid is now flowing in the high temperature region. In the whole loop, the temperature of the fluid varies from 655K to 755K.

3. Concentration Distribution:

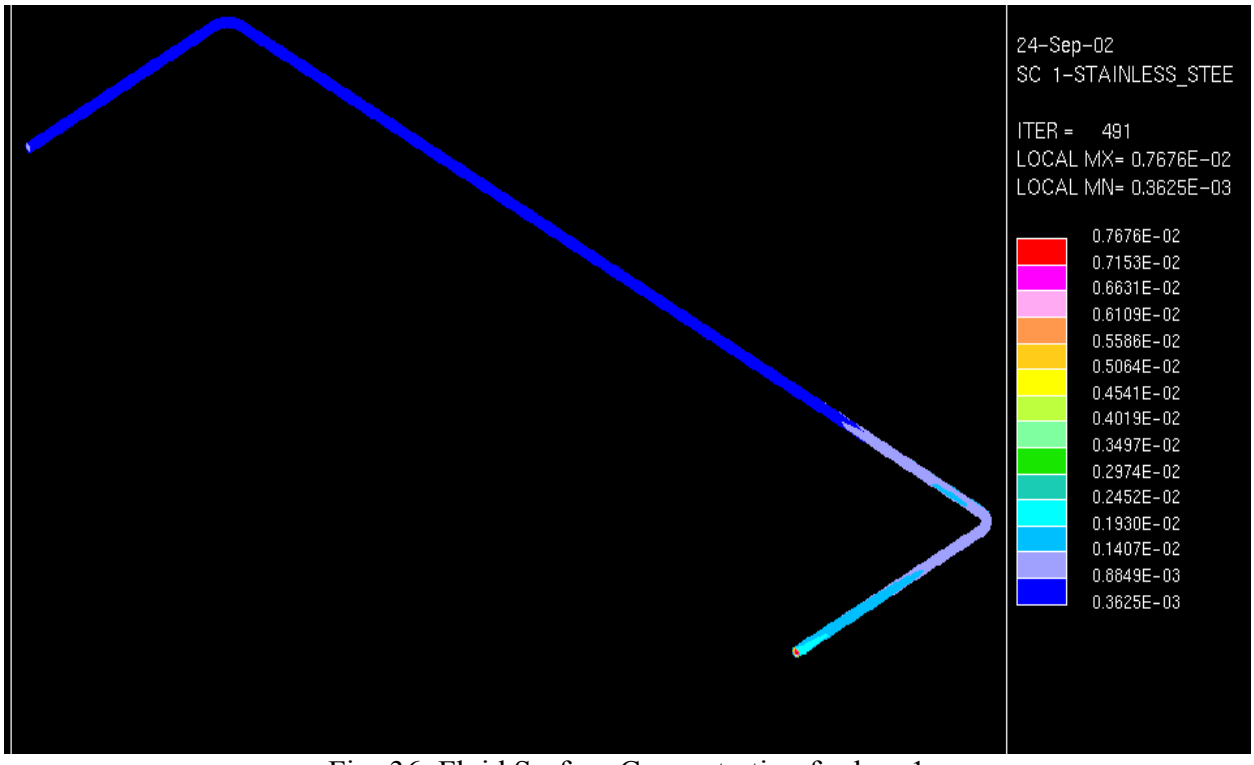

Fig -36: Fluid Surface Concentration for loop1

It can be reiterated here that the wall concentration for the loop has been calculated by the program with the help of user subroutine using equation 7. The concentration in the whole discussion is referred to the concentration of iron present in the fluid in parts per million (ppm). Figure 36 shows the concentration of iron on the fluid surface that is in direct contact with the wall. Higher concentration in some regions of the fluid compared to the maximum concentration imposed on the wall boundary can be explained with a similar analogy used for temperature distribution. Figure 37 shows the concentration along a section of the pipe cut through an axial plane. It is to be noted that the concentration decreases slowly due to diffusion as the fluid moves in the flow direction.

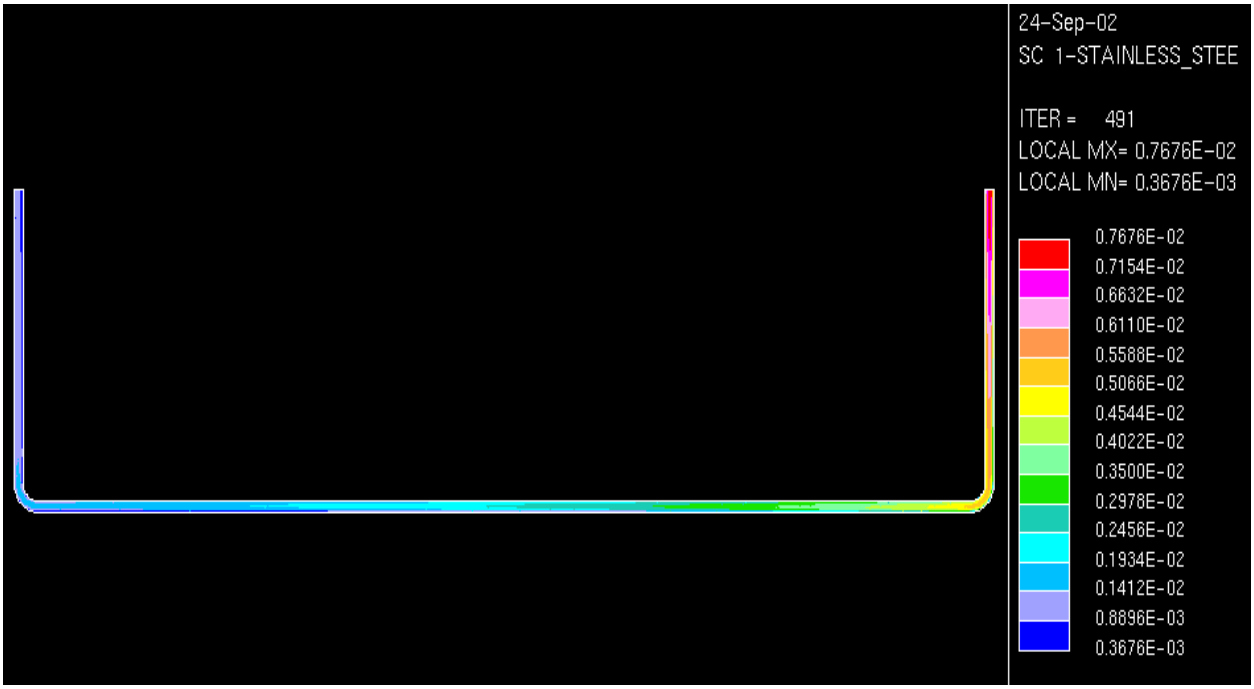

Fig -37: Fluid Concentration for Loop1 at an Axial Plane

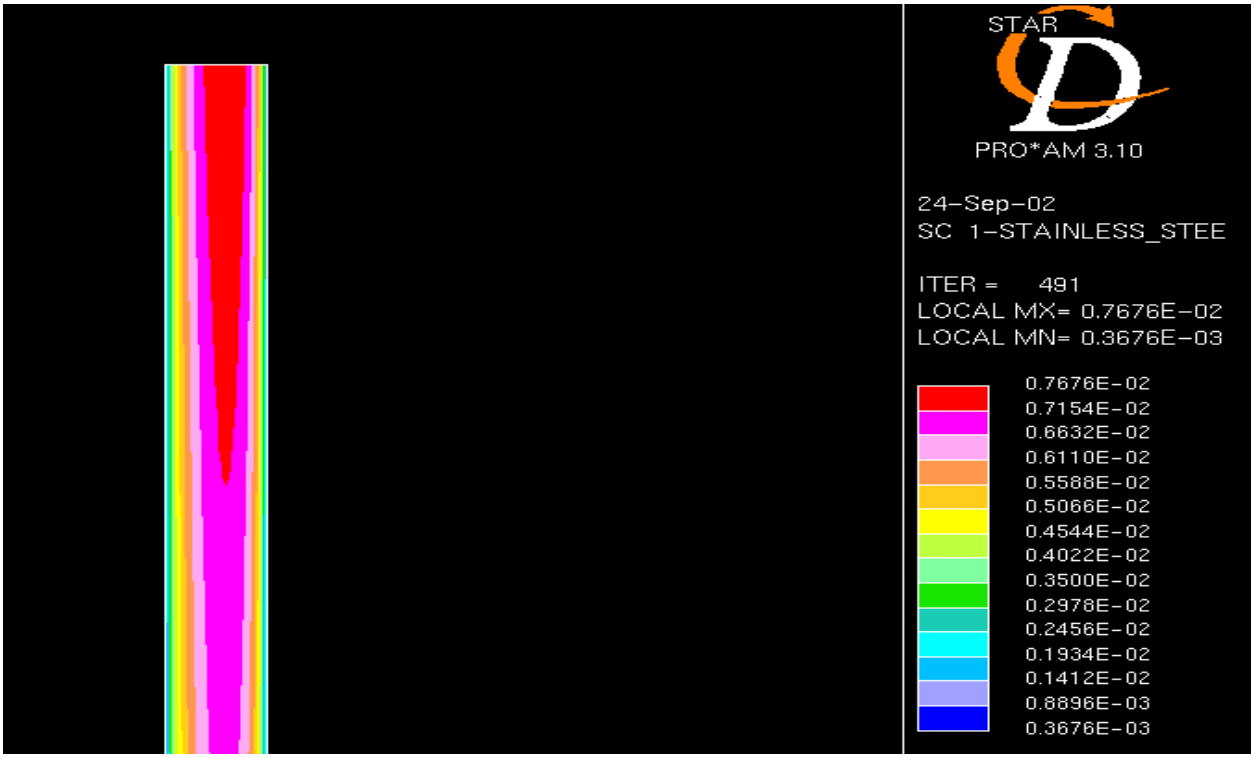

Fig -38: Fluid Concentration at the Inlet for Loop1

By the time the fluid reaches the first elbow section, as shown in figure 38, the concentration distribution becomes more uniform, as the high concentration fluid particles diffuse into the low concentration regions.

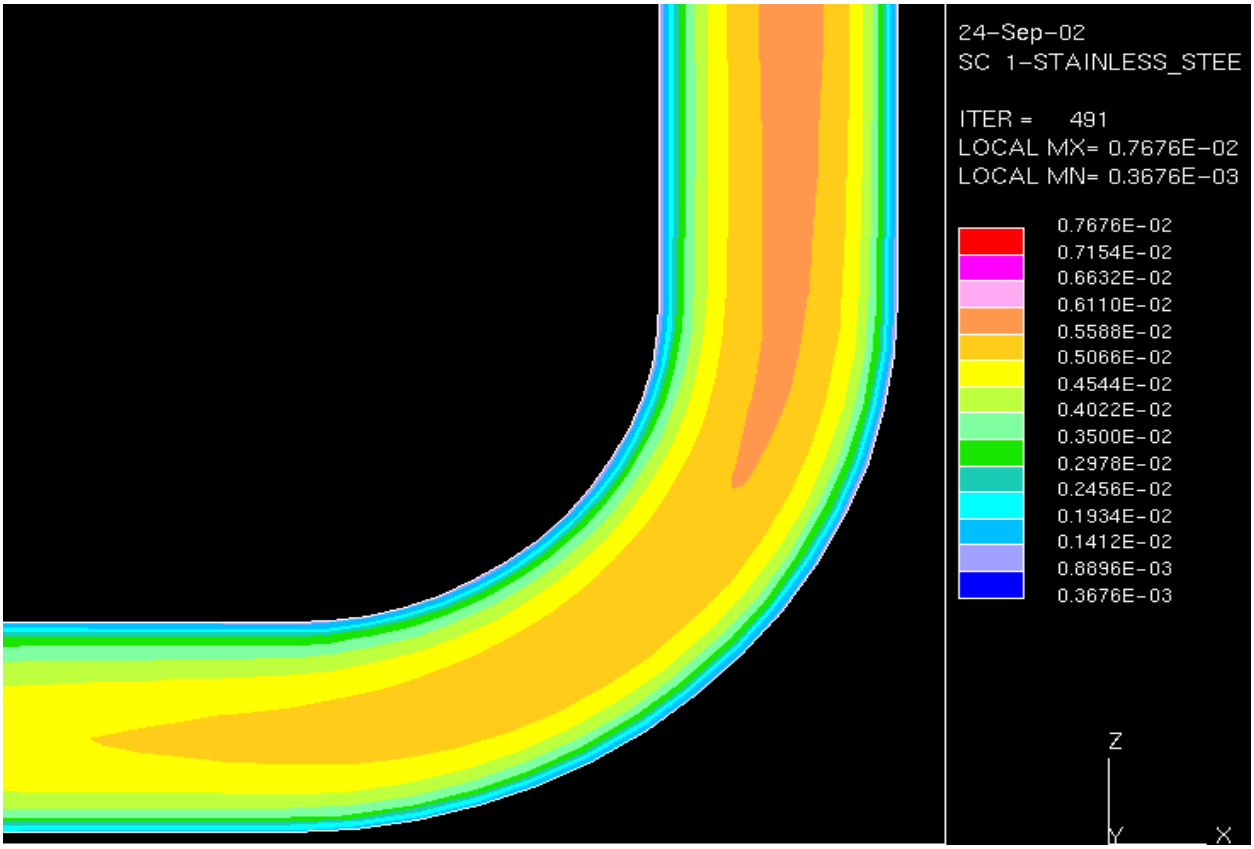

Fig -39: Fluid Concentration at the First Elbow Section for Loop1

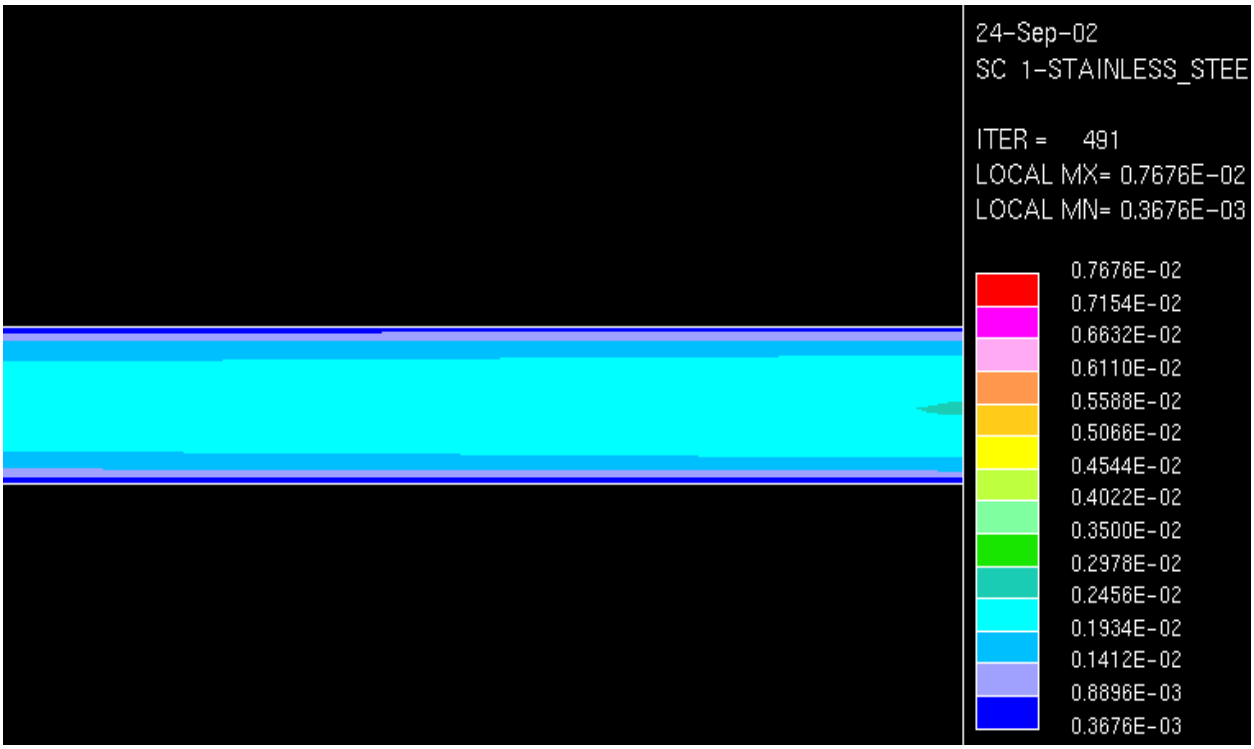

Fig -40: Fluid Concentration at the Heating Zone in the Loop1

Unlike the trend seen in the temperature distribution, where the fluid temperature first decreases and then again increases due to the varying wall surface temperatures, the fluid

concentration mainly decreases steadily all through the flow. The reason for this is when the walls are at lower temperature, the temperature diffuses into the fluid. But in case of concentration, where there is a mass transfer, there is no diffusion of the concentration into the fluid from the wall and in the whole process because the concentration of fluid entering the loop1 is higher than the concentration in any region of the wall. Hence, diffusion can only be seen within the fluid particles.

The explanation above can be justified by the figure 40, which shows the concentration distribution at the heating zone. There is no concentration diffusing into the fluid from the wall.

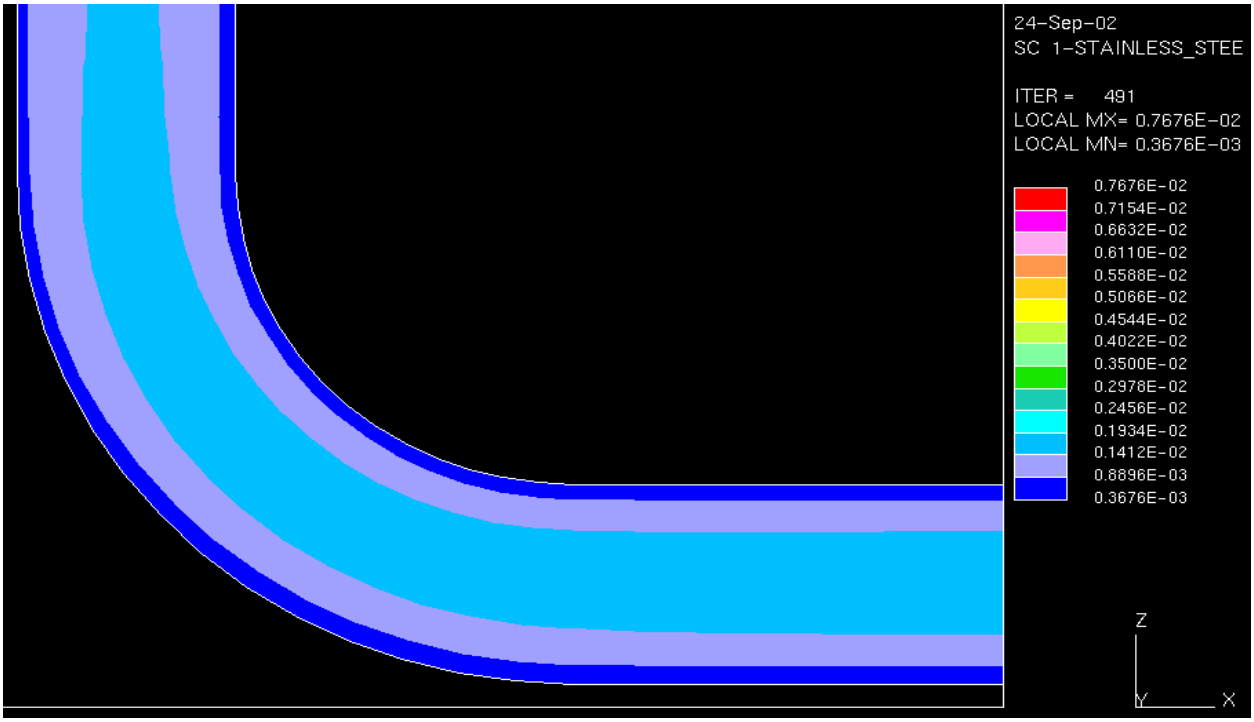

Fig -41: Fluid Concentration at the Second Elbow Section for Loop1

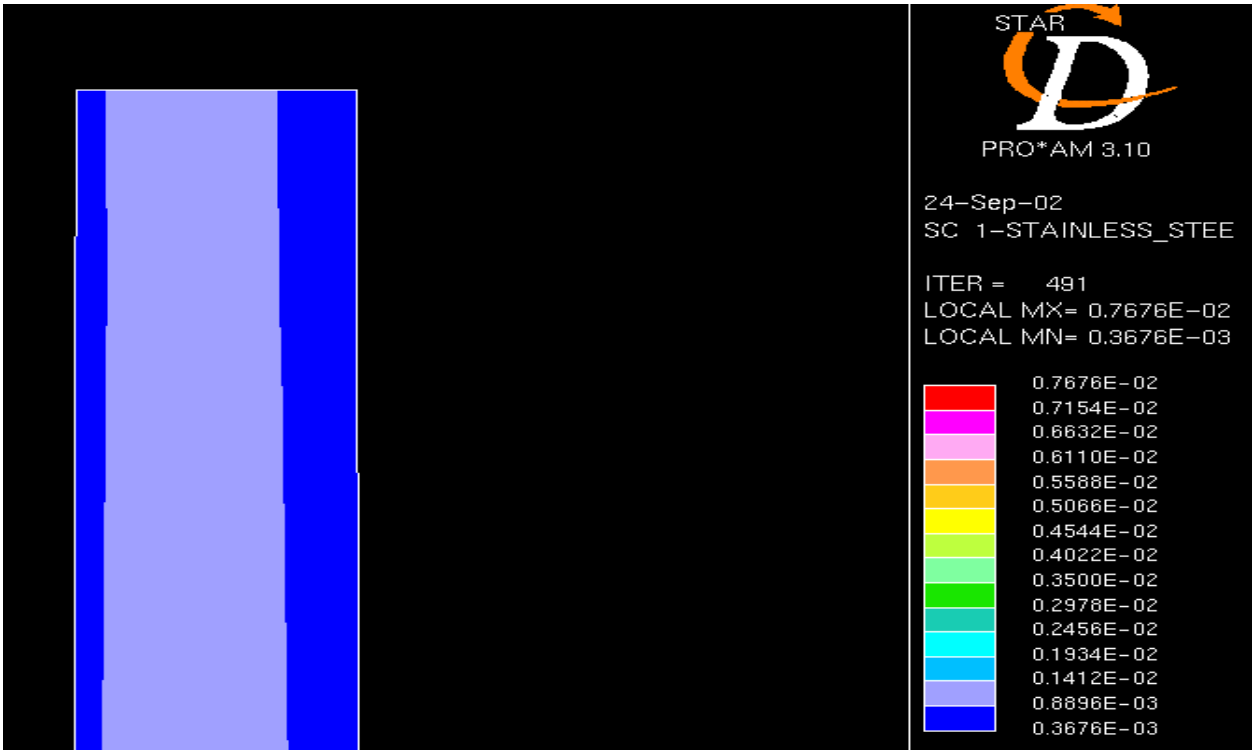

Fig -42: Fluid Concentration at the Outlet from Loop1

II) DISCUSSION ON THE RESULTS FROM LOOP2:

1. Velocity and Pressure Distribution:

The velocity and pressure distribution in the loop2 looks almost similar to the ones in the loop1. No new analysis has been mentioned hence for that loop. It is necessary to mention here that the analysis of the velocity plots from loop1 hold good for this case too.

For feeding the data from one loop to another, a semi-automatic procedure has been followed. In so doing, the values of velocity in all the three coordinates, temperature, density, k, ε and concentration values for all the cells on the outlet boundary are read into the corresponding cells on the inlet boundary.

2. Temperature Distribution:

The wall surface temperatures imposed on the loop2 are as follows:

0 – 4.5m	:	varies linearly from 723K to 823K
4.5 – 10.5m	:	823K
10.5 – 12m	:	varies linearly from 823K to 723K
12 – 13.5m	:	723K
13.5 – 15m	:	varies linearly from 723K to 623K

Figure 43 shows the temperature distribution of fluid surface that is contact with the walls. The fluid temperature in the whole loop varies from 689K to 801K.

Figure 44 shows the temperature distribution in the loop along an axial plane of the pipe. Note that the wall surface temperature for the loop1 at the outlet is 723K and the wall surface temperature at the inlet of loop2 is 723K. Similarly, the wall surface temperature at the outlet of loop2 is 623K and the wall surface temperature at the inlet of loop1 is also 623K which makes it a continuous loop.

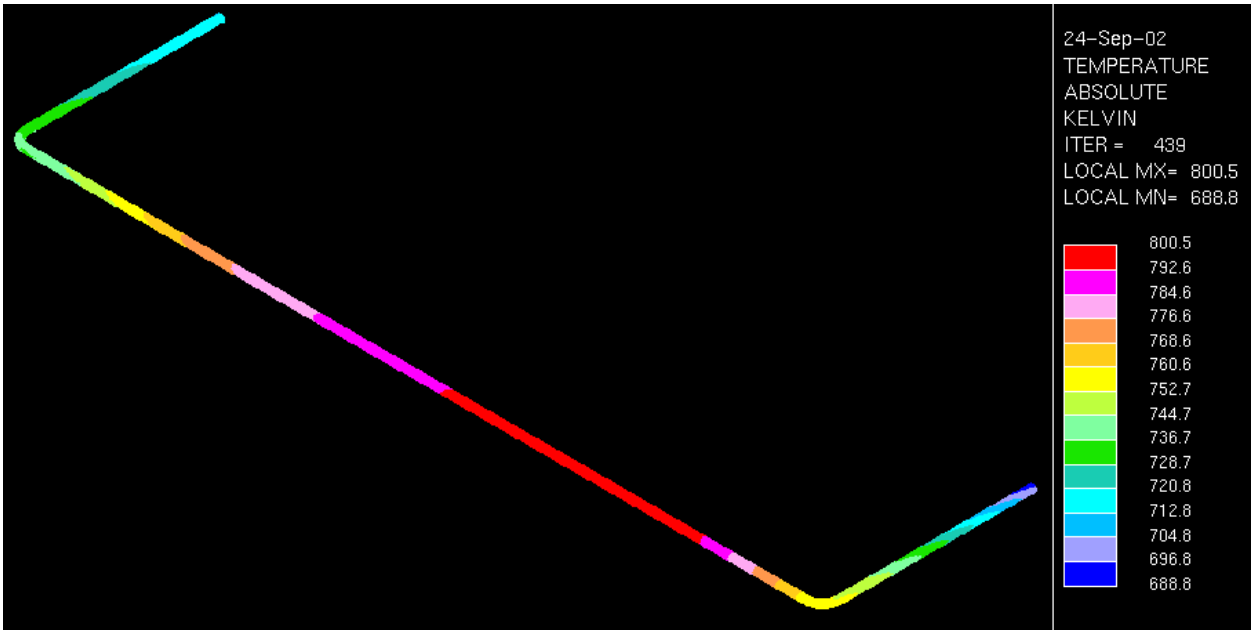

Fig -43: Fluid Surface Temperature for Loop2

Figure 45 portrays the temperature at the inlet condition of loop2. Careful observation reveals that the inlet fluid temperature for loop2 is same as the outlet fluid temperature for loop1.

It should be noted that the fluid inlet conditions for loop1 might not be same as the outlet conditions of loop2 for the cases provided, as the results are shown are from the ongoing runs and the data from the loop1 is fed into the loop2. This data from the loop2 will be fed as an input for the loop1 for the next run.

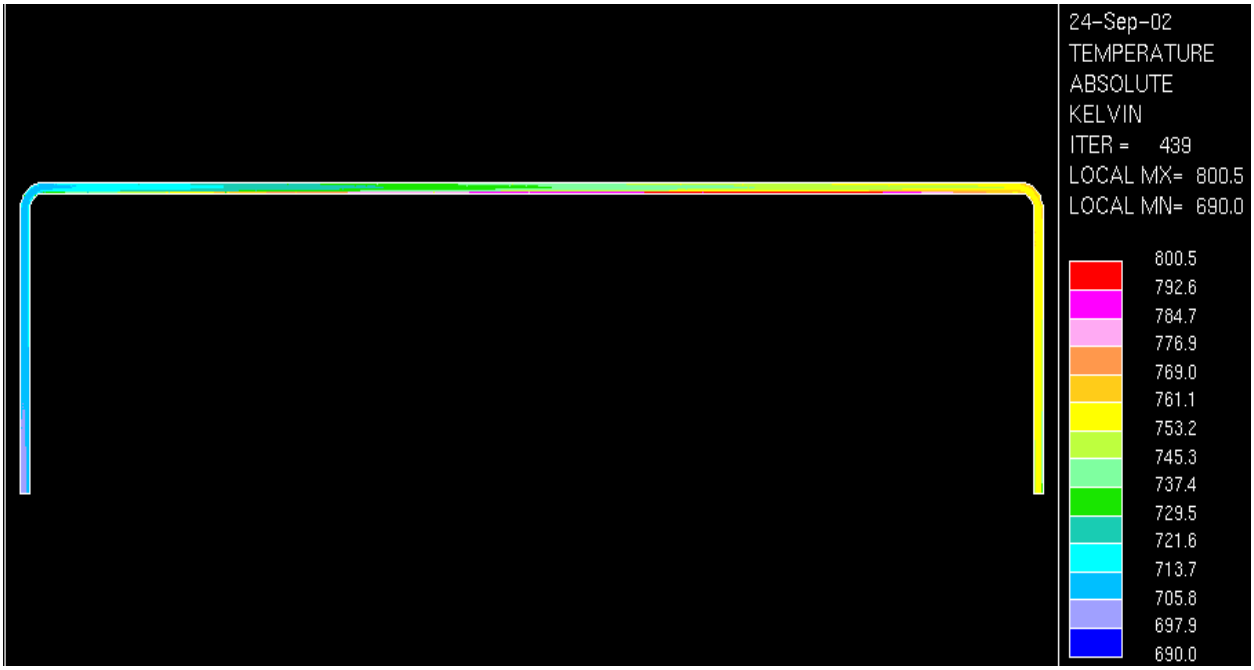

Fig -44: Fluid Temperature for Loop2 at an Axial Plane of the Pipe

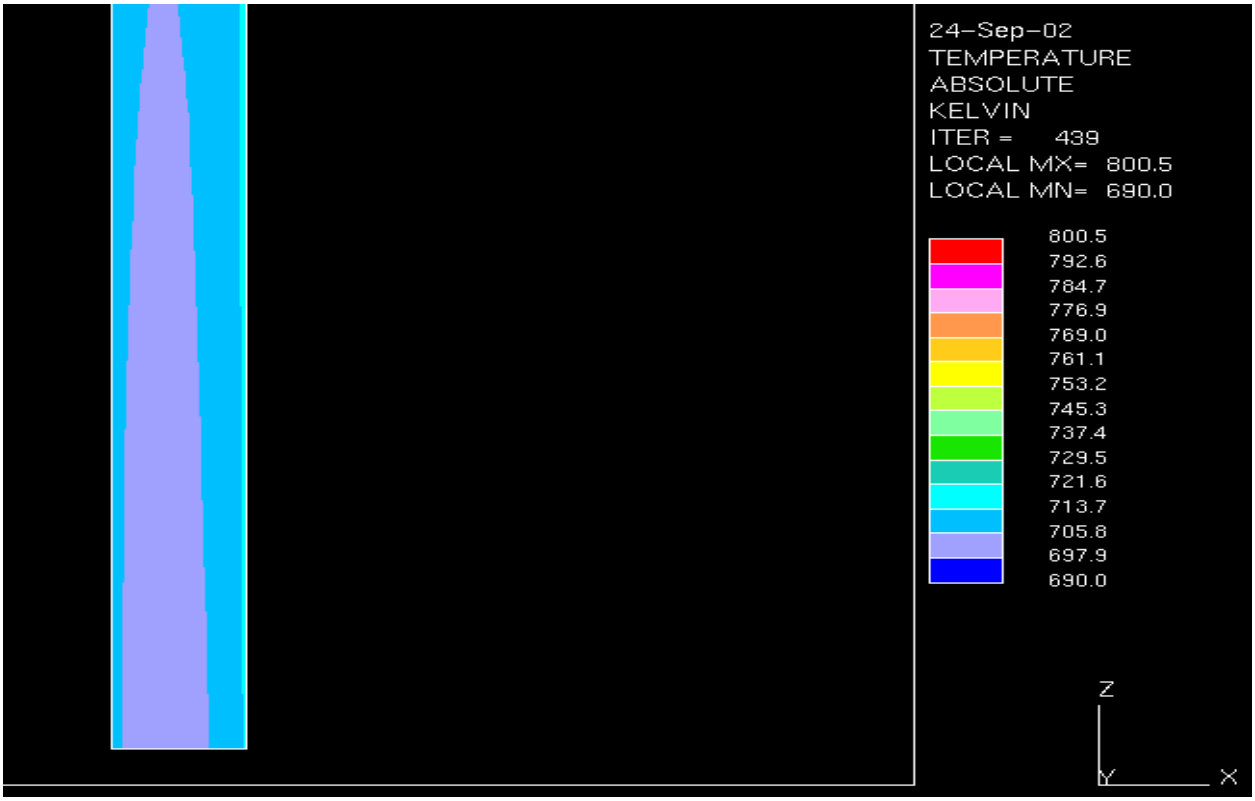

Fig -45: Fluid Temperature at the Inlet for Loop2

It can be observed from figure 45 that the temperature of the fluid slowly increases because the wall temperature rises from 450K to 550K. Figure 46 shows the temperature increase in the fluid because of constant increase in the wall surface temperature at the first

elbow section of loop2. The temperature rise is more linear because the wall temperature rise is gradual around the elbow than being abrupt.

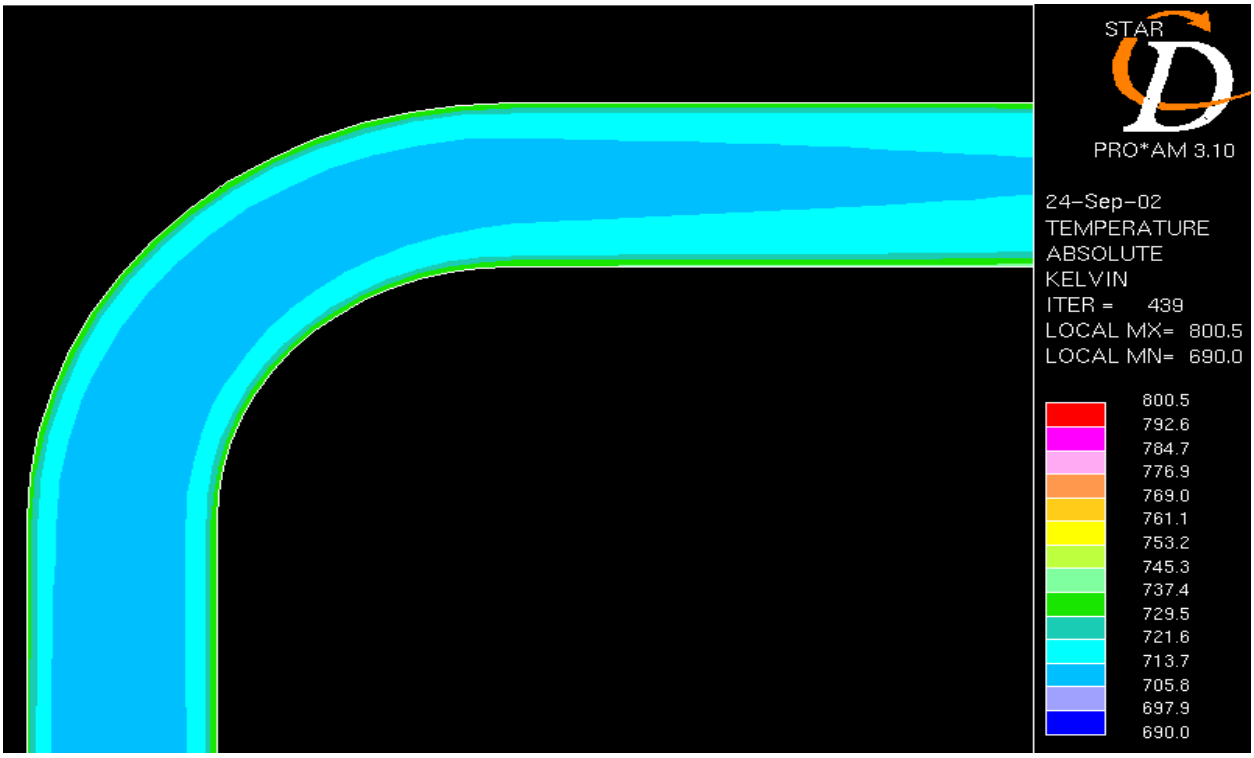

Fig -46: Fluid Temperature at the First Elbow Section for Loop2

In the next figure, the temperature of the fluid starts decreasing due to the decrease in wall temperature. In the region shown, the wall temperature drastically decreases from 823K to 723K over a short length of the pipe. Hence the fluid temperature decrease is also more drastic than in the previous case.

Fig -47: Fluid Temperature at the Cooling Zone in the Loop2

Figure 48 shows the temperature variation at the second elbow section. Again, it can be seen that the temperature of fluid at the center of the pipe is more than the fluid adjacent to it and

almost equal to the fluid temperature near the wall, the reason being the same as the one described for this trend in loop1 discussion.

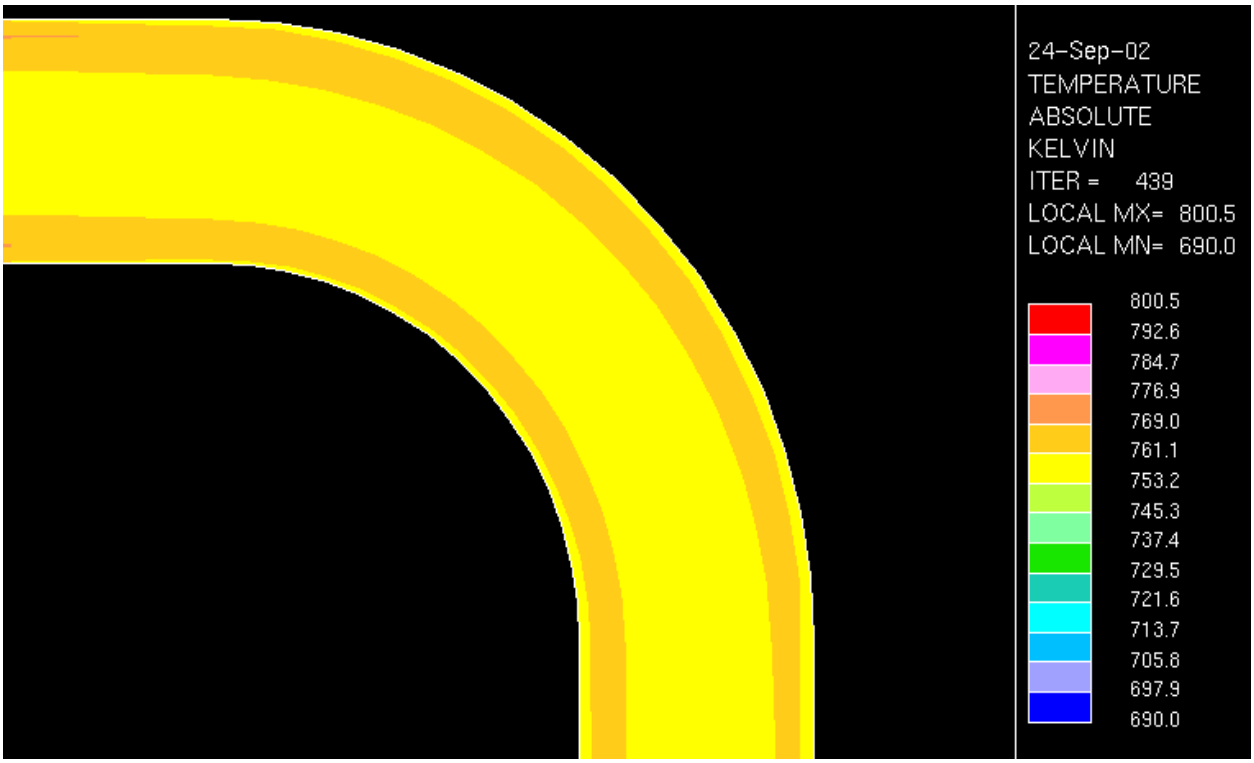

Fig -48: Fluid Temperature at the Second Elbow Section for Loop2

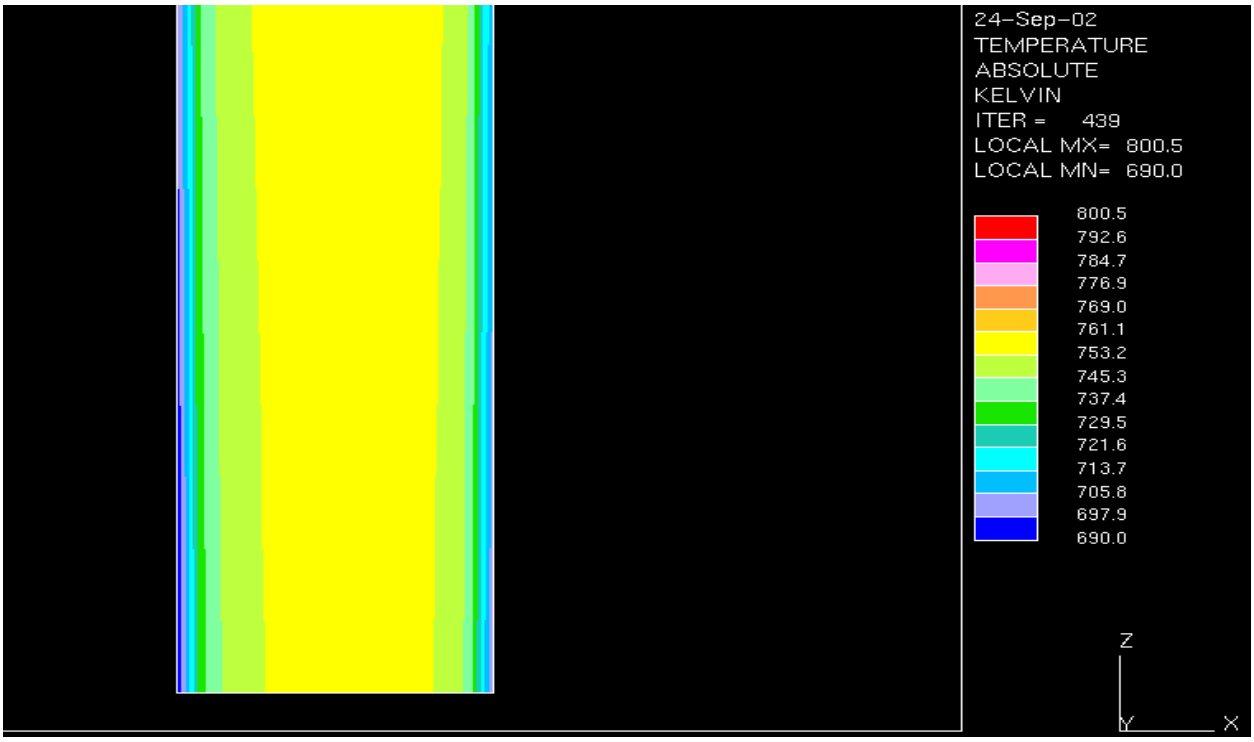

Fig -49: Fluid Temperature at the Outlet from Loop2

Figure 49 shows the fluid temperature at the outlet of loop2. The fluid temperature steadily decreases as the wall is at a lower temperature than the fluid.

3. Concentration Distribution:

Figure 50 shows the fluid surface concentration variation in the loop2 at the wall. The concentration of the fluid varies from 0.2842E-03 to 0.2038E-01 the highest concentration corresponding to the maximum temperature region.

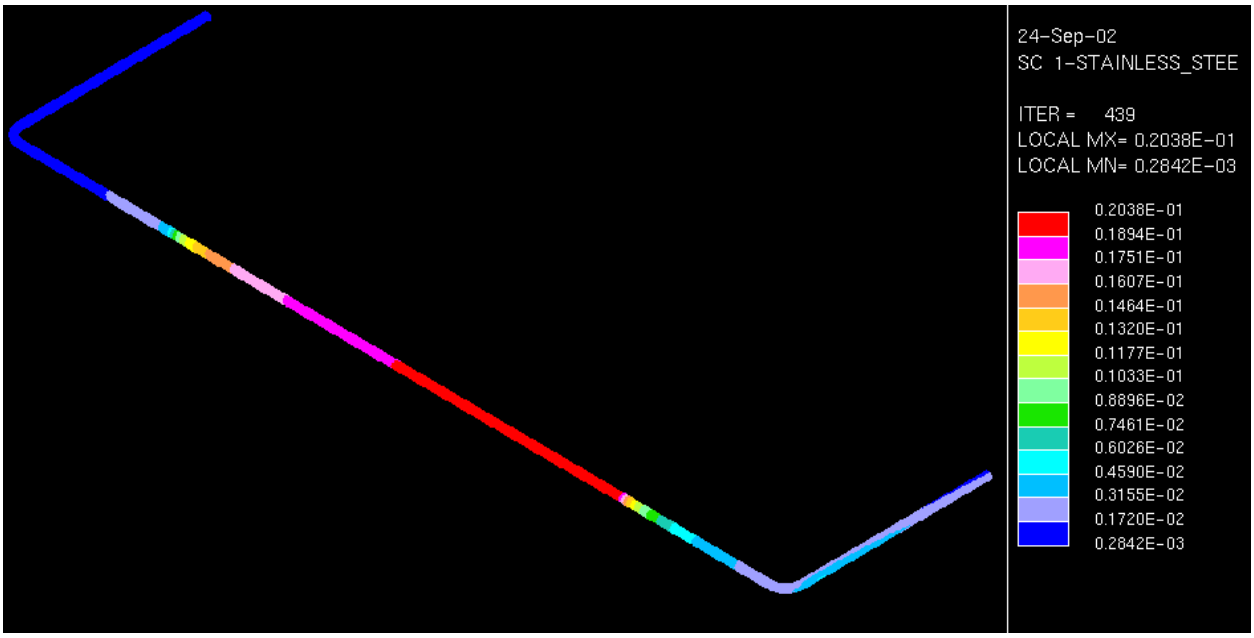

Fig -50: Fluid Surface Concentration for Loop2

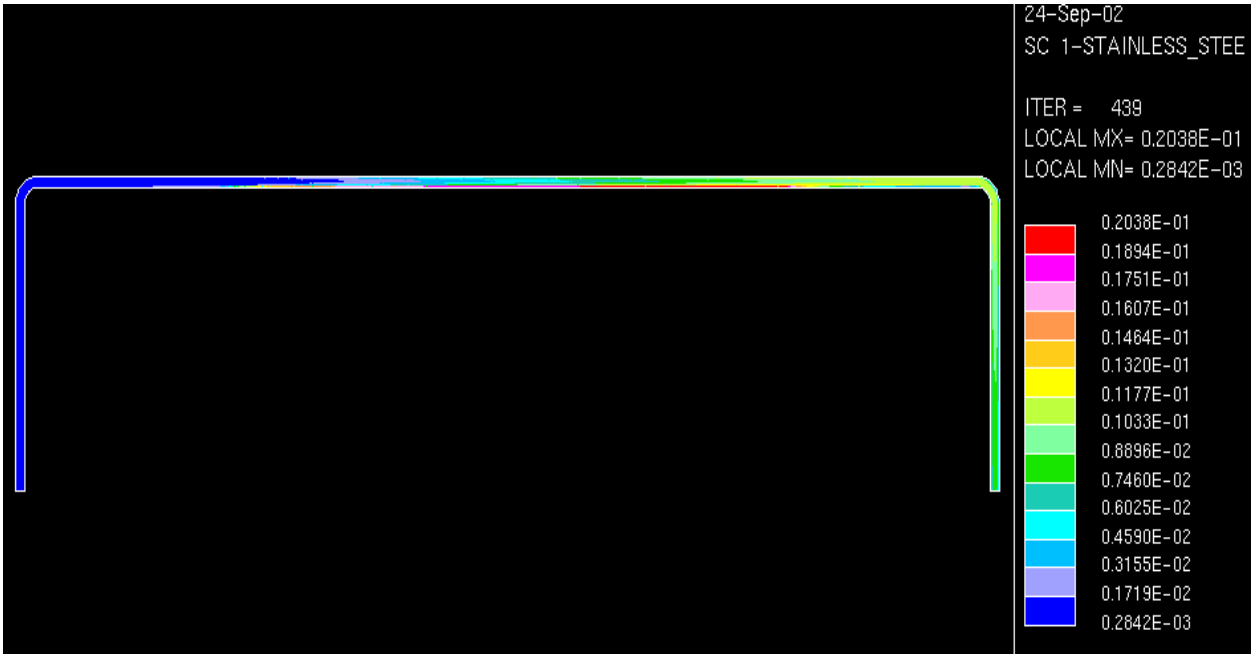

Fig -51: Fluid Concentration for Loop2 at an Axial Plane of the Pipe

The concentration of the fluid along the center of the pipe section cut in the transverse direction can be seen in figure 51. Figure 52 shows the concentration distribution at the inlet of loop2. The inlet concentration of loop2 is same as the outlet species concentration from loop1. It can be seen from figures 52 and 53 that the concentration of the fluid decreases at first and slowly increases again. This is due to the fact that the temperature of the walls increases in these regions and the concentration of iron increases with an increase in temperature. Initially, at the inlet, the concentration of the fluid shows a decreasing pattern even when the temperature increases. This is due to the fact that the concentration of fluid is more than the wall

concentration at the inlet. When the wall concentration becomes more than the fluid concentration, diffusion from the wall surface to the fluid can be seen.

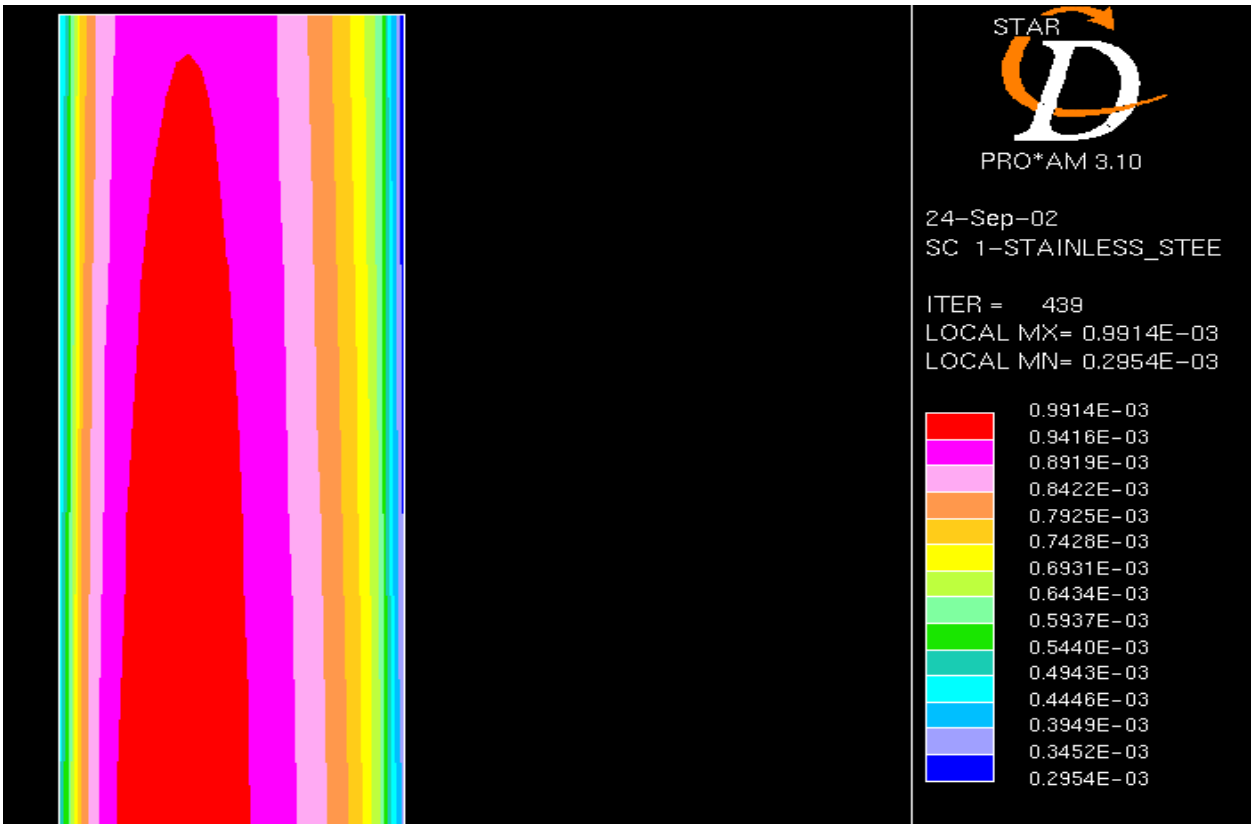

Fig -52: Fluid Concentration at the Inlet for Loop2

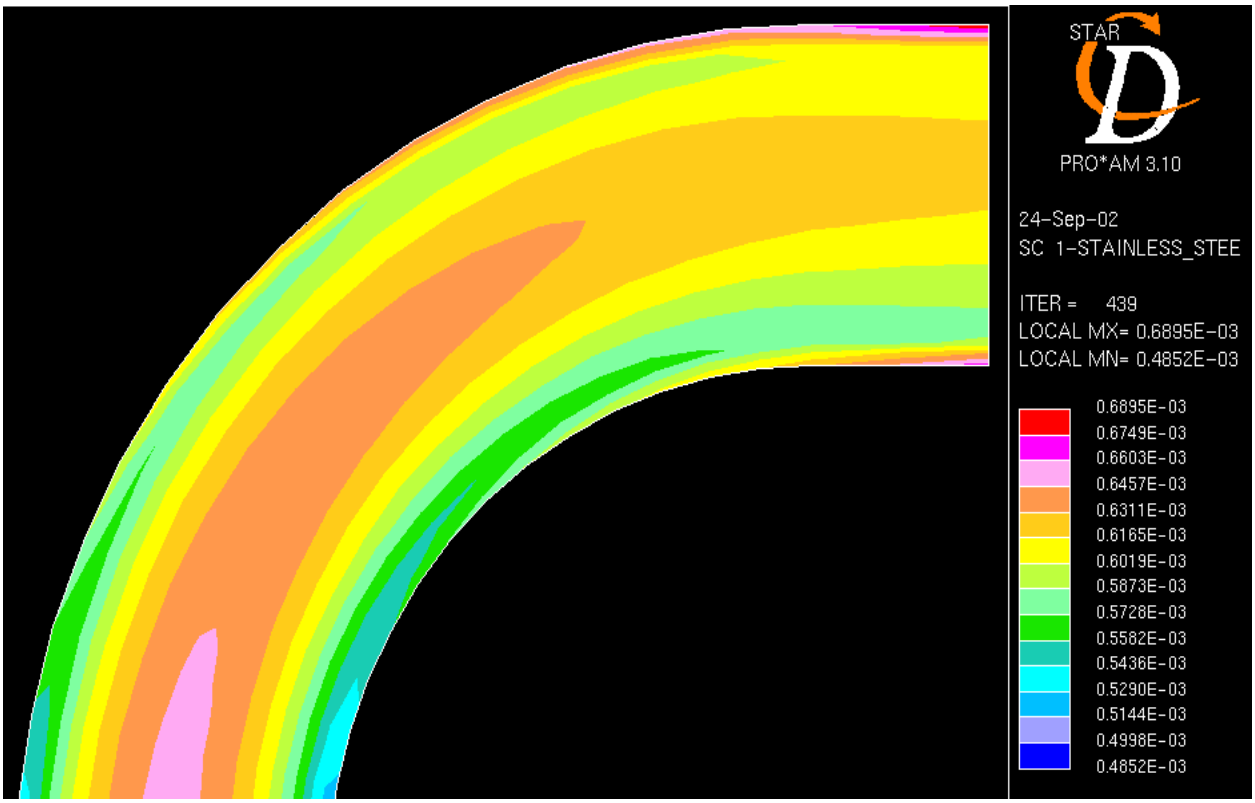

Fig -53: Fluid Concentration at the First Elbow Section for Loop2

Figure 54 shows a more pronounced increase in concentration levels in the fluid. Figure 55 shows the concentration distribution in the second elbow section in the loop2. In this section,

as mentioned before, the temperature rises. As a result of this, there is no diffusion of iron into the fluid. The decrease in concentration of the fluid is due to the diffusion of high concentration particles in the fluid to the low concentration regions. Finally, figure 56 shows the iron concentration present in the liquid LBE at the outlet of the loop2.

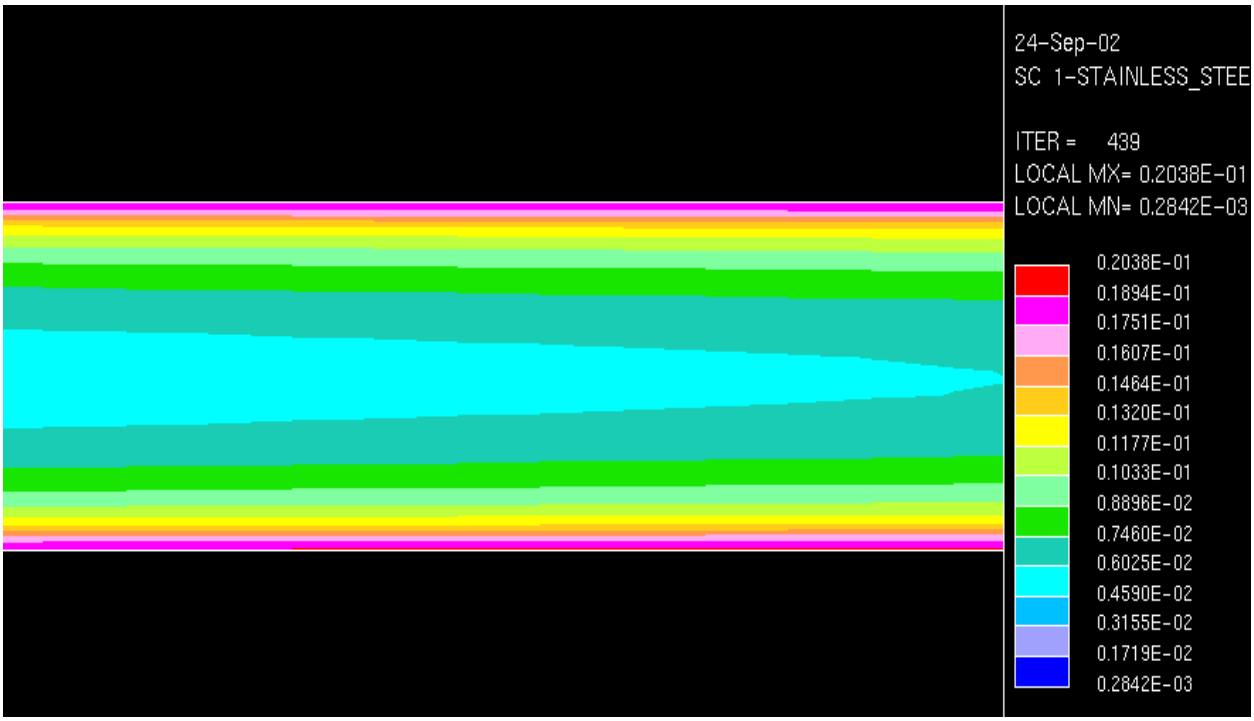

Fig -54: Fluid Concentration at the Heating Zone in the Loop2

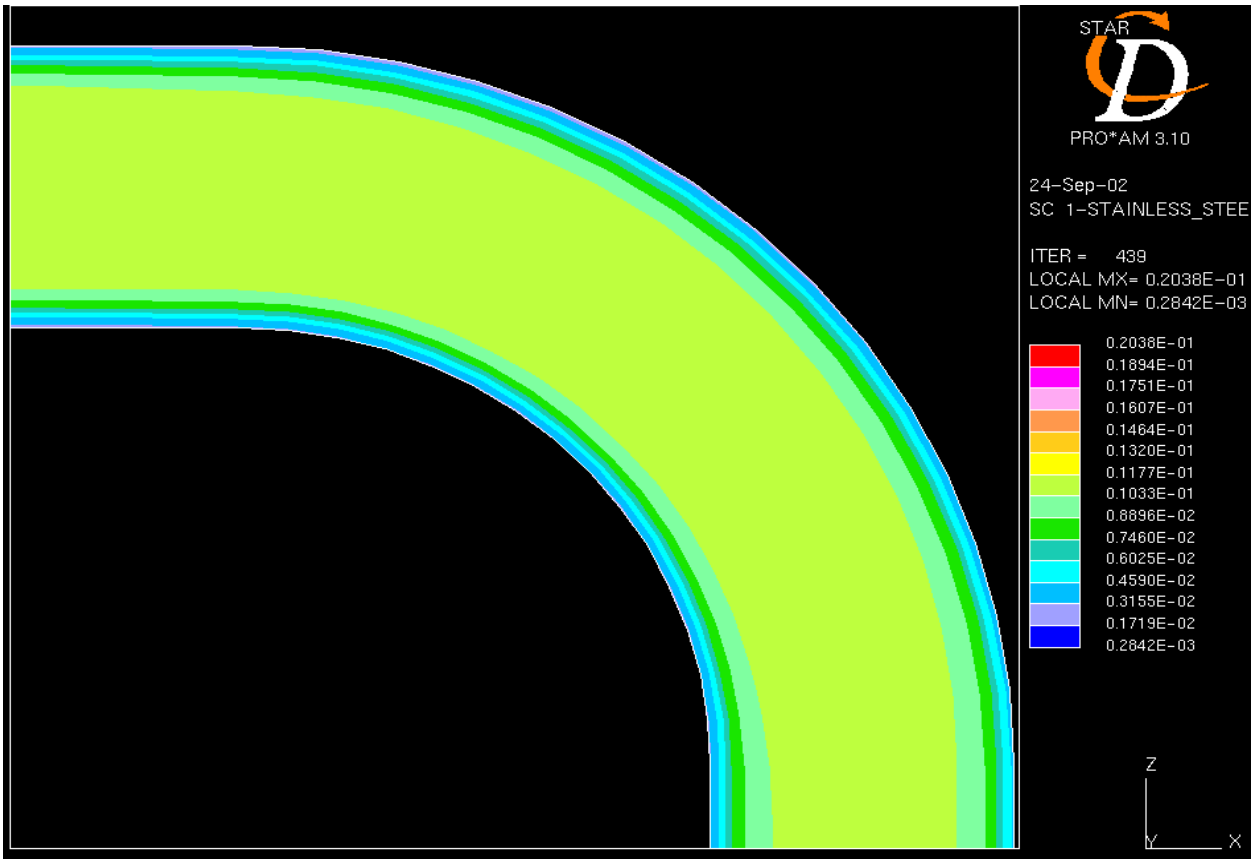

Fig -55: Fluid Concentration at the Second Elbow Section for Loop2

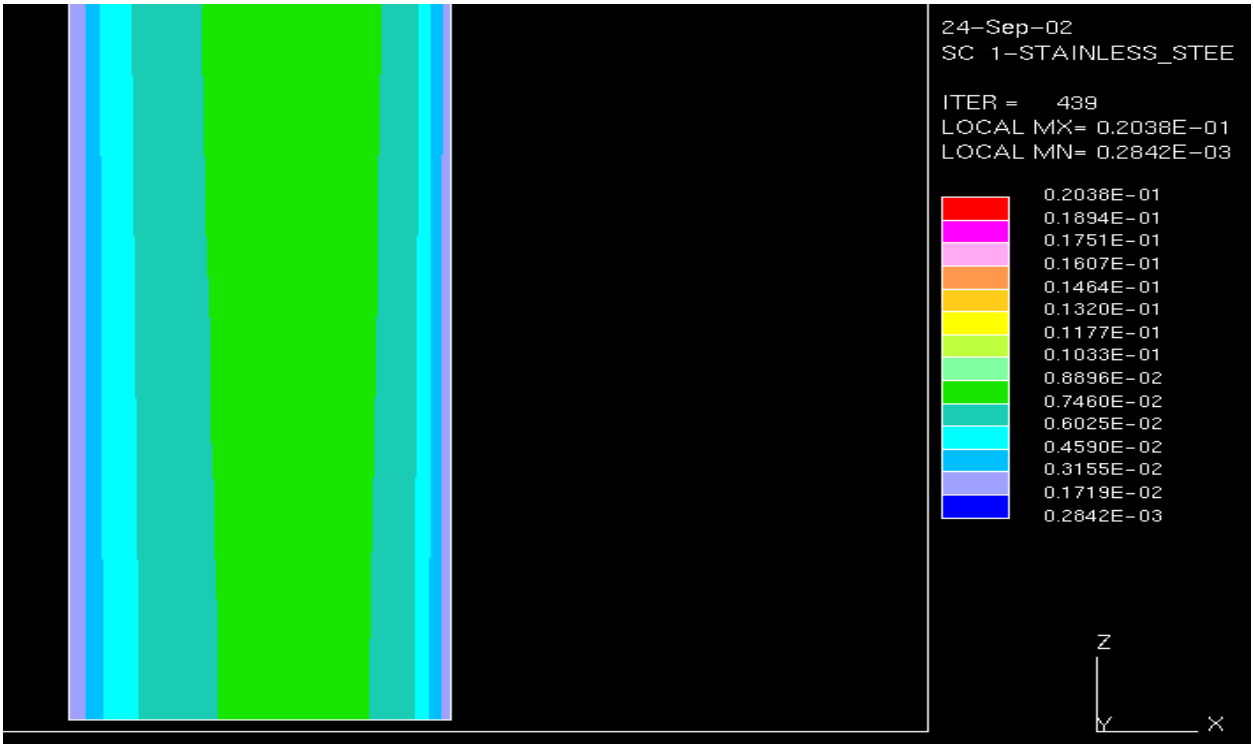

Fig -56: Fluid Concentration at the Outlet from Loop2

VALIDITY OF THE APPROACH:

As described earlier, the procedure followed is to create two U–sections and to successively feed the output of one section into another. This approach was decided on after careful discussions with our contact from LANL Dr. Li and Post-doctorate Dr. Jinsuo. Since the procedure followed is semi-manual, the convergence of the flow in the whole system has to be observed manually by comparing the result from each run on each loop with the previous run on the same loop. Convergence may be assumed to be obtained if the values between two consecutive runs are fairly close (less than 1% relative change). To keep track of how close the convergence condition is approached a method of plotting a graph between the iteration number and the concentration of the iron at a few nodes was adopted. A few nodes each from loop1 and loop2 have been selected and the concentration changes in these nodes are recorded after each run. The locations of these nodes are close to the second elbow of both loops.

Loop2 has higher temperatures than loop1. Because of this, the erosion of the surface (due to corrosion) in the loop2 should be high, resulting in high concentration at the cells near to the wall. Hence the rate of diffusion of wall concentration into the fluid reduces from one iteration to the next in loop 2. Also, the concentration of iron into the fluid for the first few iterations is higher than when compared to the values of the following graphs indicating concentrations for the last few iterations. In other words, the concentration increases steeply for the first few iterations and then the gradient of concentration change from iteration to the other decreases slowly.

When the iteration number and concentration for a given node in the loop2 is plotted for the last four iterations, they show reasonable results, depicting that the flow analysis is on the verge of convergence. Figure 57 shows this trend.

A similar argument holds good for the concentration of fluid in the loop1 except that the concentration change steadily decreases with the number of iterations. This is because relatively speaking, higher bulk concentration flows are entering the loop1 from loop2, due to higher temperatures in loop2 than in loop1. The concentration with which the fluid enters the loop1 is

higher than the concentration of the wall surface in loop1 at any part. Due to this, there is no diffusion of iron species from the wall into the fluid. Hence the concentration of the fluid in the flow decreases steadily from iteration to iteration. The plot between iteration number and the concentration at a node in loop1 is shown in figure 58.

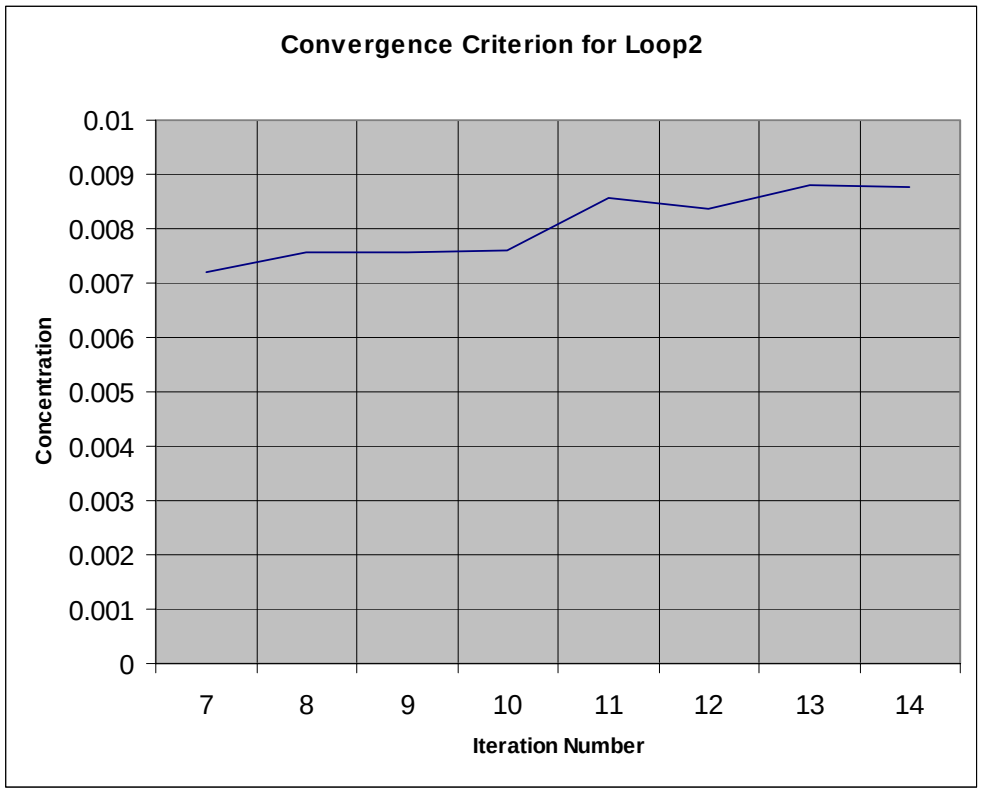

Figure -57: Convergence for Loop2

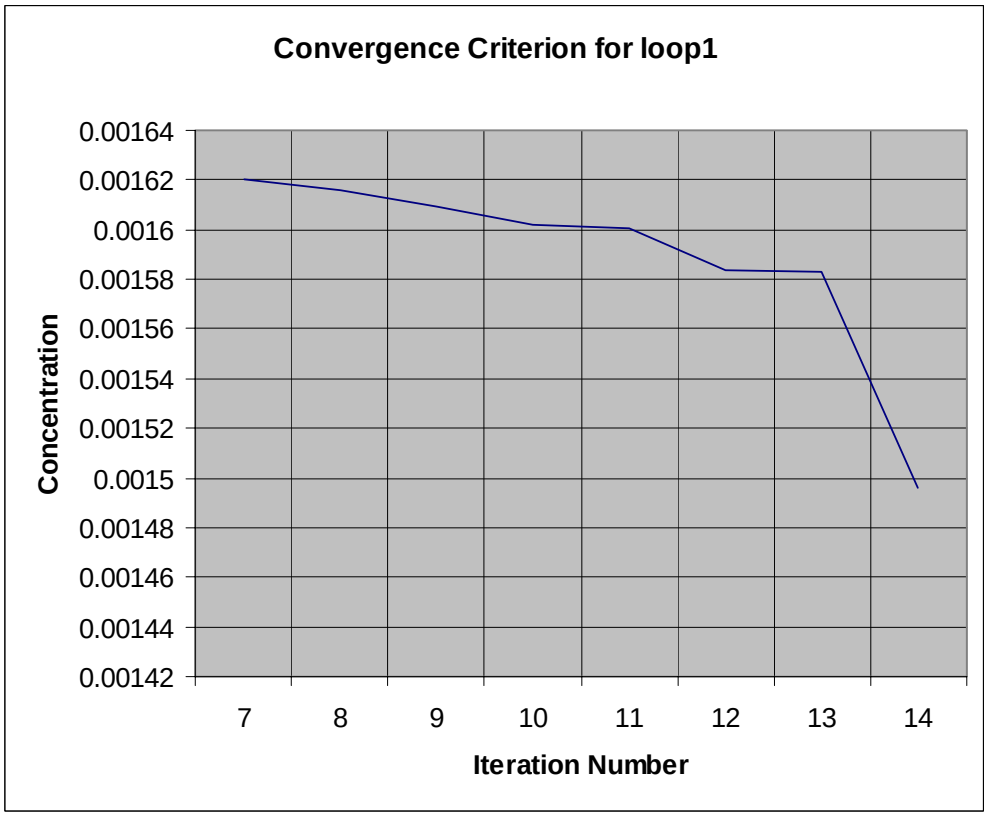

Figure -58: Convergence for Loop1

Because of the well behaved hydrodynamics of flow, temperature distributions and local concentrations and due to the fact that near convergence is observed from successive iterations, the approach is seen essentially to be a valid one in predicting concentration gradients and bulk concentration values inside the loop at various cross-sections.

Work is proceeding on refining the mesh at the wall so that a better resolution of the wall concentration gradients is obtained for comparison with the analytical model described by Li et al. 2001.

REFINEMENT OF THE MODEL

Study illustrates that the concentration gradient in the region near the wall may change dramatically and the detail information from that region is of great importance to have a better understanding to the model about how species is transported and distributes.

Based on the above-mentioned model, the outermost layer of cells are refined and divided into 10 cells equally. By this means, the details can be caught at region as close as 0.3mm to the wall. Figure 59 shows the cross section of the refined model.

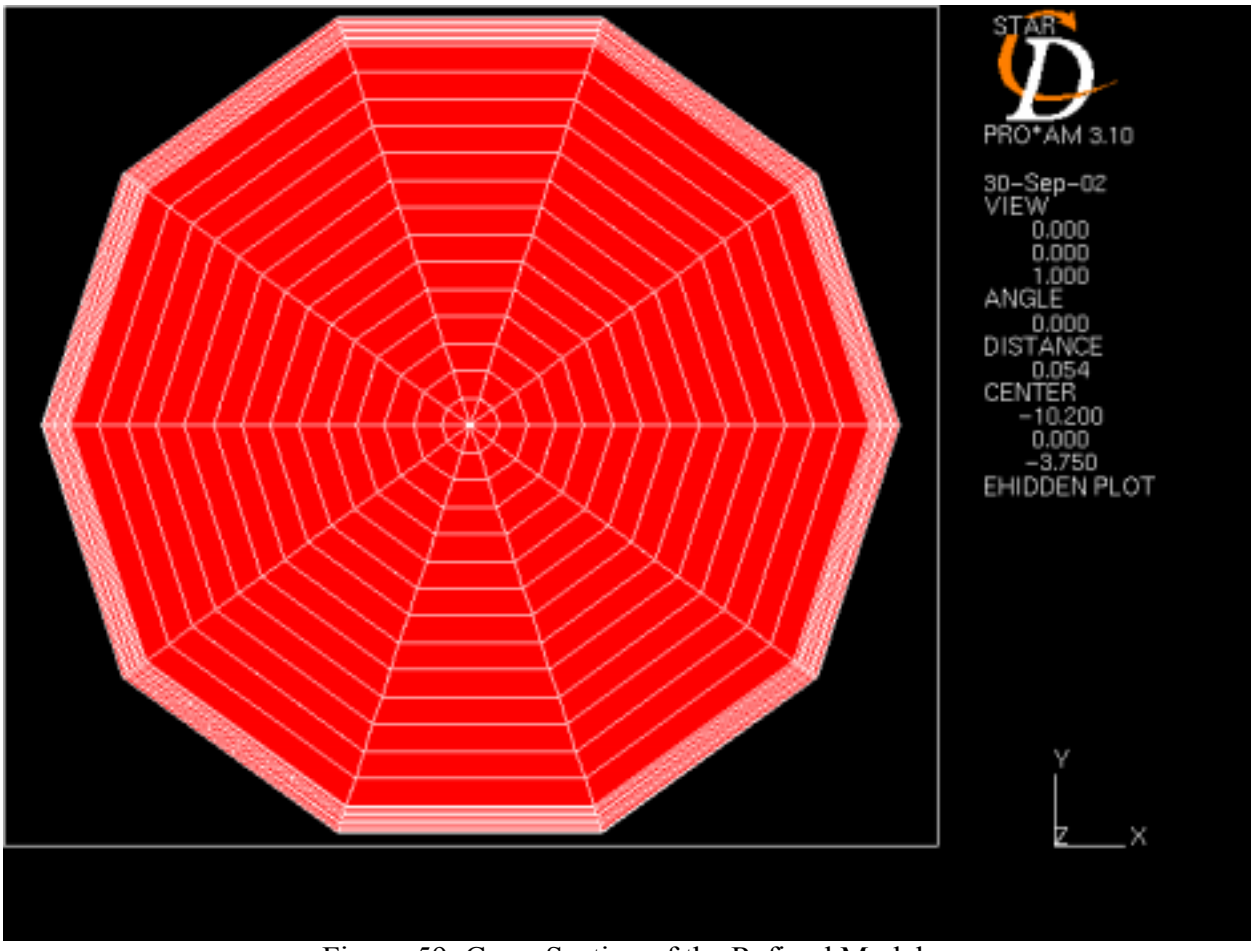

Figure-59: Cross Section of the Refined Model.

After refinement, the cell number of each half of loop increases up to 130,000. It costs nearly 15 hours for one model to reach the convergence. The same methodology is applied with unrefined model. We feed convergent results from one half to the other repeatedly. The work has given out some preliminary results (Figure-60) which provide a more detailed description of concentration at the near wall region. To get the final result, it will take some more time to present the final results.

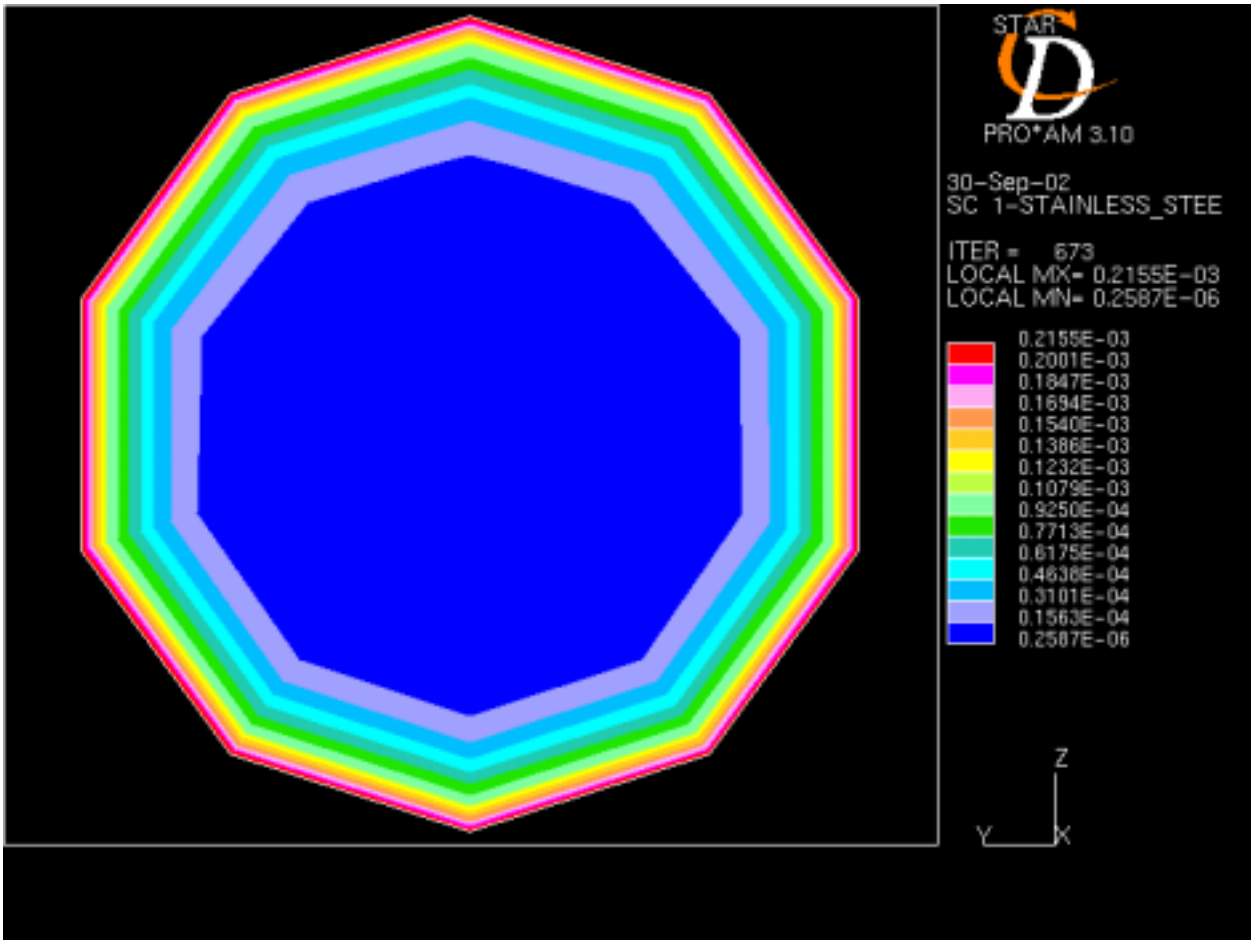

Figure-60: A Preliminary Concentration Plot at Cross Section.

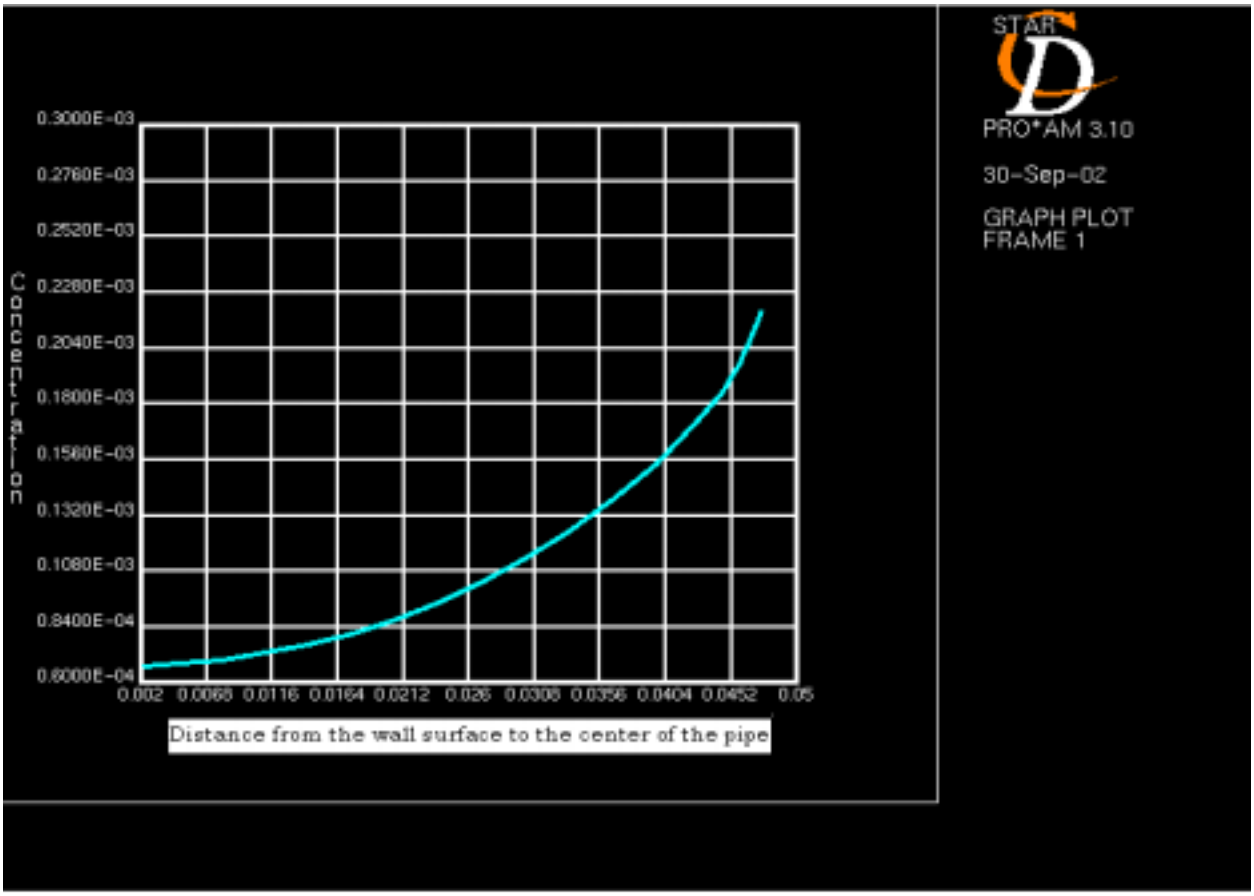

Figure 61: Concentration Variation of the Loop1 from the Wall Surface to the Center of the Pipe

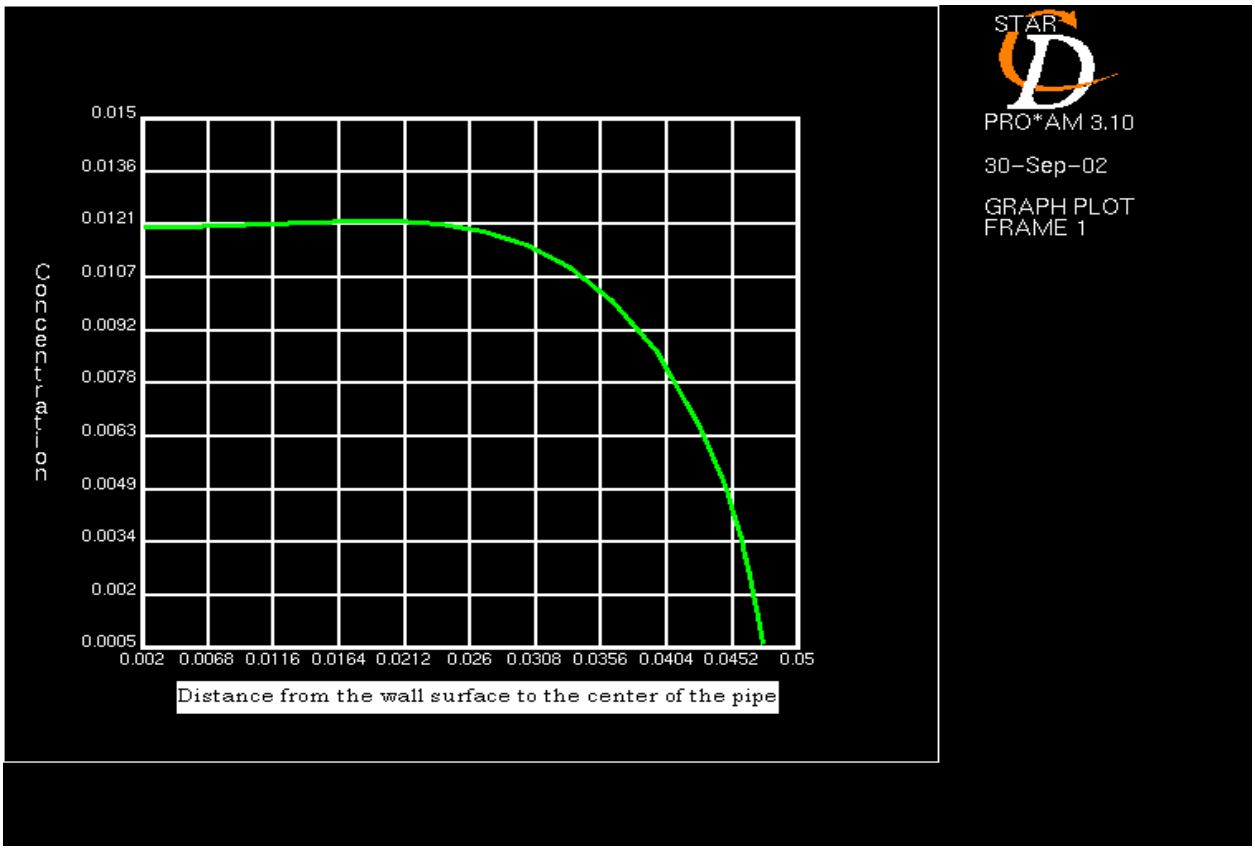

Figure 62: Concentration Variation of the Loop2 from the Wall Surface to the Center of the Pipe

Figures 61 & 62 show the variation of the concentration from the wall surface to the center of the pipe for loop1 and loop2 respectively. As expected, the concentration of the fluid in the loop1 is increasing as the distance from the wall surface is increasing and the concentration loop2 decreases as the distance from the wall surface increases.

ALTERNATIVE 2-D CONCENTRATION DISTRIBUTION MODEL FOR LAMINAR FLOW

A 2-D axisymmetric flow problem is set up. It is the upper half of the cross section along the axis of a pipe. As a result, the bottom line in the plots is the line of symmetry. The length of domain is as 50 times the diameter. A varying temperature is imposed on the upper interface. The physical problems both with increasing and decreasing temperature as a boundary condition were studied in order to capture the effects of the different temperatures on concentration profiles. For the case with increasing temperature, the upper wall is divided into three parts along the axis. The temperature remains at 623K for the first part and 723K for the last part, each of which is 45% of the whole length. The second part is where the temperature increases linearly from 623K through 723K, which only counts 5% in x direction. And for the decreasing temperature case, the temperatures for the first and the last section are 723K and 623K, respectively, 45% of length each, too. The temperature for the second region is similar to the increasing temperature case where it linearly decreases from 723K to 623K. Flow was considered as laminar and fully developed for simplicity. A FORTRAN code using Finite Difference Method (FDM) was developed to model this problem explicitly. Successive Overrelaxation (SOR) method was chosen to iterate and reach a converged solution.

RESULTS AND DISCUSSIONS:

Temperature (K)

The simplified Energy Equation (Eqn. 8) was non-dimensionalized and discretized to solve for the temperature.

$$k\left(\frac{\partial^2 T}{\partial x^2}+\frac{\partial^2 T}{\partial r^2}+\frac{1}{r}\frac{\partial T}{\partial r}\right)=u\frac{\partial T}{\partial x} \qquad (8)$$

where k is the thermal conductivity and u is the velocity in x direction.

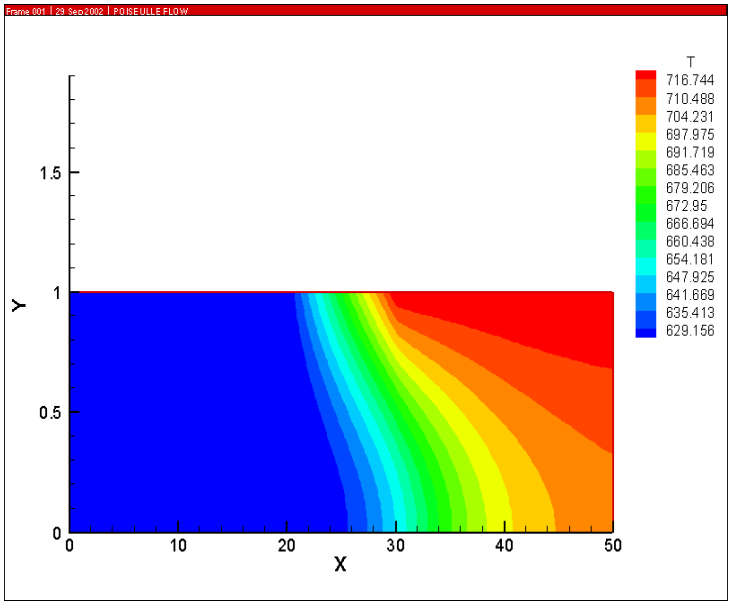

Figure-63: Temperature Distribution, Re=2300 ,Increasing Wall Temperature

The variables are non-dimensionlized by introducing the following dimensionless quantities, the governing equation transform to Eqn. 9 in which temperature depends on the Reynolds Number and Prandtl Number

$$\bar{u}=\frac{u}{u^0} \qquad \bar{x}=\frac{x}{r^0} \qquad \bar{r}=\frac{r}{r^0} \qquad \bar{T}=\frac{T}{T^0}$$

$$\mathrm{Re}=\frac{\rho u^0 r^0}{\mu} \qquad \mathrm{Pr}=\frac{C_p\mu}{k}$$

$$\left(\frac{\partial^2 \bar{T}}{\partial \bar{x}^2}+\frac{\partial^2 \bar{T}}{\partial \bar{r}^2}+\frac{1}{\bar{r}}\frac{\partial \bar{T}}{\partial \bar{r}}\right)=\mathrm{Re}\cdot\mathrm{Pr}\cdot\bar{u}\frac{\partial \bar{T}}{\partial \bar{x}} \qquad (9)$$

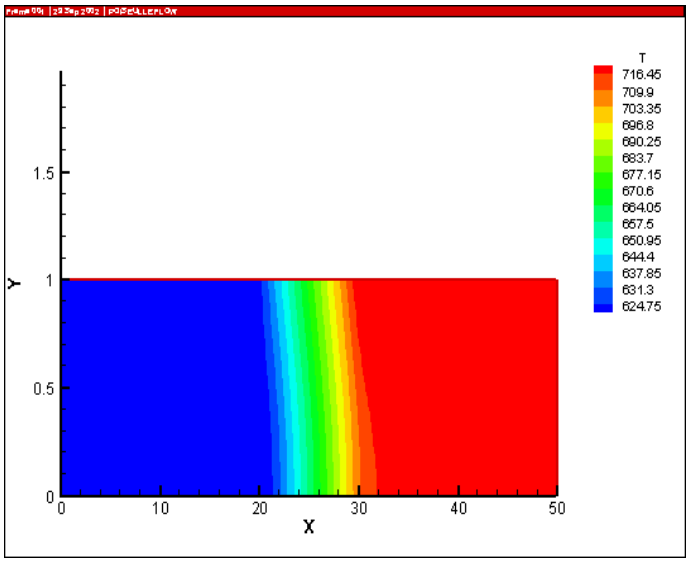

Figure- 64: Temperature Distribution, Re=230, Increasing Wall Temperature

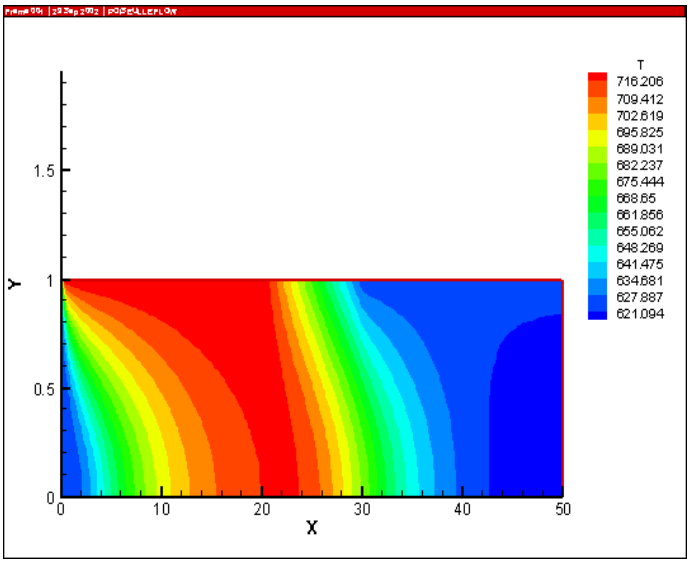

Figure-65: Temperature Distribution, Re=2300, Decreasing Wall Temperature

A 220×30 mesh is applied and Fig. 63 and Fig. 64 are the temperature distribution when Prandtl Number approximately equal to 0.01 and Reynolds Number equates to 2,300 and 230, respectively to give a range of flow rates in the pipe. Both these runs are for increasing wall-temperature cases. It can be observed that when Prandtl Number is small, the temperature diffusion in radius direction is dominant. Temperature is hardly able to diffuse in axis direction, if Reynolds Number is small. Similarly, for the temperature-decreasing cases (Fig. 65 and Fig. 66), it is much easier for the flow to cool down when the velocity is smaller. Otherwise, the impact of high temperature remains in certain distance and relatively large area.

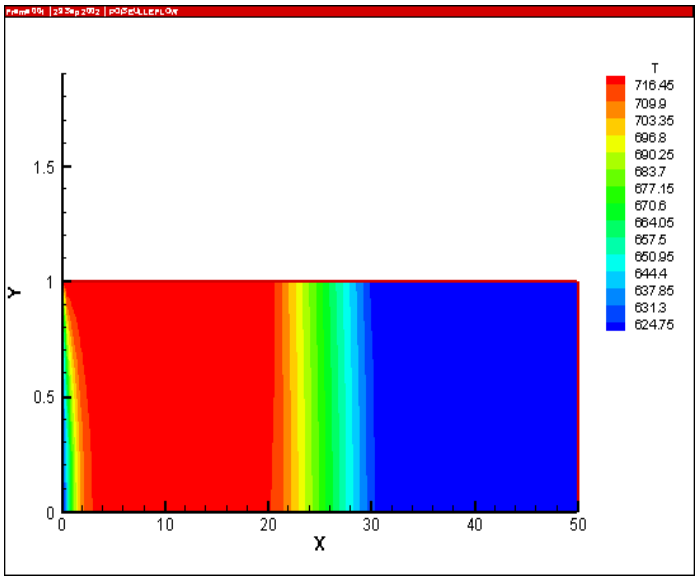

Figure-66: Temperature Distribution, Re=230, Decreasing Wall Temperature

Concentration of Fe (ppm)

The convection-diffusion equation is used as governing equation (Eqn. 10). Following the same procedure to non-dimensionalize the Eqn. 10 and obtain (Eqn. 11) similar to Eqn. 9. The only difference is with the use coefficient $\overline{D}$, instead of $\mathrm{Re}\cdot\mathrm{Pr}$.

$$D\left(\frac{\partial^2 C}{\partial x^2}+\frac{\partial^2 C}{\partial r^2}+\frac{1}{r}\frac{\partial C}{\partial r}\right)=u\frac{\partial C}{\partial x} \tag{10}$$

$$\bar{u}=\frac{u}{u^0} \qquad \bar{x}=\frac{x}{r^0} \qquad \bar{r}=\frac{r}{r^0} \qquad \bar{C}=\frac{C}{C^0} \qquad \bar{D}=\frac{D}{D^0}$$

$$\bar{D}\left(\frac{\partial^2 \bar{C}}{\partial \bar{x}^2}+\frac{\partial^2 \bar{C}}{\partial \bar{r}^2}+\frac{1}{\bar{r}}\frac{\partial \bar{C}}{\partial \bar{r}}\right)=\bar{u}\frac{\partial \bar{C}}{\partial \bar{x}} \tag{11}$$

To capture the details of the concentration profile near the wall a finer mesh was used of composed of 5000×100 nodes. This fine mesh provides a better understanding of interaction between flow and species transport.

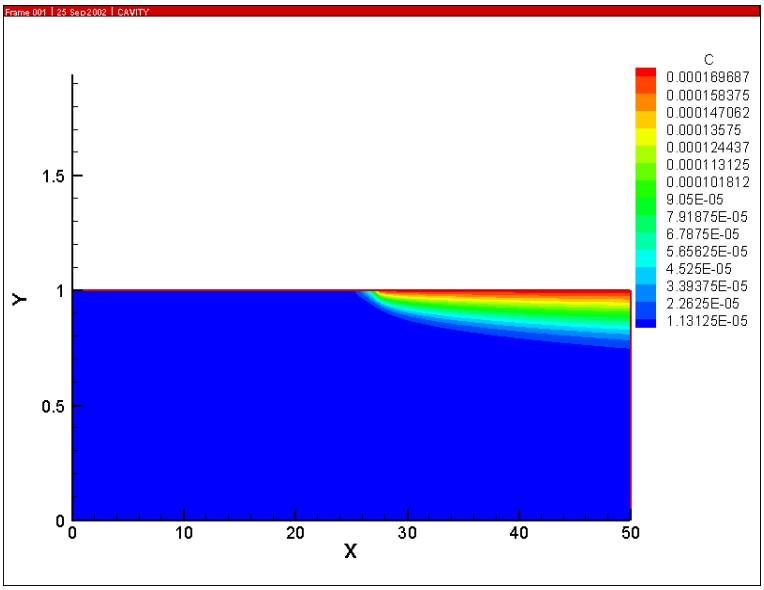

Figure-67: The Concentration Distribution of Fe with 0.01ppm O_2

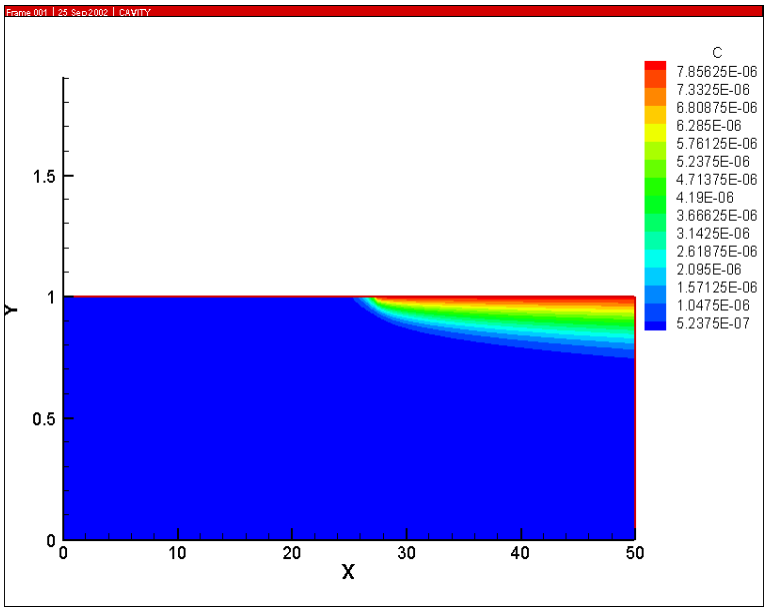

Figure-68: The Concentration Distribution of Fe with 0.1ppm O_2

Fig. 67 through Fig. 69 shows the contour of concentration with increasing temperature on the wall, but with different magnitudes of oxygen concentration. The results indicate that the contours basically have a similar pattern when the boundary conditions are the same, no matter

how much the concentration of oxygen is. But the concentration of oxygen really matters when we study the content of Fe. The concentration of Fe in the bulk flow when there is 1.0ppm oxygen in it is several orders less than the number when oxygen is at 0.01ppm. Meanwhile, as can be seen, the concentration of Fe in the flow is almost 100 times less when there is 0.1ppm oxygen, comparing with when 0.01ppm oxygen is in the flow. But if more oxygen is added into the flow, the concentration of Fe will not be reduced as dramatically as before. As the plots show, 1.0ppm oxygen can only make iron in the flow less by 10 times than when there exists 0.1ppm oxygen.

When the laminar flow is fully developed, the concentration diffuses slowly in the radial direction and only a relatively small portion of the species will transport into the bulk region.

A similar situation occurs in the decreasing temperature cases (Fig. 70 to Fig. 72). Most of the species particles remain near the wall and are transported downstream and may increase the potential risk of clogging of the pipes over a long period of time.

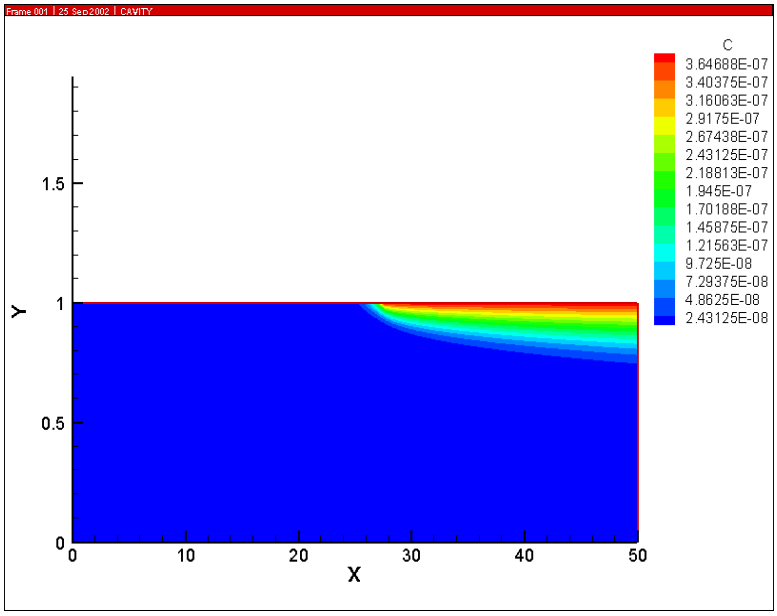

Figure-69: The Concentration Distribution of Fe with 1.0ppm O_2

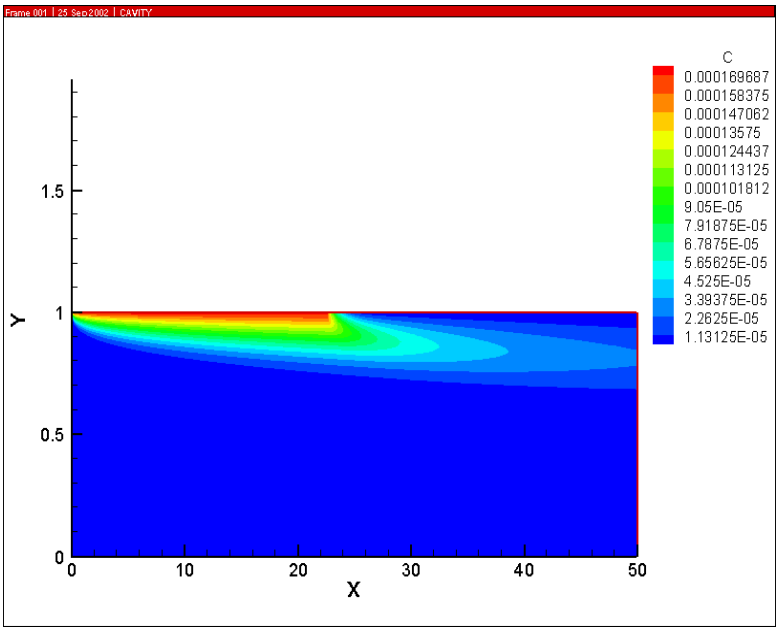

Figure-70: The Concentration Distribution of Fe with 0.01ppm O_2

CONCLUSIONS FOR 2-D CODE RESULTS

A FORTRAN code is developed to study the diffusion and convection of temperature and concentration from the pipe's wall boundary to the bulk flow assuming a fully developed flow profile and constant properties. From the results obtained one can conclude that the temperature distribution is very dependant on the properties Re*Pr number product of the flow. A low product value gives temperature more chance to spread out in the radius direction than axis direction. The information obtained by the code seems to b consistent with expected physical behavior of the temperature and concentration processes for the given boundary conditions.

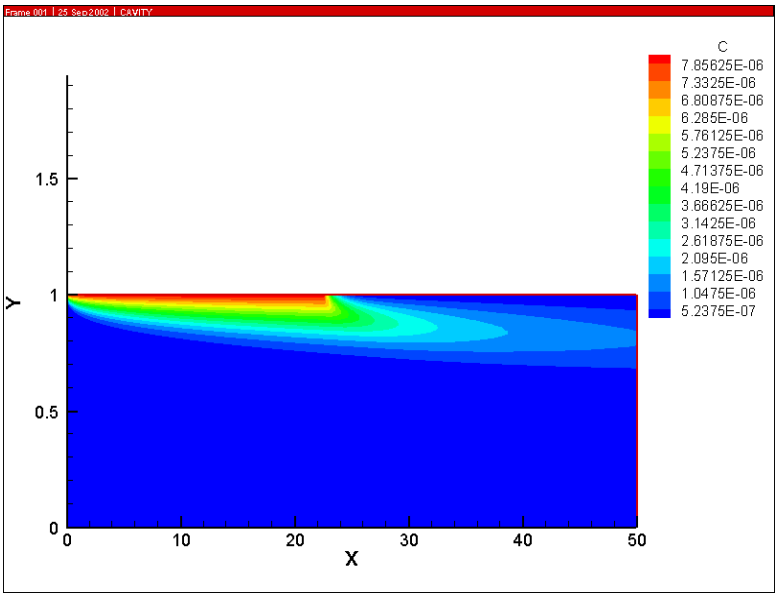

Figure-71: The Concentration Distribution of Fe with 0.1ppm O_2

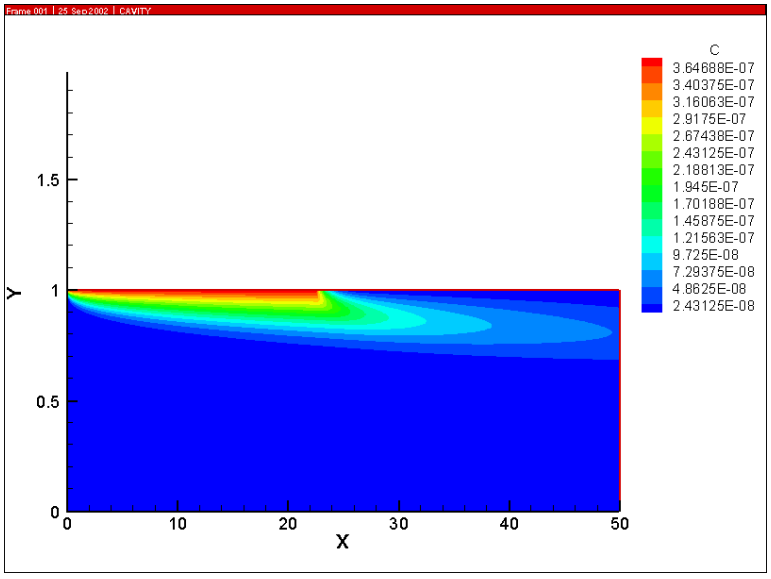

Figure-72: The Concentration Distribution of Fe with 1.0ppm O_2

As far as concentration of Fe is concerned, it shows that most of the iron particles will be transported close to the wall. This sheds some light on the concern for the precipitation and clogging problem of corrosion products on the inner walls of the loop. A preliminary result indicates from the data that active oxygen control techniques can be effective in reducing the corrosion. A higher oxygen concentration can reduce iron in the flow by several orders which are helpful to prevent the precipitation due to the above mentioned results. The relation between concentration of oxygen and Fe is not linear and the reduction of Fe will become less marked with more oxygen being added.

REFERENCES:

1. *A kinetic model for corrosion and precipitation in non-isothermal LBE flow loop*
   By Xiaoyi He, Ning Li, Mark Mineev
   Journal of Nuclear Materials, 20th April 2001.

2. *Active control of oxygen in molten lead-bismuth eutectic systems to prevent steel corrosion and coolant contamination*
   By Ning Li
   Journal of Nuclear Materials, 1st October 2001.

3. *The US accelerator transmutation of waste program*
   By Denis E. Beller, Gregory J. Van Tuyle, Deborah Bennett, George Lawrence, Kimberly Thomas, Kemal Pasamehmetoglu, Ning Li, David Hill, James Laidler, Phillip Fink.
   Nuclear Instruments and Methods in Physics Research A 463 (2001) 468-486

4. *Development of LBE technology and corrosion test of US Steels.*
   By Ning Li
   Lead-Bismuth Technology International Meeting, December 20th 2000.

5. *An oxygen control strategy for corrosion minimization in direct contact Lead-Bismuth water systems.*
   By Jacopo Buongiorno, Neil E. Todreas, Mujid S. Kazimi
   ICAPP, Florida, June 2002.

6. *Report on Bench-Mark-C study thermal hydraulic calculations of the target Mock-up.*
   By, Xiaoyi He, Ning Li
   Submitted to http://lib-www.lanl.gov/la-pubs/00796245.pdf LA-UR-99-5669

7. *Oxygen concentration measurement in liquid Pb-Bi Eutectic.*
   By T.W. Darling, Ning Li
   AccAPP – ADTTA'01 Meeting.

8. *Research activities in US related to material compatibility issues for nuclear systems using heavy-liquid-metal coolant.*
   By R.G. Ballinger, J.Y. Lim
   MIT-ANP-TR-080, MIT, Nuclear Engineering Dept., July 2001.

9. *Liquid Lead-Bismuth Materials Test Loop*
   By Valentina Tcharnotskaia, Curtt Ammerman, Timothy Darling, Joe King, Ning Li, Don Shaw, Leon Snodgrass, Keith Woloshun
   LAUR-01-5051, Internal Report submitted to Los Alamos National Laboratories.

10. *Properties of Lead-Bismuth coolant and perspectives of non-electric applications of Lead-Bismuth reactor.*
    By P.N. Martynov, K.D. Ivanov
    International Atomic Energy Agency, Vienna (Austria)

11. *Lead Bismuth Eutectic (LBE) Materials Test Loop (MTL) Test Plan.*
By Ning Li, Keith Woloshun, Valentina Tcharnotskaia, Tim Darling, Curtt Ammerman, Xiaoyi He, Joe King and David Harkleroad
LA-UR-01-4866, Internal Report submitted to Los Alamos National Laboratories. August 2001.

12. *Advanced Accelerator Applications: Addressing Nuclear Issues*
By Ed Arthur
2001 Science Day, Los Alamos National Laboratory, February 13, 2001.

13. *Introduction to heat transfer, 3rd Edition*
Frank P. Incropera, David P. DeWitt

14. *Hydraulics and Fluid Mechanics, 2001, 13th edition.*
Modi, P.N., Seth, S.M.

15. *Properties of Gases and Liquids, McGraw Book Co., 1977, 3rd Edition*
Reid, R.C.

16. *Molecular Dynamics Simulation: Elementary Methods (1992, John Wiley and Sons)*
J.M. Haile.